UiT The Arctic University of Norway

Department of Arctic and Marine Biology

The metabolic roles of astrocytes and neurons in the diving brain

A study of the mitochondrial distribution in the brain of the hooded seal (*Cystophora cristata*)

Sari Elena Dötterer

Master's thesis in Biology BIO 3950, November 2023

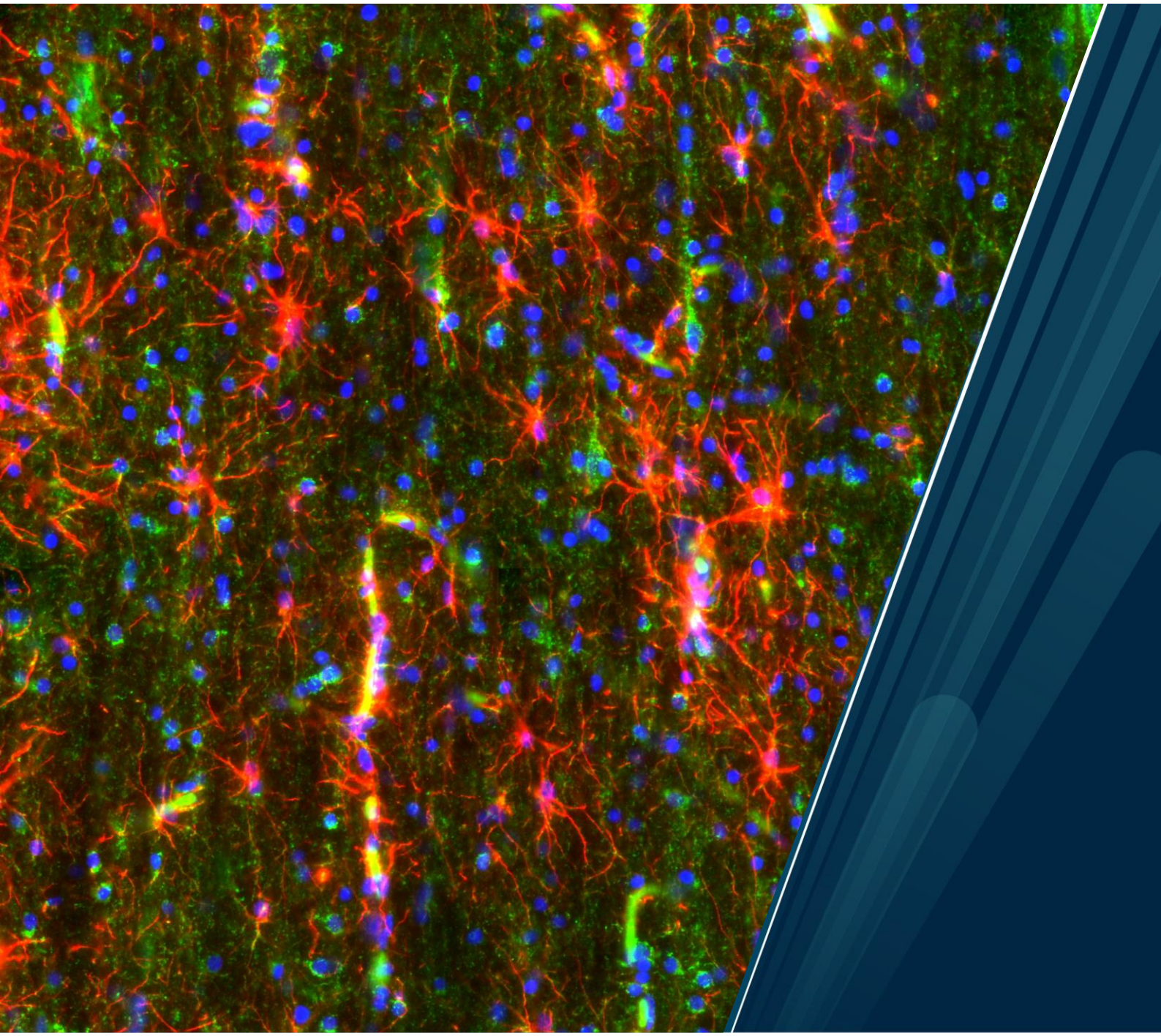

Cover photo by Dötterer, S. E. (2023): *Hooded seal visual cortex stained for GFAP, TOMM20 and DAPI. Imaged with Slide scanner VS120 (Olympus, Japan).*

University of Tromsø
BIO-3950 (60 ECTS)

Department of Arctic and Marine Biology

The metabolic roles of astrocytes and neurons in the diving brain – A study of the mitochondrial distribution in the brain of the hooded seal (*Cystophora cristata*)

Main supervisor:
PhD student MSc Chiara Ciccone

Co-Supervisor:
Prof. Lars Folkow

Acknowledgements

I want to thank my supervisors Chiara Ciccone and Lars Folkow, for trusting me with this project and being there for me through all the ups and downs. I have learned a lot from you.

I want to thank Kenneth Bowitz Larsen, Randi Olsen and Anthimi Palara for showing me immunostaining techniques and how to use a microscope. A special thanks to Roy Heijkoop who used several hours to show me how to use the wide field microscope on brain tissue and giving valuable advice about quenching. I also want to thank Fredrik Markussen and Fernando Marques for sharing valuable insights on immunostaining.

I want to thank my mom who wants to have zoom calls with me at late hours to help me with statistics. I want to thank my classmates, Sara Torppa and Anna Henriksson for struggling together with me. I also want to thank the people that I could never have done this without; Eric, Julie and Villads. In the end, a special thanks to Molly, our neighbours cat that aways finds ways to sneak into our house and cheer me up with her presence.

Abstract

The brain is highly dependent on oxygen for its metabolism and, in most mammals, major brain dysfunction occurs already within minutes of insufficient oxygen supply (hypoxia). Oxygen is the final electron acceptor in the electron transport system that drives the production of ATP through oxidative phosphorylation in the mitochondria. The rate at which oxidative phosphorylation produces ATP is dependent on the spatial organisation of the mitochondria. Studies on mice and primates have shown that mitochondria are unevenly distributed between the two major cell types of the brain: neurons and astrocytes. Neurons predominantly rely on aerobic metabolism and have higher mitochondrial density, whereas astrocytes produce energy mainly anaerobically and have lower mitochondrial density. There is evidence of a tight metabolic coupling between astrocytes and neurons especially at the brain's synapses, where the astrocytes aid the neurons in their metabolism through a mechanism called the astrocyte-neuron lactate shuttle (ANLS). Mammals that experience hypoxia regularly, like pinnipeds, show a remarkable brain hypoxia tolerance. Studies done on the visual cortex of the deep-diving hooded seal (*Cystophora cristata*) suggest that one of the mechanisms at the base of their tolerance is a metabolic shift between astrocytes and neurons. To further investigate the hooded seal brain metabolism, tissue from the visual cortex of adult hooded seals, juvenile hooded seals and mice was sampled and fixed for immunostaining and fluorescence imaging of astrocytes, neurons and mitochondria to analyse the distribution of mitochondrial sizes and densities between the two cell types. The adult hooded seals had significantly lower mitochondrial densities and larger sized mitochondria in the astrocytes compared to the neurons, whereas the opposite was found in juvenile seals and mice. This could indicate differences in the metabolic roles of astrocytes and neurons between these animals. The overall lower mitochondrial density in the adult seals compared to juvenile seals and mice is in accordance with previous findings of lower brain metabolism and supressed synaptic transmission in the adult hooded seal brain. The differences found between juvenile and adult seals indicate that mitochondrial densities and sizes may be traits that depend on age and/or development of diving abilities in the hooded seals. These findings shed new light to understating the cellular mechanisms behind the hypoxia tolerance of pinnipeds.

Keywords: Hooded seal (*Cystophora cristata*), reverse ANLS, mitochondrial density, mitochondrial size, immunostaining, fluorescence microscopy.

Table of Contents

List of Tables

List of Figures

1 Introduction

1.1 The brain and its energy metabolism

The brain is a remarkably energy demanding organ and is, in most cases, highly dependent on oxygen to meet its energy demands. In humans, the brain uses approximately 20 % of the oxygen consumed by the body, whereas it only accounts for around 2% of the total body weight (Mink et al., 1981). The need of energy comes from several energy consuming cellular processes which are mainly divided between two cell types: neurons and glia cells. In rats and humans, 75–80 % of the glucose oxidation takes place in neuronal cell processes, whereas most of the remaining 20-25 % takes place in astrocytes, a glia cell type (Hyder et al., 2013).

1.1.1 Neurons

Neurons are the primary cells for processing and transmitting information in the nervous system. They are electrically excitable and can convey signals down their axons in form of action potentials(Hill et al., 2016). Neurons transfer electrical signals to neurons or other target cells in form of synapses. When the action potential of an excited neuron reaches a synapse, it triggers the inflow of calcium ions which leads to the release of vehicles with neurotransmitters. These neurotransmitters travel over the synaptic cleft and bind to receptors of the postsynaptic cell, where a new electrical signal or cellular response is produced (Hill et al., 2016).

To be able to convey these signals, the neurons are highly dependent on balancing the ion concentrations across their cell membrane, which get repeatedly disrupted through action potentials and synaptic signalling. Most of the energy utilized by neurons is related to the activity of ion pumps, like the Na+-K+-ATPase pump in the cell membrane, working on balancing these ion concentrations (Magistretti & Allaman, 2015). Even though the action potentials create a rapid increase in positive intracellular ions through the of opening voltage gated Na+ channels, the bulk flow of Na+ ions is minimal, suggesting that only little energy spent on restoring the ion balance disrupted by action potentials (Alle et al., 2009). The main energy consumption in neurons seems to take place at the synapses (Harris et al., 2012). Re-establishing ion concentrations in the postsynaptic neuron after synaptic signal transmission account for a large

fraction of the consumed energy, while in the presynaptic terminal, the balancing of ion concentration and recycling of neurotransmitter vesicles contribute to the energy consumption (Harris et al., 2012). The high energy demand at synapses indicates the presence of local metabolic processes inside the neurons or from supporting cells, like astrocytes (Magistretti & Allaman, 2015).

1.1.2 Astrocytes

Astrocytes are the most abundant glia cells in the central nervous system. They are named after *ástron,* the Greek word for "star", because of their star shaped appearance (Figure 8, Methods) (Hill et al., 2016). Astrocytes were long considered to only serve as "structural fill" and connective tissue in the brain. In the last few decades however, it was discovered that these cells play important roles especially around neuronal synapses (Kimelberg & Norenberg, 1989). Astrocytes take up neurotransmitters from the synaptic cleft and thereby help terminating the stimulation of the postsynaptic cell (Rothstein et al., 1996). In addition, astrocytes aid the neurons in their metabolic needs by supplying them with metabolites like lactate (Pellerin & Magistretti, 1994). One single astrocyte can be connected to up to 100 000 neuronal synapses (Halassa et al., 2007).

The main energy expenditure in astrocytes emerges from the uptake of neurotransmitters and the ion imbalance that comes with it. Glutamate is the most abundant excitatory neurotransmitter of the nervous system (Meldrum, 2000). For glutamate to be taken up by astrocytes, it has to be co-transported over the membrane together with Na+ (Bouvier et al., 1992). This increases the intracellular levels of Na+, which gets actively pumped out of the cell by the energy demanding Na+-K+-ATPase pump. In addition, astrocytes spend energy on the conversion of glutamate into glutamine (Magistretti and Chatton 2005). Glutamine can be transported back into the neurons, where it gets converted back into glutamate and is packed into vesicles awaiting new synaptic release. Thereby the astrocytes can aid the neurons in the recycling of neurotransmitters (Waniewski & Martin, 1986).

Most of the brain glycogen stores are found in the astrocytes and due to its low overall concentrations, it is suggested to be mainly utilized for local energy supply (Brown, 2004).

Glycogen is a branched glucose polymer that essentially functions as an energy storing molecule. It can be broken down by glycogen phosphorylase into glucose molecules that fuel the energy metabolism of the cell. Glycogen is found at low levels in the brain (6-12 µmol) compared to the levels in liver or skeletal muscles (100-500 µmol) (Chryssanthopoulos et al., 2004; Cruz & Dienel, 2002). In the brain, the highest concentration of glycogen is located around synapses (Phelps, 1972) and studies on the expression of mRNA coding for enzymes involved in glycogen metabolism, showed that these are upregulated in astrocytes when neurons are present (Mamczur et al., 2015). This suggests that glycogen is an important energy substrate for synaptic metabolism when the supply of glucose is low (Allen et al., 2005).

1.1.3 Neuron-Astrocyte metabolic coupling

Since synapses are the main sites of energy consumption in neurons (Harris et al., 2012), these regions are dependent on the supply of energy substrates to sustain their metabolic needs. In 1994, the astrocyte-neuron lactate shuttle (ANLS, Figure 1A) hypothesis was first described, as a mechanisms of metabolic coupling between astrocytes and neurons and between neuronal activity and energy supply (Pellerin & Magistretti, 1994). As described above, when glutamate enters an astrocyte, it triggers several energy consuming processes inside the cell. This leads to an increase in the uptake of glucose from the blood (Pellerin & Magistretti, 1994). Astrocytes are closely associated with the capillaries of the brain: they can enclose capillaries with several of their "end feet" creating a large surface for the uptake of glucose and oxygen from the blood (Kimelberg & Norenberg, 1989). Most of the glucose taken up by astrocytes is broken down to lactate through glycolysis (Walz & Mukerji, 1988) and the lactate is released into the extracellular space through specific monocarboxylate transporters (Pierre & Pellerin, 2005). Studies on cell cultures showed that during resting metabolic rates, as much as 85 % of the glucose used by astrocytes is released as lactate (Bolaños et al., 1994). The lactate is taken up by neurons and serves as an energy substrate for their metabolism (Schurr et al., 1988). The neuronal lactate uptake is suggested to be driven by the glutamate-glutamine cycling in the astrocytes, indicating that the supply of lactate is regulated by neuronal activity (Pellerin & Magistretti, 1994).

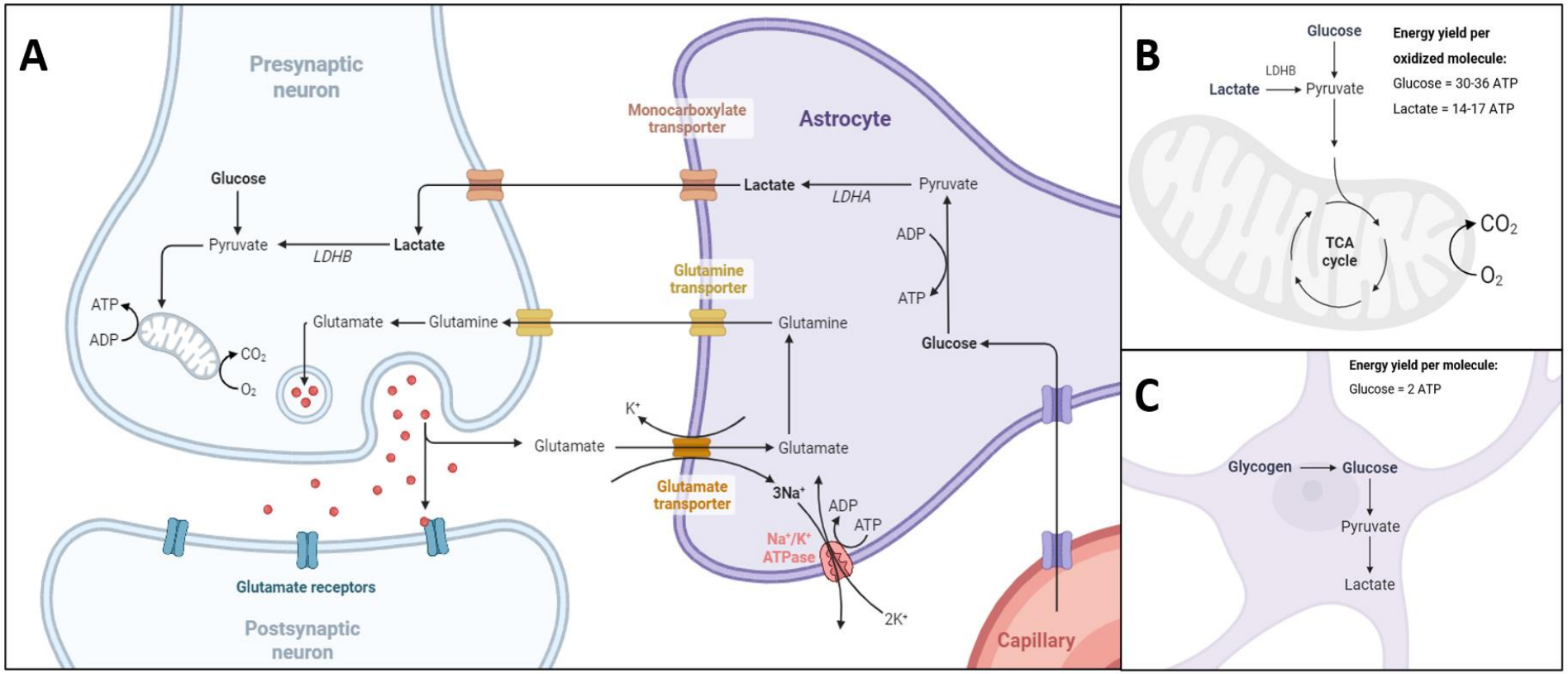

Figure 1. Schematic representation of A) The astrocyte-neuron lactate shuttle, and the predominant metabolic pathways in B) neurons and C) astrocytes. LDHB = lactate dehydrogenase type B. LDHA = lactate dehydrogenase type A. TCA cycle = tricarboxylic acid cycle. Figures created in BioRender.com.

Therefore, according to the ANLS theory, neurons are mainly dependent on oxidative metabolism, while astrocytes primarily use glycolysis as a mean of energy production (Bélanger et al., 2011; Hyder et al., 2006). To get an understanding of the differences between these metabolic mechanisms, I need to mention the role of mitochondria.

1.2 Mitochondria

Mitochondria are known in simple terms as "the powerhouse of the cell". They are small, double-membraned organelles found int the cytoplasm of cells (Lewis & Lewis, 1915). The inner membrane of mitochondria, has a series of enzymatic complexes (from I to IV) which constitute the electron transport system (ETS) (Chance & Williams, 1956). They are the drivers of the production of the universal energy carrier adenosine triphosphate (ATP), through oxidative phosphorylation. For ATP to be produced in the mitochondria, oxygen is required as the final electron acceptor of the electron transport system (Chance & Williams, 1956; Hill et al., 2016).

1.2.1 Mitochondrial metabolism in neurons

Neurons primarily produce ATP by using oxygen though the oxidative phosphorylation process (Hyder et al., 2006). To meet the high energy demands at synapses, neurons transport mitochondria from the soma, where they are manufactured, to pre- and post-synaptic areas (Chang et al., 2006). When glucose is available, it is used by the cell to produce pyruvate through a series of biochemical reactions referred to as glycolysis (Figure 1B). Pyruvate can get transported into the mitochondria and enter the tricarboxylic acid cycle (TCA). During this cycle, important substrates like NADH and $FADH_2$ together with CO_2 and few molecules of ATP are produced. NADH and $FADH_2$ are further used as substrates by the complexes of the ETS to transport electrons along the inner mitochondrial membrane and produce an electrochemical gradient of protons across it. The proton gradient is then used by an ATPsynthase (also referred to as complex V) to produce ATP. The energy yield of oxidative glucose metabolism is high, producing 30-36 ATP per molecule of glucose. Similar to glucose, lactate can serve as an energy substrate for oxidative phosphorylation. It can be converted into pyruvate by lactate dehydrogenase (LDH) enzymes and pyruvate can then enter the TCA cycle in the mitochondria. The ATP yield from the oxidative metabolism of lactate is lower than from glucose, producing between 14-17 ATP per lactate molecule. Evidence suggests that lactate is one of the main energy substrates in neurons and that pre-

and postsynaptic neurons show high expression of lactate dehydrogenase enzymes in the neocortex of humans (Duka et al., 2014). One form of lactate dehydrogenase (LDHB) is predominantly found in cells that convert lactate into pyruvate and is selectively expressed in neurons, while another form of lactate dehydrogenase (LDHA) is involved in reducing pyruvate into lactate (Figure 1). LDHA is almost exclusively found in astrocytes in the central nervous system (Bittar et al., 1996). These observations support the evidence of an astrocyte-neuron lactate shuttle (Pellerin & Magistretti, 1994).

1.2.2 Mitochondrial metabolism in astrocytes

As mentioned above, astrocytes produce lactate (Bolaños et al., 1994). This is done through an energy yielding process called glycolysis, where ATP can be produced without the presence of oxygen. The process takes place in the cytoplasm of the cell and does not require mitochondria. In glycolysis, glucose is broken down into pyruvate, which in turn is reduced into lactate (Figure 1C). The energy yield of glycolysis is low, producing only 2 ATP per molecule of glucose. Given this low energy yield and the accumulation of lactate inside the cell, glycolysis is mostly known to be the favoured process of energy production when oxygen supply is scarce. However, it has been shown that 10% of the glucose entering the brain is turned into lactate through aerobic glycolysis, which produces lactate while oxygen is present (Vaishnavi et al., 2010). The enzymes that drive aerobic glycolysis are highly expressed in astrocytes (Bélanger et al., 2011), meaning that these cells do not only turn to glycolysis when tissue oxygen levels are low, but also when oxygen is present.

Astrocytes have mitochondria and are therefore also able to produce ATP through oxidative phosphorylation. Molecular studies have however shown that the entering of pyruvate into the TCA cycle in the mitochondria is regulated by a specific pyruvate dehydrogenase enzyme (Halim et al., 2010). In astrocytes, this enzyme is found in a less active state due to it showing a higher degree of phosphorylation (Zhang et al., 2014). This suggests that the astrocytes are not able to increase the rate of oxidative phosphorylation from the levels at resting metabolic rate, and therefore have to turn to other ways of energy production, like glycolysis, when the metabolic needs increase (Magistretti and Allaman 2015).

1.2.3 Mitochondrial densities

The differences in metabolic pathways between neurons and astrocytes is reflected in the densities and morphology of the cell's "powerhouses", the mitochondria. Quantitative analyses of mitochondria in the primate visual cortex through transmission electron

microscopy, has revealed that mitochondrial densities differ between neurons and glia cells (Figure 2A). According to Wong-Riley (1989), there is a substantially higher mitochondrial density in neurons compared to glia cells. This is consistent with western blot analyses of mitochondrial proteins and enzymes, which are found in significantly higher quantities in neurons compared to astrocytes in mouse cortical cell cultures (Figure 2B) (Alano et al., 2007). The predicted energy expenditure is higher in the postsynaptic compartment of neurons than in the presynaptic axon terminal (Harris et al., 2012). However, the higher proportion of mitochondria relative to energy expenditure in the axon terminal (Figure 2B) might indicate that there are some energy consuming processes that are not accounted for in the analysis of Harris et al. (2012). The low mitochondrial density relative to energy expenditure in glia cells is another indication that energy is produced outside of the mitochondria in these cells, presumably through glycolysis (Harris et al., 2012).

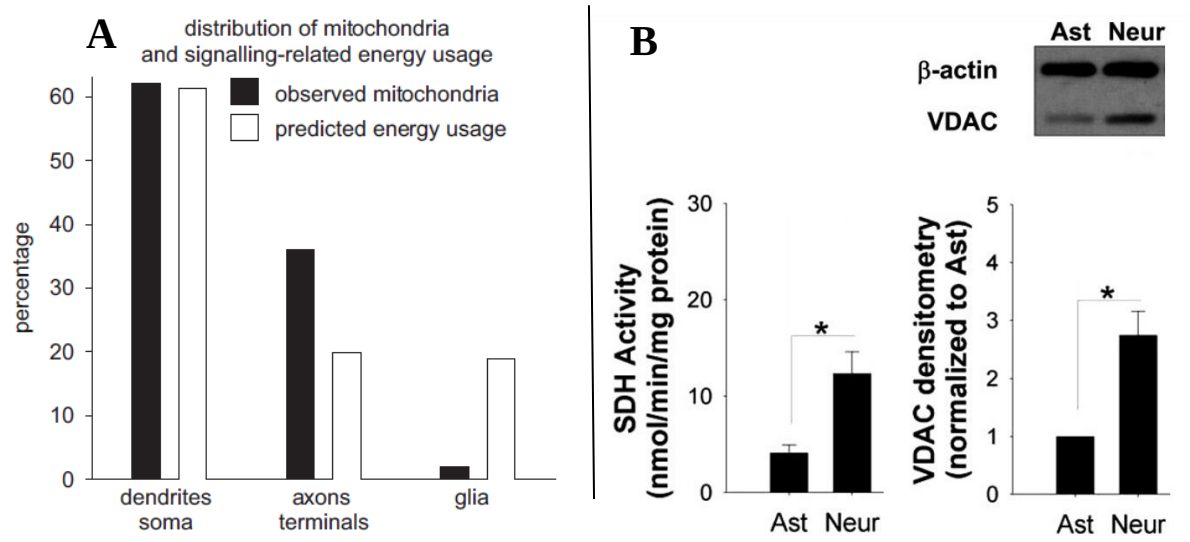

Figure 2. A) Percentage of total mitochondrial density (black) observed in transmission electron microscopy studies on primate visual cortex (Wong-Riley, 1989) and predicted energy expenditure by the different cellular compartments (Attwell & Laughlin, 2001). Updated and redrawn by Harris, Jolivet, and Attwell (2012) to include housekeeping energy which is added as 25% of the total predicted energy usage. **B)** Succinate dehydrogenase (SDH, complex II in the ETS) activity and western blots of outer mitochondrial protein, voltage-dependent anion channel (VDAC), in mouse cortical neurons (Neur) and astrocytes (Ast). * =$p < 0.01$. Redrawn from Alano et al. (2007).

1.2.4 Mitochondrial plasticity

Mitochondria are organelles of high plasticity that can undergo multiple cycles of fission, the splitting of one mitochondrion into two smaller mitochondria, and fusion, the merging of two mitochondria into one larger mitochondrion (Lewis & Lewis, 1915). Fusion and fission of mitochondria is controlled by multiple factors which can differ between different cell types of the body (Collins et al., 2002), or may occur in response to cellular stressors (Westermann, 2012). In general, it has been shown that the balance between fusion and fission is determined by the metabolic demands of the cell, where cells with lower respiratory activity have more fragmented, small mitochondria, and cells with higher respiratory activity have a higher density of fused mitochondrial networks (Westermann, 2012). The rate of fusion and fission largely affects the mitochondrial density and mitochondrial sizes within cells. Therefore, mitochondria are not organelles of a constant size and number, but can change throughout the cell's life cycle and metabolic needs.

1.2.5 Mitochondrial densities through life stages

Mitochondrial densities in the brain are known to increase from birth to maturation (Blomgren & Hagberg, 2006; Pysh, 1970). Quantitative transmission electron microscopy studies of rat brains revealed that the most rapid increase in mitochondrial densities occurs in the postnatal stages, during the time the development and maturation of the brain occurs (Pysh, 1970). The activity of the mitochondrial protein cytochrome c oxidase increases parallelly with mitochondrial densities, being low at birth and highest in adulthood (Blomgren & Hagberg, 2006). A study by Curti et al. (1990) on isolated mitochondria from the rat brain, showed that there is a significant decline in cytochrome c oxidase activity at old age in rats. If this decline is accompanied by a decrease in mitochondrial density has to my knowledge not yet been investigated.

1.2.6 Mitochondrial size

The mean mitochondrial size in rat brains, appears to remain constant through a rats life stages (Pysh, 1970). However, a cell's cytochrome c oxidase activity has been found to be positively correlated to its size, indicating that cells with larger mitochondria have a higher rate of oxidative phosphorylation (Mjaatvedt & Wong-Riley, 1988; Wong-Riley, 1989). One explanation for this is that larger sized mitochondria have more space for an increased inner membrane area (which is where cytochrome c oxidase activity occurs, as a part of the electron transport system), and can therefore drive oxidative phosphorylation at a higher rate.

However, respiratory activity of mitochondria is not only dependent on size but has also been linked to the morphology and organization of the inner mitochondrial membrane (Kristián et al., 2006a). This indicates that both size and membrane morphology are important factors in determining the oxidative capability of mitochondria.

1.3 Effects of hypoxia on the brain

We have already established that the brain requires substantial amounts of oxygen to meet its energetic needs (Mink et al., 1981) and that oxygen must be present for oxidative phosphorylation to occur in mitochondria. So, what happens during hypoxia, when the oxygen tension in the brain is too low to enable aerobic oxidation to meet its metabolic needs? One of the leading causes of death and disability in human adults worldwide is stroke (WHO 2020). During a stroke, the vascular system in the brain is damaged, causing an impairment of oxygen and glucose supply to parts of the brain. A wide range of energy demanding cellular processes are disrupted when oxygen tensions are low. One of them is the balancing of ion concenetrations across the cell membrane which, when disrupted in neurons eventually causes a massive and potentially detrimental increase in intracellular Ca^{2+} levels (Hansen & Nedergaard, 1988). The increase in calcium is a result of the so-called excitotoxic cascade which triggers a hightend realease of glutamate in the synaptic cleft causing ecxessive stimulation of the postynaptic cell (e.g., Katayama et al., 1991). Major brain disfuction occurs in most animals already within few minutes of insufficient oxygen supply (Katsura et al., 1994).

The energy metabolism described so far, has been based on the brains of humans, mice and rats, which are terrestrial animals with largely uninterrupted access to oxygen, and are highly dependent on this oxygen for meeting their brains energy needs. There are, however, animals that are exposed to oxygen-deprived environments, either seasonally, throughout their whole life or intermittently because of their foraging behaviour (Larson et al., 2014). Studying the mechanism that enable these animals to cope with cerebral oxygen deprivation gives new insights into their physiological adaptations and responses to hypoxia.

1.4 Diving mammals as natural models of hypoxia

Seals and whales are marine mammals that forage below the water surface. Although they live most of their lives under water (Blix, 2005), they have lungs that similarly to the lungs of humans, are designed for gas exchange with the surface air (Hill et al., 2016). This means that during breath-hold dives, these animals face the challenge of not being able to acquire

oxygen. In some seal species the arterial oxygen pressure has been measured to drop to only 12 – 20 mmHg during dives (Meir et al., 2009; Qvist et al., 1986) which is much lower than the levels that typically cause neuronal malfunction metabolic deficiency in human brains; 25-40 mmHg (Erecińska & Silver, 2001). With these low levels of arterial oxygen supplied to the brain during dives, the seals appear to still be able to meet the brain's energetic needs, thereby avoiding extensive brain tissue damage (Larson et al., 2014). The question therfore arises as to what mechanism allow their brains to cope with hypoxemia? In order to gain more insight into these mechanisms, one of the animals that can be studied is an exeptional diver, the hooded seal (*Cystophora cristata*).

1.4.1 Hooded seal

The hooded seal (*Cystophora cristata*) is an Arctic and sub-arctic phocid species. Its distribution is limited to the North Atlantic Ocean and the population is mainly divided into two stocks: the Greenland Sea stock of around 76 000 individuals and the Northwest Atlantic stock with an estimated 600 000 individuals (ICES., 2019). Hooded seals are sexually dimorphic where the males are substantially larger, weighing between 200-360 kg, than the females, weighing between 150-250 kg (Blix, 2005). Males also have the characteristic "hood", a nasal sac that has given the species its name. The hood is believed to be a sexual selected trait and is not present in females (Jefferson et al., 2015). Hooded seal become sexually mature at the age of 4-5 years (Frie et al. 2012) and their average life expectancy is approximately 25-30 years (Kovacs & Lavigne, 1986)

Hooded seals are dependent on sea-ice for breeding and whelping. They return to the same breeding colonies each March to give birth to their pups on ice floes (Blix, 2005). The pups are nursed for only 2-4 days (Bowen et al., 1985), the shortest lactation period for any mammal, before the adults breed and disperse to their foraging grounds in open water. They are known to feed on squid (*Gonatus fabricii*), polar cod *(Boreogadus saida),* capelin *(Mallotus villosus*), Greenland halibut *(Reinhardtius hippoglossoides),* Atlantic cod *(Gadus morhua*) and redfish *(Sebastes mentella),* although their diet can vary between feeding grounds (Hammill & Stenson, 2000; Haug et al., 2004; Hauksson & Bogason, 1997).

1.4.2 Adaptations to diving

Telemetry studies on the diving behaviour of hooded seal have shown that they spend more than 90% of their life below the water surface (Folkow and Blix 1999). The hooded seal is categorized together with Weddell seals (*Leptonychotes weddellii*) and elephant seals

(*Mirounga sp*.) as deep-diving seal species. Free-diving hooded seals have been recorded to dive down to depths of 1600 m and stay submerged of up to 1 hour (Folkow & Blix, 1999; Vacquie-Garcia et al., 2017). However, most dives are to 100-600 m depth and last between 5-25 min (Folkow and Blix 1999).

Pinnipeds have several adaptations that enable them to endure long breath-hold dives. Metabolic depression is achieved by an extensive reduction in heart rate (bradycardia) that is accompanied by a re-distribution of blood flow to the most hypoxia-sensitive tissues, through peripheral vasoconstriction. These key adaptations enable them to economize with a limited oxygen supply (Bron et al., 1966; Thompson & Fedak, 1993; see Blix, 2018 for review). The peripheral vasoconstriction may, when fully engaged, reduce flow of blood to almost all organs of the body substantially, with the exception of the brain, where the blood flow is, in fact, slightly increased (Blix et al., 1983; Zapol et al., 1979). Hooded seals are, moreover, capable of reducing brain metabolism during diving, through brain cooling (Blix et al., 2010; Ramirez et al., 2007). This is a mechanism that diverts cooled venous blood from the flippers to the brain (Blix et al., 2010). Added to this, hooded seals have particularly large internal oxygen stores (Burns et al., 2007), almost four times as large as those of humans (Blix, 2018). Together with a large blood volume, they have high amounts of haemoglobin in the blood. Additionally, their skeletal muscles have the highest levels of myoglobin recorded in any species (Burns et al., 2007). Both haemoglobin and myoglobin are proteins that can reversibly bind oxygen, and therefore play important roles in the transport and storage of oxygen in the body (Hill et al., 2016). Despite this, deep-diving seals may experience very low arterial oxygen levels during routine diving, as mentioned above (Meir et al., 2009, Qvist et al., 1986), which leave their brain in a hypoxic condition.

During hypoxia experiments in vitro, neurons from the visual cortex of hooded seals maintain neuronal activity for a significantly longer period than the neurons of mice (Folkow et al. 2008). Synaptic signalling measured in vitro in the hippocampus of hooded seal, has moreover been shown to be diminished but active for up to 3 hours of hypoxia, in addition to displaying a recovery after re-oxygenation (Geiseler et al., 2016). Significantly higher levels of glycogen have been documented in the hooded seal cortex compared to mouse cortex (Czech-Damal et al., 2014), leading to the hypothesis that glycogen is not only present in the astrocytes but also in the neurons, to serve as a energy source when the supply of glucose is low (Czech-Damal et al., 2014). How the hooded seal brain is able to maintain its function and meet its metabolic needs during diving-induced hypoxemia is still fully not understood.

1.4.3 The hypothesis of reverse metabolic roles in seal astrocytes and neurons

One study trying to shed new light on hooded seal brain metabolism was done by Mitz et al. (2009), investigating the distribution of neuroglobin and cytochrome c in the hooded seal brain. Neuroglobin is an oxygen binding protein, that - similarly to haemoglobin and myoglobin - may potentially serve as an oxygen storage in the brain (Burmester et al., 2000). In terrestrial mammals, neuroglobin is exclusively found in the neurons and have there been shown to have neuroprotective properties and to be closely associated with mitochondria (Burmester & Hankeln, 2009). (Khan et al., 2006). It was first hypothesized that hooded seals might have substantially higher levels of this protein in their brain (Folkow et al. 2008), but it was discovered that their neuroglobin levels are similar to those of non-diving species (Mitz et al., 2009; Schneuer et al., 2012). The distribution of neuroglobin between astrocytes and neurons did however differ between hooded seal and mouse brains. Immunolabelling and fluorescence microscopy suggested that neuroglobin is highly present in the astrocytes of hooded seal, whereas in mouse, the neuroglobin is restricted to the neurons, as expected (Mitz et al., 2009). Mitz et al. (2009) additionally discovered high levels of cytochrome c in the hooded seal astrocytes. This could indicate that the hooded seal astrocytes have a high rate of oxidative phosphorylation compared to the astrocytes e.g., of rodents. Furthermore, it may indicate a metabolic switch between neurons and astrocytes, where neurons depend less on oxidative metabolism than the astrocytes. This is contrary to the observed metabolic roles of astrocytes vs neurons in rodents (Pellerin & Magistretti, 1994), to which Mitz et al. (2009) proposed the presence of a reverse astrocyte-neuron lactate shuttle in hooded seals. According to this hypothesis, neurons may resort to anaerobic glycolysis during severe hypoxia, then shuttling the produced lactate to the astrocytes, in which lactate may be re-converted to pyruvate when oxygen again becomes readily available during surfacing events. In this way, astrocytes may alleviate neurons from lactate overload, as well as post-dive reperfusion oxidative stress. The observation of LDHB being highly expressed in seal astrocytes supports this hypothesis (Hoff et al., 2016).

1.4.4 Mitochondrial densities in the hooded seal brain

The high presence of neuroglobin and cytochrome c (Mitz et al., 2009) could additionally indicate a higher mitochondrial density in the astrocytes compared to neurons in hooded seals. Firstly, this could reflect a shift in oxidative metabolism, that could indicate that neurons are less dependent on oxygen to meet their metabolic needs (Mitz et al., 2009). Secondly, the

astrocytes might have a higher rate of energy production due to oxidative metabolism in mitochondria, which means that they could increase the rate of their neuroprotective functions, like the uptake of glutamate from the synaptic cleft to minimize excitotoxicity (Katayama et al., 1991). Thirdly, the main source of reactive oxygen species (ROS) comes from mitochondria, and during hypoxia and re-oxygenation after diving in seals the production of ROS is substantially increased (Elsner et al., 1998; Halliwell, 2006). A lower density of mitochondria in the neurons could therefore be a mechanism to avoid neuronal damage (Mitz et al., 2009).

1.5 Aims and hypotheses

The aim of this thesis is to give new insights into the cellular mechanisms that contribute to hypoxia tolerance in the brain of hooded seals. I will do this by investigating the size and density of mitochondria in neurons and astrocytes of adult and juvenile hooded seals. The size and density of mitochondria will additionally be measured in the brains of mice, which will serve as a non-hypoxia-tolerant control species.

Hypotheses to be tested:

1. **In hooded seals there is a similar or higher mitochondrial density in astrocytes compared to neurons.**

This would be in accordance with the immunohistochemistry data presented by Mitz et al. (2009) who found high intensity staining of neuroglobin and cytochrome c in hooded seal astrocytes. This finding forms the basis for the 'reversed ANLS hypothesis, whereby the astrocytes have an increased aerobic metabolism and the neurons produce energy anaerobically.

2. **In hooded seals the mitochondria are larger in the astrocytes than in the neurons.**

Large astrocytic mitochondria would imply that they have a higher rate of oxidative phosphorylation (Mjaatvedt & Wong-Riley, 1988; Wong-Riley, 1989), which would be in support of the 'reversed ANLS hypothesis' in hooded seals mentioned above (Mitz et al. 2009).

3. **The mitochondrial density in hooded seal astrocytes is higher than the density in the astrocytes of mice.**

This would be in accordance with the immunohistochemistry data presented by Mitz et al. (2009), which found no staining of cytochrome c and neuroglobin in mouse astrocytes, but a high presence of the staining in hooded seal astrocytes.

4. **The mitochondrial sizes in astrocytes of hooded seals are larger than those in the astrocytes of mice.**

Implying that the astrocytic mitochondria in hooded seals have a higher capacity of oxidative phosphorylation than the mitochondria in mouse astrocytes, supporting the theory of different metabolic roles of astrocytes and neurons in hooded seals compared to mice (Mitz et al. 2009).

5. **The ratio of mitochondrial density between astrocytes and neurons is similar in adult and juvenile seals.**

Based on observations from rat brain, the overall mitochondrial density might increase from birth to adulthood (Blomgren & Hagberg, 2006; Pysh, 1970). However, if a metabolic switch between astrocytes and neurons exists, and is an intrinsic adaptation to hypoxia in hooded seals, regardless of age, the mitochondrial density ratio between neurons and astrocytes might stay the same.

2 Materials and methods

To measure mitochondrial density and size distribution, fixed tissue of the visual cortex from adult hooded seals, juvenile hooded seals and mice were immunolabeled for mitochondria, neurons and astrocytes and imaged with fluorescence microscopy. Using the image analysis software *FIJI* (version 1.54f, 2023) a manual and automated cell selection methods were conducted to specify the area of astrocytes and neurons within the tissue. Within the cells, mitochondrial size as well as two types of measurements of mitochondrial density were recorded: *mean fluorescence intensity* and *mitochondrial counts*. These measurements were analysed using mixed linear models in RStudio (version 4.3.1, 2023).

2.1 Animal sampling

Three adult female hooded seals (*Cystophora cristata*) (Table 1) were captured at their breeding grounds in drift ice at approx. 72°N, 016° W in the Greenland Sea ("the West Ice"), in March 2022, during a research/teaching cruise with the R/V Helmer Hanssen, by permit from relevant Greenland and Norwegian authorities. The seals were all lactating and between 1-4 days postpartum at time of capture.

The captured seals were immediately sedated by an intramuscular injection of zolazepam/tiletamine (Zoletil Forte Vet., Virbac S.A., France, 1.0-1.5 mg/kg) and then anaesthetised via endotracheal ventilation with 2-3% isoflurane (Forene, Abbott, Germany) in air. When fully anaesthetized, they were euthanized by exsanguination via the carotid arteries, all in accordance with a permit issued by the Norwegian Food Safety Authority (NFSA ('Mattilsynet') - permit no. 29013).

Six fully weaned hooded seal pups were live-captured from the same breeding colonies as the adult females, in March 2022. Their health was carefully monitored during the return to the approved research animal facility (NFSA approval number 089) of the Department of Arctic and Marine Biology at UiT – The Arctic University of Norway. Here, they were maintained for other research purposes (NFSA permit 29080) in two 40 000 L sea water pools and were trained and fed (thawed fresh-frozen herring (*Clupea harengus*)) supplemented with vitamin (SeaTabs®, Pacific Research Labs, Inc., USA) by UiT staff members. In June 2023, at the age of 15 months, the seals were euthanized as described above, again with reference to NFSA permit 29080.

Eight adult male mice, strain C57BL6, were gifted to this project from Samuel Geisler during his works on electrophysiology in seal and mouse (Sara Torppa master's thesis, unpublished). The mice were euthanized using cervical dislocation, in accordance with "Regulation concerning the use of animals for scientific purposes" (FOR-2017-04-05-451; https://lovdata.no/dokument/SF/forskrift/2015-06-18-761).

Brain tissue from a total of eight adult mice and six juvenile hooded seal was sampled and fixed during May-June 2023. However, only tissue from three juvenile seals and three adult mice (Table 1) was further used in staining and analysis. The analysis of tissue from all the sampled animals was beyond the scope of this thesis.

Table 1. Overview of the animals included in staining and analysis. F = female, M = male.

Animal ID	Species	Age	Sex	Sampling date	Brain region	Location
K1-22	Hooded seal	Adult	F	20/03/2022	Visual cortex	Greenland Sea
K2-22	Hooded seal	Adult	F	21/03/2022	Visual cortex	Greenland Sea
K7-22	Hooded seal	Adult	F	23/03/2022	Visual cortex	Greenland Sea
K2A-22	Hooded seal	Juvenile (15 months)	M	20/06/2023	Visual cortex	Captive UiT
K7A-22	Hooded seal	Juvenile (15 months)	F	14/06/2023	Visual cortex	Captive UiT
K10A-22	Hooded seal	Juvenile (15 months)	F	06/06/2023	Visual cortex	Captive UiT
M5-23	Mouse	Adult (13 weeks)	M	25/05/2023	Visual cortex + white matter	Captive UiT
M6-23	Mouse	Adult (16 weeks)	M	31/05/2023	Visual cortex + white matter	Captive UiT
M7-23	Mouse	Adult (16 weeks)	M	01/06/2023	Visual cortex + white matter	Captive UiT

2.2 Tissue sampling

The brains of adult hooded seals, juvenile seals and adult mice (Table 1) were immediately removed after decapitation and placed in ice cold artificial cerebrospinal fluid (aCSF) (128 mM NaCl, 24 mM $NaCHO_3$, 0.5 mM NaH_2PO_4, 3 mM KCl, 1 mM $MgCl_2$, 10 mM D-glucose, 20 mM sucrose, 3.5 mM $CaCl_2$) to slow the degradation process of neuronal tissue. The

average time from capitation to immersion in aCSF was 15 minutes for the hooded seals and 35 seconds for the mice.

Subsamples of the visual cortex were placed in a petri dish lined with dental wax containing aCSF. The visual cortex was chosen for this study because previous research on neuroglobin distribution in hooded seal has been done on the visual cortex (Mitz et al. 2009). Furthermore, the number of synapses per neurons is higher in the cerebral cortex compared to the rest of the brain (Abeles 1991), presumably making the visual cortex an area with high astrocyte-neuron metabolic coupling. The cortex, therefore, serves as a good model for studying cell metabolism and mitochondrial density.

The tissue was carefully cut into cubes of 1 cm^3 (hooded seal) and 1 mm^3 (mouse) using two sterile razor blades. This size was chosen in consideration to the formalin-based fixatives' ability to penetrate the tissue which is known to be approx. 1 mm per hour (Medawar, 1941). For hooded seal brain tissue, pieces of 1.5 cm^3 can be successfully fixed in formaldehyde solutions (Mitz et al. 2009). This is, firstly, due to the brain size being much larger, and therefore the visual cortex region having a higher volume compared to the size of the same region in a mouse brain. Secondly, hypoxia experiments on hooded seal brain have shown that the tissue can endure longer periods of no oxygen supply (Folkow et al., 2008; Geiseler et al., 2016). This is an advantage when fixating the tissue, as no visible degradation of the tissue was observed even in regard to the slow penetration rate of the formaldehyde fixations that was used.

To be able to detect enough astrocytes, a sufficient tissue area with white matter was needed. Since the visual cortex of mice is physically smaller than the hooded seal visual cortex, it was difficult to sample enough material. In mice, the sections stained for astrocytes were therefore sampled from white matter found beneath the visual cortex in the inner brain. However, the sections stained for neurons were from the visual cortex.

The samples were moved to sampling tubes with fixative (see paragraph 2.3 for details), with a no higher than 1:10 tissue to fixative ratio. All handling of the tissue, such as cutting and moving, was done carefully to not cause any squeezing and deformation of the cells.

2.3 Tissue fixation

Adult hooded seal brain tissue was fixed overnight in 4% paraformaldehyde (PFA) in PBS (140 mM NaCl, 2.7 mM KCl, 8.1 mM Na_2HPO_4, 1.5 mM KH_2PO_4). It was further transferred to 0.4% PFA + 0.01 % NaN_3 in PBS for long term storage.

Three different fixatives (Table 2) were used for the fixation of brain tissue from juvenile hooded seal and adult mice. The tissue was immersed in the respective fixatives overnight and washed 3x 1 min in PBS before being transferred to 0.04% PFA + 0.01 % NaN_3 in PHEM (60mM PIPES, 25mM HEPES, 10mM EGTA, and 4mM $MgSO_4 \cdot 7H_20$) for long-term storage.

2.3.1 Paraformaldehyde fixatives

The “PFA fix”, a paraformaldehyde fixative (Table 2), was used to prepare the tissue for immunostaining. The formaldehyde recipe was updated to fit the standard PFA fix protocols used at the Core Facility of Advanced Microscopy (KAM) at UiT, and the tissue sampled in 2023 was therefore fixed using 8% PFA in PHEM. Compared to the adult seal samples fixed in 2022, the PFA concentration was increased, and PBS was switched to PHEM, which has a higher capability to preserve cell ultrastructure and intracellular antibody binding (Montanaro 2016).

2.3.2 Glutaraldehyde fixatives

The fixatives containing glutaraldehyde (Table 2) were used to prepare the tissue for correlative light and electron microscopy (CLEM) and/or transmission electron microscopy (TEM). Glutaraldehyde (GA) creates covalent bonds in the tissue and therefore has a stronger tissue stabilizing ability than PFA (Hopwood 1972). This is important when looking at e.g. mitochondrial morphology as it preserves the structure of cells and organelles in the tissue. However, a too high GA concentration can make the receptors in the tissue unavailable for antibody binding and is therefore not suitable for immunostaining (Weber 1978).

The “Morphology fix” was prepared with a 2.5% GA concentration, using a 25% GA stock. This stock solution additionally contained ethanol which further decreases antibody binding (Otali et al. 2009). This fixative prepared the tissue for TEM imaging with the goal to look at mitochondrial morphology, such size and inner membrane structure. The “GA fix” was prepared with 0.5 % GA in PHEM, using a GA stock of 8% GA that didn’t contain any additional ethanol. This fix prepared the tissue for CLEM, which combines both immunostaining and TEM imaging techniques.

Table 2. Fixatives for immunostaining and electron microscopy. *8% Glutaraldehyde stock not containing ethanol. **25% Glutaraldehyde stock with ethanol.

Fixative name	Used for	Recipe
PFA fix	Immunostaining	8% PFA in PHEM
GA fix	Immunostaining with glutaraldehyde for correlative light and electron microscopy (CLEM)	4% PFA + 0,5 % Glutaraldehyde* in PHEM
Morphology fix	Microwave-assisted processing with osmium for transmission electron microscopy (TEM)	4% PFA + 2,5% Glutaraldehyde** in PHEM

2.4 Sectioning

The tissue was sectioned using two different methods: the Tokuyasu cryosectioning method and the cryostat sectioning method.

2.4.1 The Tokuyasu cryosectioning method

This method was used to make very thin slices (70-700 nm thickness) with a surface area of around 1 mm^2. These slices were made for the purpose of CLEM, which uses immunostaining and fluorescence microscopy to label the cells and combines this with TEM to look at mitochondrial morphology within the cells. The sections for CLEM need to be cut with a ultramicrotome to make them thin enough for electrons to pass through them (De Boer et al., 2015). The CLEM approach was however abandoned in this project, due to difficulties in finding staining signal in these slices (as described in section 2.7.2). The slices were also deemed to be inadequate for mitochondrial quantification, as due to their thickness, the sections would only show a small slice of a cell. The Tokuyasu sections were however still used in the initial testing of antibodies for astrocytes, neurons, and mitochondria with fluorescence microscopy. In addition, the specificity of the mitochondrial antibody was tested through gold-immunostaining and TEM.

Preparation of the tissue for sectioning followed the “Tokuyasu cryosectioning method” described by Webster and Webster (2014). Fixed tissue from hooded seal was carefully cut into 1 mm^3 pieces using two razor blades and dental wax. The pieces were placed in 2.3 M

sucrose (#SO389, Sigma-Aldrich) in PBS and overnight for cryoprotection. Some of the pieces were immersed in gelatine before cryoprotection to create tissue blocks suitably shaped for cryosectioning. Further, the tissue was mounted on metal pins, used for mounting the tissue on the cryostat, and immersed in liquid nitrogen at -80°C. The EM UC7 ultramicrotome (Leica, Germany), equipped with a diamond knife was used to cut tissue sections, keeping the tissue frozen in a -80°C chamber while cutting.

The sections used for fluorescence light microscopy were cut to 700-1000 nm thickness. The tissue sections were picked up by placing a drop of a 1:2 solution of 2.3 M sucrose and 2% methylcellulose onto an aluminium loop. When slightly placing the loop on top the cut section, the section froze onto the drop and could be picked up and placed on poly-L-lysine (#P1399, Sigma) coated coverslips. The sections made for TEM were cut to 70 nm thickness and placed onto formvar- /carbon-coated specimen grids. These sections were thin enough for electrons to transfer through them and they were placed on grids on the grounds of a electrons inability to penetrate glass. The coverslips and specimen grids were stored at 4° C until staining.

2.4.2 The cryostat sectioning method

The cryostat sectioning method was used to make sections of a much larger thickness (20-40 µm) and with a larger surface area (ca 1 cm^2) than the Tokuyasu sections. These sections were made as a second approach to immunostaining and fluorescence microscopy after running into difficulties in the staining of Tokuyasu sections. The cryostat sections resulted more suitable for mitochondrial quantification, as the larger surface area and increased section thickness made it possible to quantify mitochondria in a large tissue area containing whole cells. As will be mentioned later in the *2.6.2 Immunostaining of cryostat section* paragraph, the 20 µm section thickness gave the best results and was the one used in the final experiment for measuring mitochondrial sizes and densities.

To prepare the tissue for cryosectioning, the fixed tissue was cryoprotected by being placed in a 30% sucrose + 0.01% NaN_3 in PBS solution overnight or until it had sunk to the bottom of the solution, indicating that the tissue was fully saturated (Rosene et al., 1986). Further, the tissue was embedded in Tissue-Tek (Tissue-Tek ® O.C.T. Compound) on a holder in the cryostat chamber for increased stabilization while cutting. Excess Tissue-Tek around the tissue was removed with a scalpel to create a small cutting surface. The tissue was cut with a CM3050 S cryostat (Leica, Germany) into sections of 20-40 µm thickness at a chamber

temperature of -19° C and object temperature of -20 °C. The sections were moved directly into petri dishes containing room temperature PBS using a paintbrush. The sections were washed 3x 1 min in PBS and mounted on positively charged microscopy slides (Superforst™ Plus Gold Microscope Slides, Epredia™) using a drop of distilled water and a paintbrush. The slides were stored at 4 °C in an airtight box overnight before staining.

2.5 Immunofluorescence

Immunofluorescence is the process of labelling specific proteins with fluorophores (Odell & Cook, 2013). This is done by using primary antibodies that are manufactured to bind a desired antigen (e.g., a protein). Then, secondary antibodies are used that specifically bind to the primary antibodies. The secondary antibodies have a fluorophore bound to them which, when exited by light at a certain wavelength, will emit light at another wavelength. This light can get detected by a fluorescence microscope. The desired features in a tissue, like cells or cell organelles, can be distinguished from each other by using several primary antibodies that bind to proteins within those specific features and secondary antibodies with non-overlapping excitation and emission spectra (Figure 3). When exited with a fluorescence microscope, the stained features can be distinguished from each other by emitting different wavelengths of light (Odell & Cook, 2013).

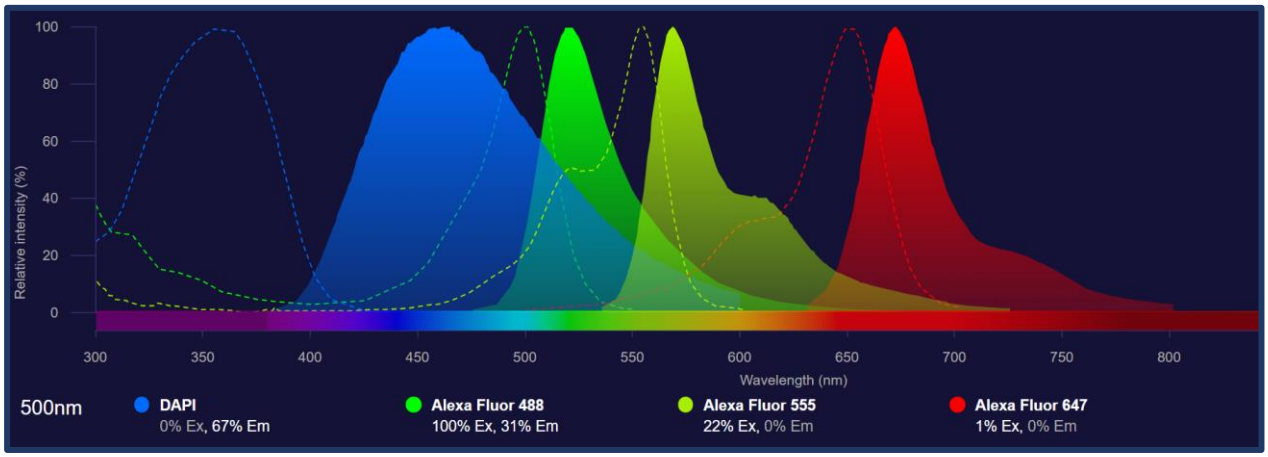

Figure 3. Overview of the excitation (stippled line) and emission (filled area) spectra of the nuclear stain DAPI and the three most used secondary antibodies in this project: Alexa Fluor 488, Alexa Fluor 555 and Alexa Fluor 647. Percentages below the fluorophores indicate the relative intensity of excitation (Ex) and emission (Em) for each fluorophore seen at 500 nm wavelength. Figure created with Thermo Fisher Fluorescence SpectraViewer.

Three primary antibodies specific for protein receptors in astrocytes, neurons and mitochondria were used for staining in this project. In addition, Alexa Fluor (AF) secondary antibodies were used to label cells and mitochondria with different fluorophores (emission wavelengths).

2.6 Immunostaining protocols

Two different protocols were used for immunostaining the tissue, one for the Tokuyasu sections and one for the cryostat sections. For the Tokuyasu sections, the reagents only needed to penetrate the very low section thickness, which meant that short incubation times were needed, and the staining procedure could be done within a few hours. For the cryostat sections, the protocol had to be adjusted to the larger section thickness. Therefore, longer incubation times and multiple steps to remove noise made this protocol into a two-day procedure.

For both protocols, the antibodies were incubated together when staining the tissue with multiple antibodies at the same time. The specific primary- and secondary antibody concentrations for mitochondria, astrocytes and neurons is described in the *2.7 Antibodies used for immunostaining* paragraph. For each staining experiment, negative controls were made by staining tissue sections with only secondary antibodies. This was important to make sure that the secondary antibodies did not specifically attach themselves to other structures other than the primary antibody and for measuring the background fluorescence intensities created by the secondary stains.

2.6.1 Staining of Tokuyasu sections

The initial immunostaining protocol was used for the staining of Tokuyasu sections and followed standardized staining procedures at the Core Facility of Advanced Microscopy (KAM) (Appendix I). Adjustments were made to the staining protocol to increase specific antibody binding. Incubation with primary antibody was changed from 20 min at room temperature to overnight at 4°C, and incubation with secondary antibody was changed from 15 min to 30 min at room temperature.

The tissue sections were attached on poly-L-lysine coated circular coverslips during the whole process of staining. To wash off any remaining sucrose or methylcellulose, the coverslips were placed into petri dishes with double-distilled water (ddH_2O) with the tissue facing down towards the water surface. They were washed 2x 10 min at room temperature ddH_2O and 1x 10 min at 37°C ddH_2O. The incubation and washes were done with drops on parafilm

(Parafilm ® “M”, Bemis Company, Inc). Parafilm was spread out over the lab bench and the desired amount of liquid of the reagents were placed as series of drops on the parafilm. The coverslips (with the tissue facing the drop) were moved with tweezers from drop to drop throughout the staining process.

To block any unspecific binding sites, the coverslips were placed on drops with blocking solution (0.8% cold water Fish Skin Serum (#G7765, Sigma-Aldrich) + 0.1% Bovine Serum Albumin (#A6588, ITW reagents) in PBS) for 15 min at room temperature. Further, the tissue was incubated on 40 µl drops with primary antibody diluted in blocking solution at 4°C overnight. The coverslips were placed in a chamber with moist tissue paper and covered with a lid to avoid evaporation. After staining, the tissue was washed 5x 2 min in PBS. Further, they were incubated with 40 µl drops with secondary antibody diluted in blocking solution for 30 min at room temperature. A lid was placed over the coverslips in this and all the next steps to avoid fluorescence bleaching by exposing the secondary antibodies to light. After staining, the tissue was washed 5x 2 min with PBS. They were then incubated with the nuclear stain DAPI in PBS at a 1 µl/ml concentration, 2 min at room temperature. After staining, the tissue was washed 3x 1 min with ddH_2O. The coverslips with tissue were mounted on microscope slides using 10 µl Mowiol. The slides were stored in the dark at 4°C until imaging.

2.6.2 Staining of cryostat sections

The standardized staining protocol had to be adjusted when staining the thicker brain sections (20-40 um) cut with a cryostat (Appendix II) Through several staining experiments the protocol was optimized, including: adjusting the section thickness, adjusting the antibody concentrations and increasing the incubation times and adding several steps of tissue processing. This was also the chosen staining protocol used to prepare sections for the final analysis of mitochondrial size and density.

To make sure that the tissue attached itself to the microscope slides, they were dried at 50°C for 30 min. Right after drying, a circle was drawn around the sections with a Super PAP hydrophobic pen (Daido Sangyo, Japan) to allow any reagents added through the staining process to stay on the slide. The sections where further post-fixed with 4% PFA in PBS for 20 min. The post-fixation was done to prepare the tissue for the though antigen-retrieval steps in this protocol. After fixation, the sections were washed with PBS 3x 5 min. Further, the slides were placed in boxes with slide holders containing citrate buffer (0.1 M $Na_3C_6H_5O_7$ *$2H_2O$ in PBS, pH = 6) and incubated 80°C for 30 min. This was done as an antigen retrieval step, to

improve the binding of antibodies to receptors (Shi et al., 2001). After antigen retrieval, the sections were let cool down to room temperature before moving them out of the citrate buffer. They were then washed with PBS 2x 5 min. To reduce autofluorescence in the section, they were incubated with 3% H_2O_2 + 10% MeOH in PBS for 10 min. They were then washed with PBS 3x 5 min. To block unspecific binding sites, the sections were incubated with BS-T: blocking solution with 0.2% Trion-X (#T8787, Sigma) for 30 min at room temperature. The addition of Triton-X serves to permeabilize the tissue, making it more accessible to the binding of antibodies to intracellular proteins. The tissue was then incubated with primary antibody diluted in BS-T at 4°C overnight. After incubation, the tissue was washed with PBS 3x 10 min. The tissue was then incubated with secondary antibody diluted in BS-T for 90 min at room temperature. The slides were put in a chamber with moist tissue paper to avoid evaporation. They were also covered with a lid in this and all following steps, to minimize fluorescence bleaching of the secondary antibody. After incubation, the tissue was washed with PBS 3x 10 min. It was then incubated with DAPI in PBS at a 1 µl/ml concentration. Further, the tissue was washed with PBS 2x 5 min. To quench autofluorescence, the sections were incubated in with TrueBlack® Lipofuscin Autofluorescence Quencher (#23007, Biotium) that had been diluted 1:20 in 70% ethanol. The slides were dipped in the quencher for 30 seconds and then put directly in a container with PBS for washing. The tissue was washed with PBS 3x 10 min after quenching. The tissue was additionally washed with distilled water 1x 2 min, before coverslips were mounted on top of the tissue sections using DABCO 2.5% anti-fade solution (#290734, Sigma-Aldrich) and nail polish.

2.6.3 Staining protocol adjustments

2.6.3.1 Noise from erythrocytes in blood vessels

When working with thicker sections, there is more of what one wants to detect, for instance more cells of astrocytes and neurons, but one also runs into the problem that there is more structure that creates noise in the image. The structures that mainly created noise in the cryostat sections were erythrocytes inside blood vessels.

Since the brain of the sampled animals was utilized in other research experiments (e.g., the harvesting of live neurons and astrocytes), the tissue could not be fixed through perfusion fixation. Perfusion fixation is the preferred method of tissue fixation for immunostaining as it firstly, can fix larger sizes of tissue in one piece and secondly, washes out any remaining

blood cells from the blood vessels. The brain tissue was instead cut into smaller sections and fixed by immersion fixation as described above. This created the problem of erythrocytes still being stuck inside the vessels and thereby creating noisy fluorescent images.

The hooded seal brain has been seen to be densely vascularized (Ludvigsen, 2010), which also was evident when studying the 20-40 µm sections in the microscope. Blood vessels can be identified based on their thickness, shape, and the presence of oval nucleuses in the epithelial cells along the capillary walls (Figure 4) (Yeon et al., 2012). However, to test if the structures creating noise were really capillaries, some sections were stained with a primary antibody binding to a receptor in Collagen IV, which is part of the basal lamina in capillaries. The staining followed the protocol for cryostat sections and rabbit anti-collagen IV (#ab6586, Abcam) was diluted 1:200 in BS-T and used as a primary antibody, while Goat Anti-Rabbit Alexa Fluor 488 (#A32731, Invitrogen Thermo Fisher) diluted 1:500 in BS-T was used as a secondary antibody. Fluorescence imaging showed that the same structures being stained with Coll IV where the one present in other stains (Figure 4).

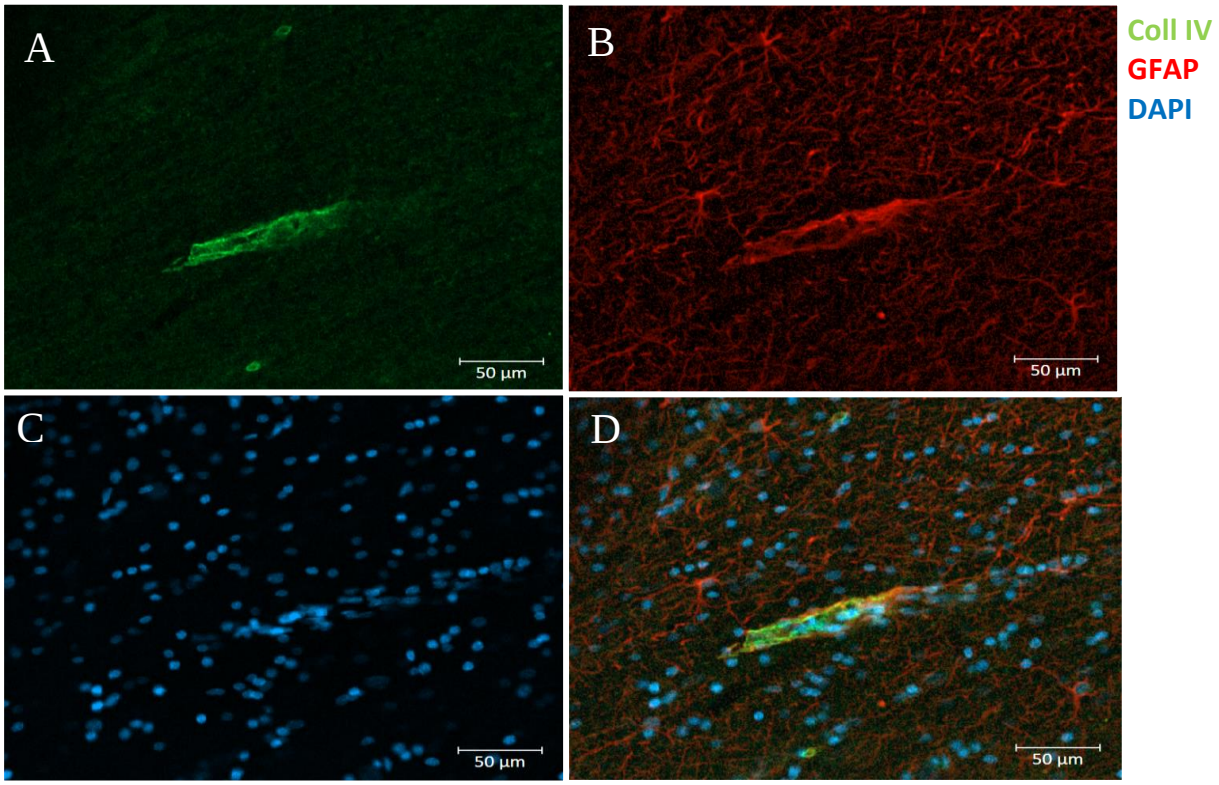

Figure 4. Hooded seal visual cortex imaged with confocal microscope LSM800. Stained for A) Collagen IV (green) with Coll IV 1:200 + AF488 1:500, B) Astrocytes (red) with GFAP 1:300 + AF568 1:200, C) Cell nucleuses (blue) with DAPI [1µl/ml], D) merge all channels.

In addition to seeing the capillary walls, the erythrocytes in the capillaries had a strong autofluorescence property (Whittington & Wray, 2017). In some cases, the signal from the erythrocytes was so bright that it "overtuned" other stained features in the image (Figure 5). The erythrocytes could easily be distinguished from other cells because of their lack of a nucleus.

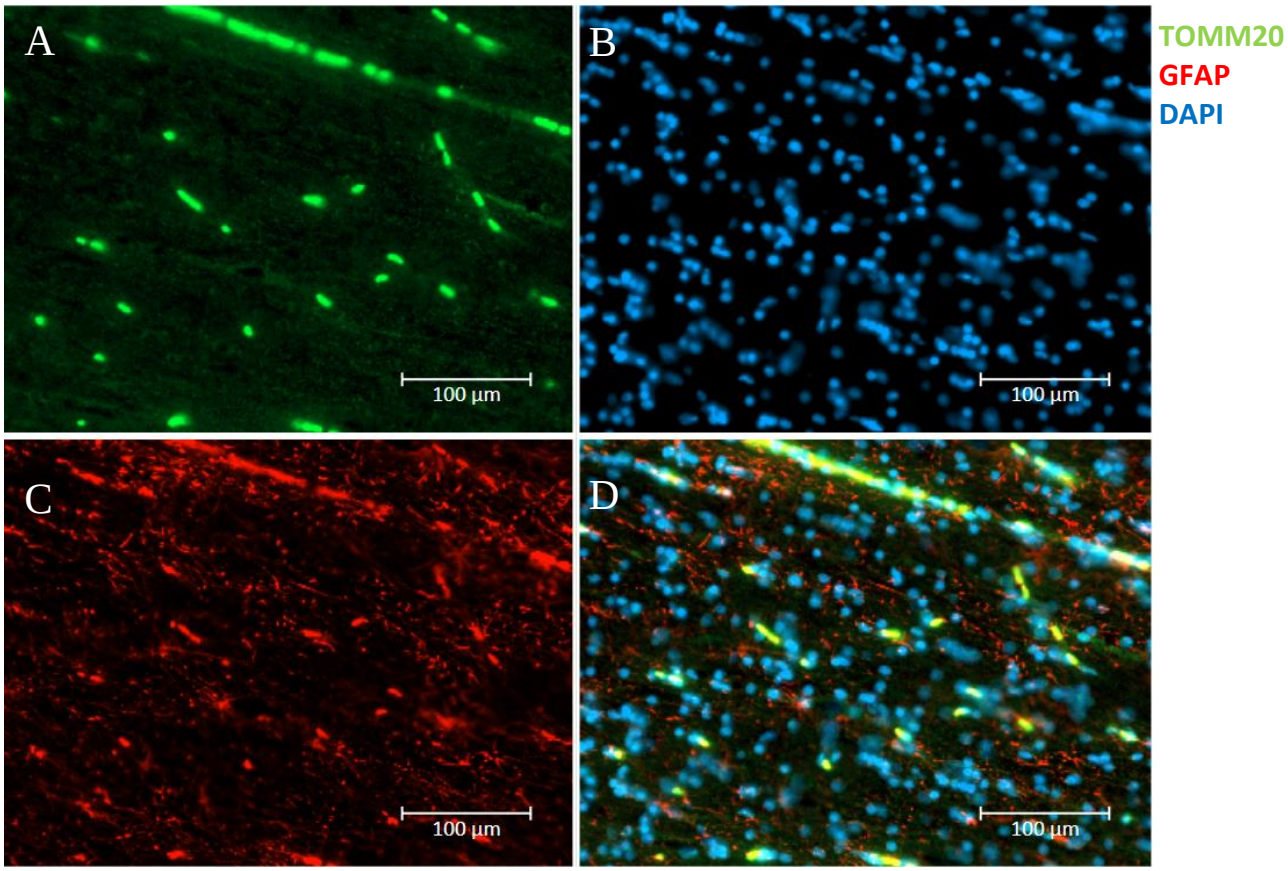

Figure 5. Juvenile hooded seal white matter from visual cortex, showing bright autofluorescence from erythrocytes. Imaged with widefield microscope Axio Zoom v.16. Stained for A) Mitochondria with TOMM20 1:500 + AF488 1:500, B) Cell nucleuses with DAPI [1µl/ml]., C) Astrocytes with GFAP 1:300 + AF568 1:200, D) All stains merged.

Several quenching steps were applied to minimize the noise from the erythrocytes as described in the cryostat section staining protocol (paragraph 2.6.2). The tissue was treated with a mix of hydrogen peroxide and methanol which is commonly used in blocking the endogenous peroxidase activity found in erythrocytes (Bussolati & Radulescu, 2011). The tissue was additionally treated with True Black ® Lipofuscin Autofluorescence Quencher (#23007, Biotium) as a step which reduces autofluorescence from erythrocytes. These techniques reduced the noise from erythrocytes, although not removing the signal from them altogether. The quenching steps were however also shown to be useful in reducing regular background noise.

2.6.3.2 From triple to double staining

The initial approach was to use "triple-staining", to stain for astrocytes, neurons and mitochondria on the same tissue sections, meaning that the two cell types could be imaged together. To achieve this, three secondary antibodies with non-overlapping wavelengths had to be used. However, the erythrocytes had the strongest fluorescent intensities when exited at lower wavelengths (450-500 nm), similar to the excitation wavelengths of AF 488 (Figure 3). This was evident when looking at the images with mitochondrial stain, which used AF488 as a secondary antibody (Figure 5). In addition, the negative control sections (only stained with secondary antibody) showed a higher presence of noise from capillaries when stained with AF 488 (Figure 6). The noise from the erythrocytes created difficulties in the detection of mitochondria and the quenching steps were not able to sufficiently reduce the erythrocyte fluorescent signal. It was therefore decided to not use any AF 488 secondary antibody, which meant that it was not possible to find three secondary antibodies with non-overlapping emission and excitation spectra. The attempt on triple-staining was therefore abandoned and astrocytes and neurons were stained on separate tissue sections. Astrocytes and neurons were stained with AF 647 secondary antibodies and mitochondria with an AF 555 secondary antibody (see Table 3, 4 and 5 with overview of the antibodies used).

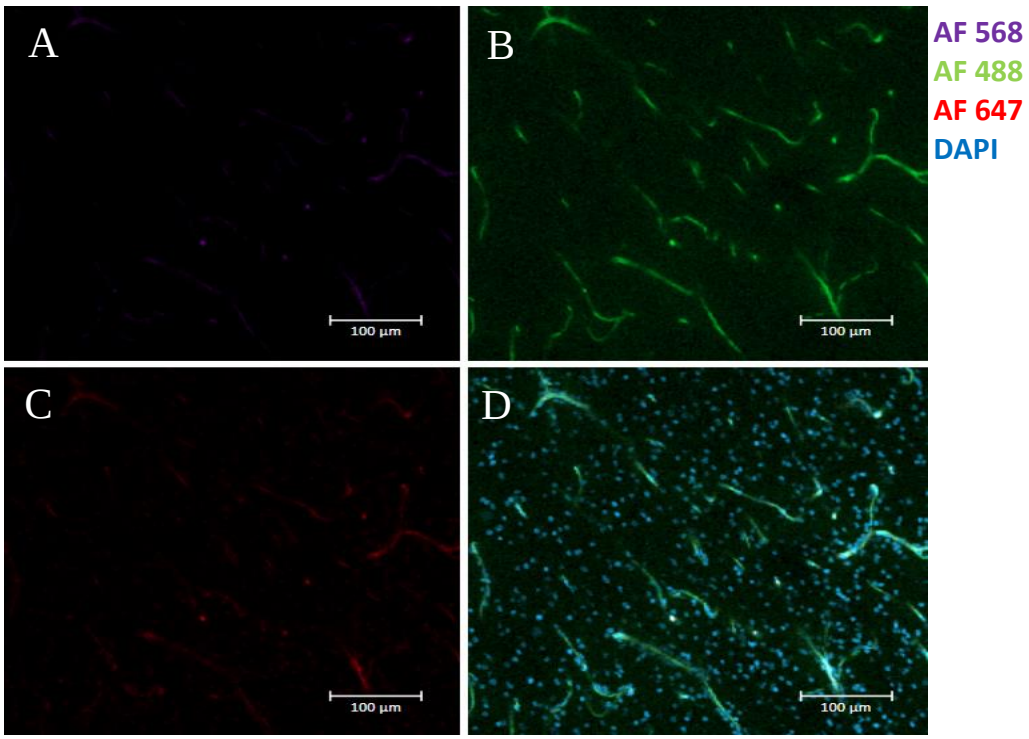

Figure 6. Negative control of hooded seal visual cortex. Imaged with LSM 800. Stained with only secondary antibodies A) AF568 1:200, B) AF488 1:500, C) AF647 1:500, D) All channels merged + DAPI [1µl/ml].

2.7 Antibodies used in Immunostaining

Three primary antibodies specific for protein receptors in astrocytes, neurons and mitochondria were used for staining. In addition, Alexa Fluor (AF) secondary antibodies were used to label cells and mitochondria with different fluorophores (emission wavelengths).

2.7.1 Staining of Hooded Seal mitochondria

Although Mitz et al (2009) stained for cytochrome c in hooded seal tissue, there are to my knowledge no previous studies using antibodies targeting the outer mitochondrial membrane in hooded seals. Therefore, different antibodies and concentrations had to be investigated. Two different versions of the TOMM20 primary antibody were tested. TOMM20 is a gene coding for one of the receptor systems in the translocase of the outer mitochondrial membrane (TOM complex) (Yano et al., 1998). The TOMM 20 Rabbit Monoclonal (#ab186734, ABCAM) did not give any specific staining, while the TOMM20 Rabbit Monoclonal (#MA5-32148, Invitrogen) gave promising results at a 1:100 concentration. The final concentration was decreased to 1:500 when staining cryostat sections for mitochondria (Table 3).

Table 3. Mitochondrial staining experiments on hooded seal visual cortex. Staining quality is marked with "x" when the stain was weak or noisy, and with "-" when no specific staining was found. The process that was used in the final staining experiment is highlighted in green.

Target	Sectioning method	Section thickness	Microscope	Primary antibody	Secondary antibody	Primary conc.	Secondary conc.	Staining quality
Mitochondria	Ultramicrotome	700 nm	LSM 800	TOMM 20 Rabbit monoclonal ABCAM #ab186734	Alexa Fluor 488 Goat Anti-Rabbit #A32731	1:50	1:500	-
						1:100	1:500	-
						1:200	1:500	-
				TOMM20 Rabbit monoclonal Invitrogen #MA5-32148	Alexa Fluor 488 Goat Anti-Rabbit #A32731	1:100	1:500	Good, but noisy
						1:200	1:500	x
		70 nm	TEM	TOMM 20 Rabbit monoclonal ABCAM #ab186734	PAG -10 Gold particles	1:12.5	1:50	Unspecific
						1:25	1:50	Specific
	Cryostat	40-20 um	LSM 800 Axio Zoom V.16 Slide scanner VS 120	TOMM 20 Rabbit monoclonal ABCAM #ab186734	Alexa Fluor 488 Goat Anti-Rabbit #A32731 Alexa Fluor 555 Goat Anti-Rabbit #A-21428	1:100	1:500	x
							1:1000	x
						1:200	1:500	x
							1:1000	x
						1:500	1:500	Best
							1:1000	x

2.7.1.1 Immunogold labelling to determine specificity

Mitochondria are small (0.75 – 3 μm^2), have a range of different shapes and are numerous in brain tissue (Bereiter-Hahn, 1990; Wiemerslage & Lee, 2016). This makes it challenging to determine if the fluorescent signal is only originating from the mitochondria or if there is unspecific staining of other cell organelles, in particular when working with tissue from hooded seal in which the antibody specificity is unknown. To test the specificity of the TOMM20 antibody (#MA5-32148, Invitrogen), 70 nm Tokuyasu sections of 4% PFA fixed hooded seal visual cortex were prepared for transmission electron microscopy (TEM) following the Tokuyasu staining protocol (2.6.1). TOMM 20 was used as the primary antibody and a secondary antibody bound to gold particles (PAG10) was used. With a HT7800 transmission electron microscope (Hitachi, Japan), the mitochondria could be identified based on their inner membrane morphology (Figure 7). The immunogold labelling

technique uses gold bound to antibodies which will appear as dark particles in the imaged tissue (Birrell et al., 1987). It could thereby be determined that at the right concentrations of TOMM20, the gold particles primarily attached themselves to the mitochondria (figure 7B). The TOMM20 (#MA5-32148, Invitrogen) primary antibody was therefore accepted as a specific antibody for mitochondria in hooded seal brain tissue.

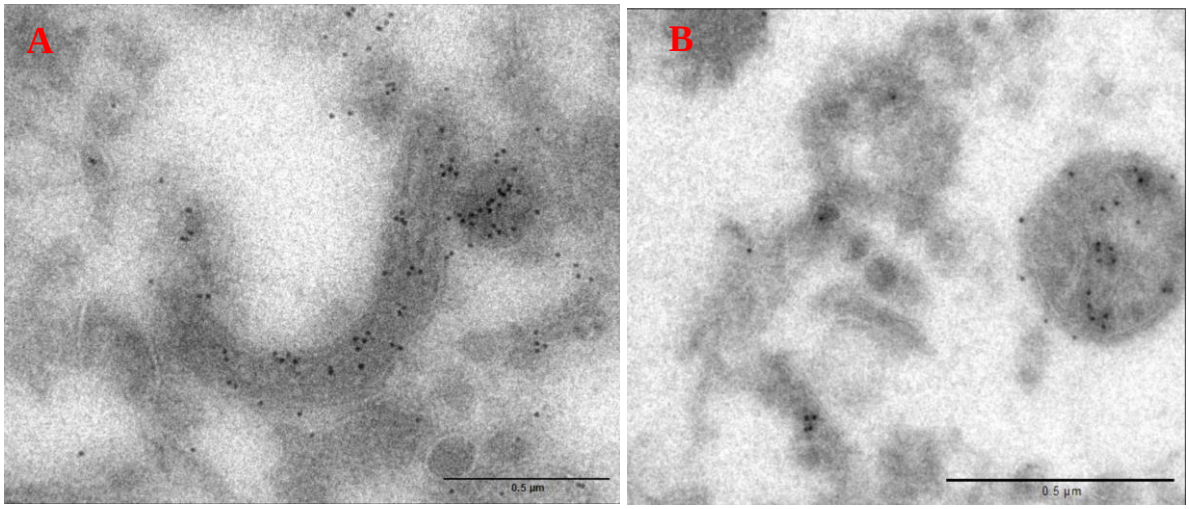

Figure 7. Adult female hooded seal (animal ID: K7-22) visual cortex imaged with HT7800 transmission electron microscope. Black spots are gold particles (PAG10) used as a secondary at 1:50 concentration. Mitochondrial primary antibody concentration was A) TOMM20 1:12.5, 12 000x magnification. B) TOMM20 1:25, 10 000x magnification. The gold particles adhere to organelles that are mitochondria, thus confirming the mitochondrial specificity of TOMM20.

2.7.2 Staining of Hooded Seal Astrocytes

The astrocytes were stained with GFAP Mouse monoclonal (#G6171, Sigma-Aldrich) primary antibody. This antibody binds to glia fibrillary acidic protein (GFAP) receptors which is an intermediate filament-III protein only found in astrocytes in the brain (Eng et al., 2000). GFAP has been used in previous immunostaining studies of astrocytes in the hooded seal brain (Mitz et al., 2009) and therefore the reported working concentrations could be used for testing.

There was however, not found any astrocyte staining signal in the Tokuyasu sections (Table 4). This was probably due to these sections being from regions in the visual cortex without astrocytes. Tokuyasu sections have a surface area of about 1 mm^2, which means that they cover only a small area of the visual cortex in hooded seals. When switching to staining cryostat sections, with a surface are of about 1 cm^2, it was evident that most astrocytes in the hooded seal visual cortex are present in the white matter (Figure 8). This shows the

importance of working with larger tissue area especially in the beginning of staining trials to have a better overview of the cell layers in the tissue and increase the chances of specific cell detection. The astrocytes were detected in the cryostat sections using the same initial antibody concentrations that had been tested on Tokuyasu sections (Table 4).

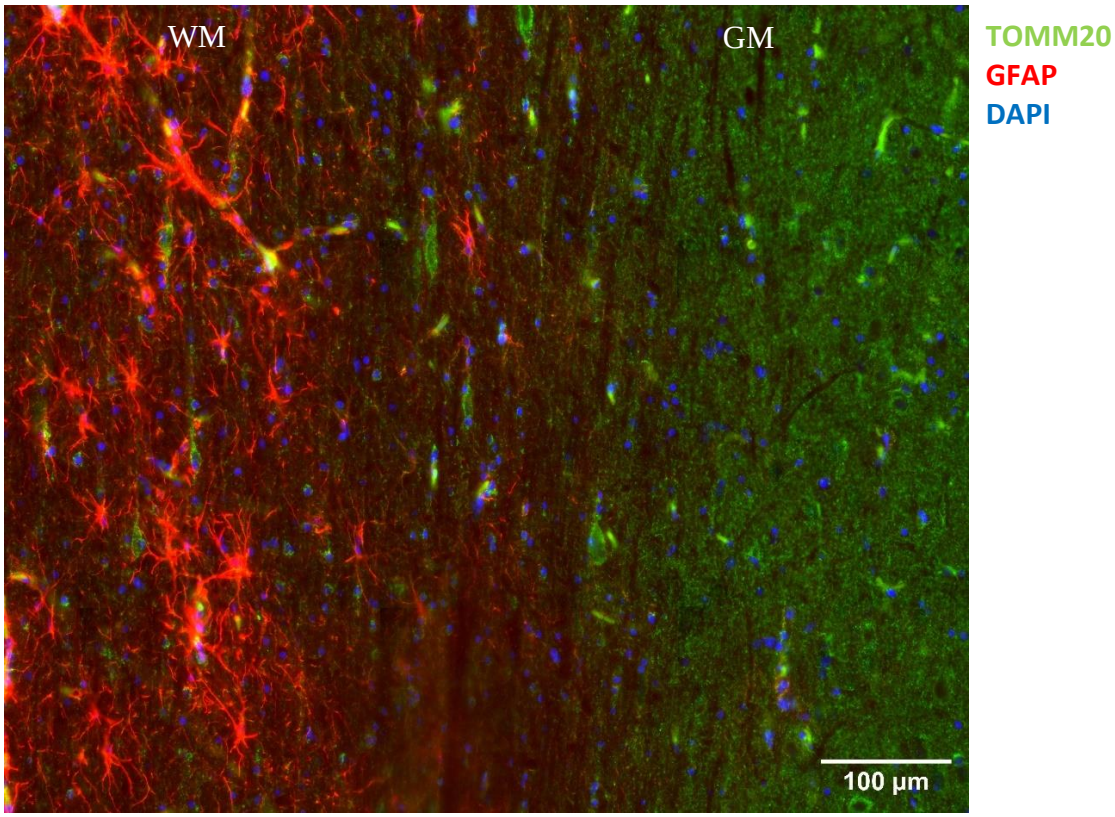

Figure 8. Juvenile hooded seal visual cortex (animal ID: K2A-22) imaged with VS120 Slide Scanner, showing the transition between the grey matter (GM) and white matter (WM) region. Astrocytes (red) stained with GFAP 1:300 + AF 647 1:200 are mainly located in WM. Mitochondria (green) stained with TOMM20 1:500 + AF 555 1:500 are more prominent in GM. Cell nucleuses (blue) are stained with DAPI [1µl/ml].

Table 4. Astrocyte staining experiments on hooded seal visual cortex. Staining quality is marked with "x" when the stain was weak or noisy, and with "-" when no specific staining was found. The process that was used in the final staining experiment is highlighted in green.

Target	Sectioning method	Section thickness	Microscope	Primary antibody	Secondary antibody	Primary conc.	Secondary conc.	Staining quality
ASTROCYTES	Ultramicrotome	1000 nm	LSM 800	GFAP Mouse monoclonal #G6171	Alexa Fluor 568 Donkey Anti-mouse #ab175700	1:50	1:200	-
							1:500	-
							1:1000	-
						1:100	1:200	-
							1:500	-
							1:1000	-
						1:200	1:200	-
							1:500	-
							1:1000	-
						1:300	1:200	-
							1:500	-
							1:1000	-
	Cryostat	40-20 um	LSM 800 Axio Zoom V.16 Slide scanner VS 120	GFAP Mouse monoclonal #G6171	Alexa Fluor 568 Donkey Anti-mouse #ab175700 Alexa Fluor 647 Goat anti-mouse #A-21235	1:100	1:200	x
							1:500	x
						1:300	1:200	Best
							1:500	x
						1:500	1:500	x
							1:200	x

2.7.3 Staining of Hooded Seal Neurons

There are to my knowledge no previous studies using neuronal antibodies in hooded seals. Neuronal staining was achieved by using the MAP2 Chicken polyclonal (#ab92434, Abcam) primary antibody (Figure 9). Microtubule-associated protein 2 (MAP2) is a protein found in the cytoskeleton of neurons and is primarily distributed in the cell body and dendrites (Dehmelt & Halpain, 2005). The neurons were visible in the staining of both Tokuyasu and cryostat sections (Table 5).

Table 5. Neuron staining experiments on hooded seal visual cortex. Staining quality is marked with "x" when the stain was weak or noisy, and with "-" when no specific staining was found. The process that was used in the final staining experiment is highlighted in green.

Target	Sectioning method	Section thickness	Microscope	Primary antibody	Secondary antibody	Primary conc.	Secondary conc.	Staining quality
NEURONS	Ultramicrotome	1000 nm	LSM 800	MAP2 Chicken polyclonal #ab92434	Alexa Fluor 647 Goat Anti-Chicken #ab4600179	1:500	1:500	x
							1:1000	x
						1:1000	1:500	x
							1:1000	x
						1:2500	1:500	Best
							1:1000	x
	Cryostat	40-20 um	LSM 800 Axio Zoom V.16 Slide scanner VS 120	MAP2 Chicken polyclonal #ab92434	Alexa Fluor 647 Goat Anti-Chicken #ab4600179	1:2500	1:500	Best
							1:1000	x

The neurons in the visual cortex were not as clearly separated from each other as the astrocytes. The images showed neuronal cell bodies surrounded by numerous dendrites and axons (Figure 9), making it difficult to determine where one cell starts and another one ends.

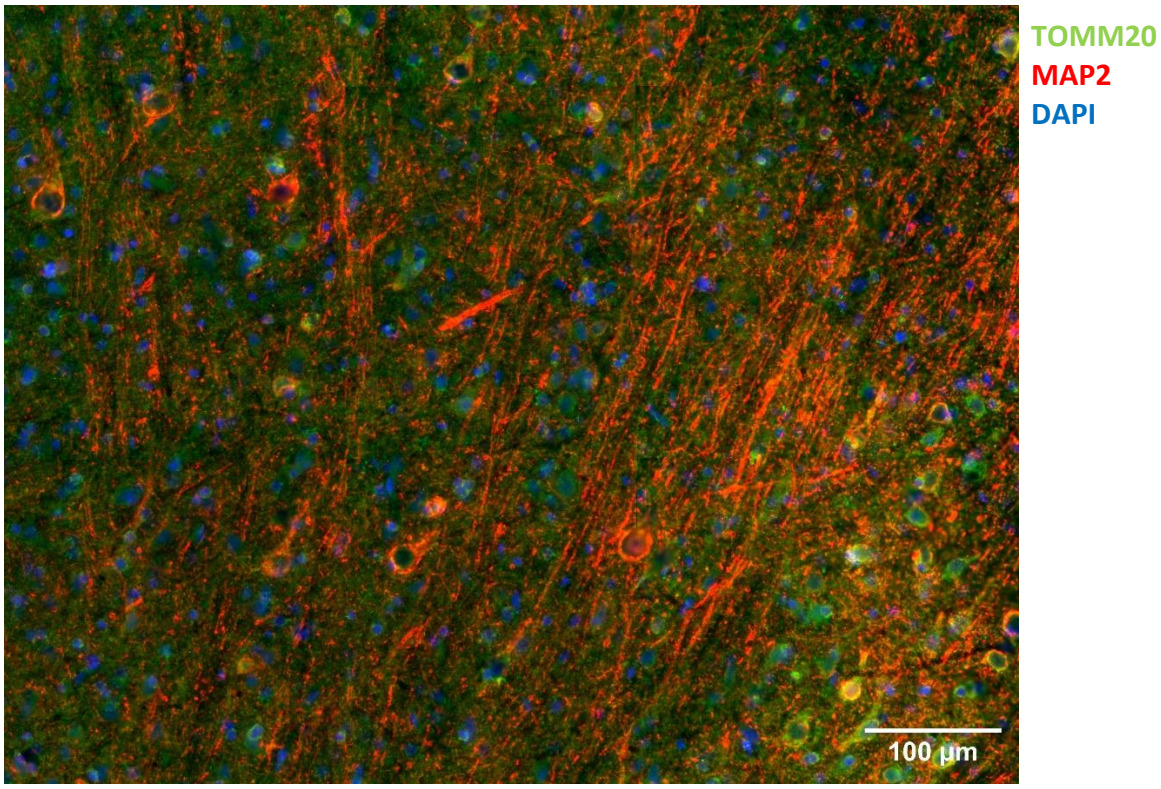

Figure 9. Adult hooded seal visual cortex (Animal ID: K1-22), imaged with VS120 Slide Scanner. Neurons (red) stained with MAP2 1:2500 + AF 647 1:500. Mitochondria (green) stained with TOMM20 1:500 + AF 555 1:500. Cell nucleuses (blue) are stained with DAPI [1µl/ml].

2.7.4 Staining of mouse visual cortex

Adjusting the antibody concentrations for immunostaining in mouse brain tissue was less time consuming, since most of the concentrations that were tested gave adequate staining. The final concentrations were therefore mostly based on the lowest concentrations that were tested to minimize antibody waste (Table 6).

Section thickness had a significant effect on the presence of noise when imaging the mouse brain tissue. The 40 µm thick sections included much out-of-focus light, making the detection of mitochondria difficult. This effect was however not found when imaging hooded seal brain. Based on this observation, the final section thickness was adjusted to 20 µm for all animals.

Table 6. Immunostaining experiments on mouse visual cortex. Staining quality is marked with "x" when the stain was weak or noisy, and with "-" when no specific staining was found. The process that was used in the final staining experiment is highlighted in green.

Target	Sectioning method	Section thickness	Microscope	Primary antibody	Secondary antibody	Primary conc.	Secondary conc.	Staining quality
MITOCHODNRIA	Cryostat	40-20 um	LSM 800 Axio Zoom V.16 Slide scanner VS 120	TOMM20 Rabbit monoclonal Invitrogen #MA5-32148	Alexa Fluor 555 Goat Anti-Rabbit #A-21428	1:100	1:500	x
							1:1000	x
						1:250	1:500	x
							1:1000	x
						1:500	1:500	x
							1:1000	Best
ASTROCYTES	Cryostat	40-20 um	LSM 800 Axio Zoom V.16 Slide scanner VS 120	GFAP Mouse monoclonal #G6171	Alexa Fluor 568 Donkey Anti-mouse #ab175700 Alexa Fluor 647 Goat anti-mouse #A-21235	1:150	1:200	x
							1:500	x
						1:300	1:200	x
							1:500	x
						1:600	1:200	x
							1:500	Best
NEURONS	Cryostat	40-20 um	LSM 800 Axio Zoom V.16 Slide scanner VS 120	MAP2 Chicken polyclonal #ab92434	Alexa Fluor 647 Goat Anti-Chicken #ab4600179	1:1250	1:500	x
							1:1000	x
						1:2500	1:500	x
							1:1000	Best
						1:5000	1:500	x
							1:1000	x

2.8 Final staining procedure

The 20 µm cryostat sections used for the final analysis were all stained simultaneously (with the same incubation times, ambient temperature, antibody concentrations and light exposure) to exclude differences in the staining process. For each animal, five sections were stained for astrocytes and mitochondria, and five sections for neurons and mitochondria. All five sections were placed on the same microscope slide and labelled from A-E (Figure 10). There was also made four negative control sections, one fore astrocytes and mitochondria and one for

neurons and mitochondria for both hooded seal and mouse tissue, using only the secondary antibodies.

2.9 Microscopy

Three microscopes in the Advanced Microscopy Core Facility (AMCF) at UiT were used for fluorescence imaging in this study. The LSM 800 Confocal Microscope (Zeiss, Germany) was used to determine the best working antibody concentrations. This microscope could capture sharp images at high magnifications by the mechanism that the light gets detected through a pinhole that blocks most of the out-of-focus light in the sample.

The widefield microscopes Axio Zoom v. 16 (Zeiss, Germany) and Slide Scanner VS 120 (Olympus, Japan) were used in creating z-stacks of larger areas of the sections. Z-stacks are created when multiple images are taken through the depth of the tissue, each image being a z-slice. The widefield microscopes reduced the sharpness of the images as they detected more of the out-of-focus light in the tissue. They were however significantly faster at image acquisition and therefore more relevant considering the amount of tissue needed to be imaged for this project. Due to a technical problem with the Axio Zoom v.16 connected computer, this microscope was no longer available for image acquisition during parts of the project. Therefore, all the imaged used for the final analyses were acquired using the VS120 slide scanner.

2.9.1 Slide scanner settings

To ensure that the images could be used for quantificational studies, the image acquiring settings had to be uniform across all samples. First, a brightfield overview image was made of each microscopy slide at 2x magnification. This was done to make it possible to choose which area that should be imaged for each of the five tissue sections on the microscope slide. An area of 2 mm^2 was selected for fluorescence imaging for each of the sections. The selected region was based on the presence of the desired cell type. For detection of astrocytes, the region was placed in the white matter areas of the tissue section. For the detection of neurons, the region was placed in both white and grey matter areas. A high focus point density was chosen, and each focus point was adjusted manually to exclude any pollution (e.g bubbles, dust) or wrinkles on the sections. A z-stack was acquired of each selected area, using 40 x magnification. The z-stacks consisted of 13 z-slices with 1 µm distance between each slice. The exposure settings were carefully adjusted to fit each stain and then kept uniformly across all samples (Table 7).

Table 7. Exposure settings for image acquisition with Olympus Slide Scanner VS 120.

Stain	Exposure channel - fluorophore	Exposure time (ms)
Mitochondria/TOMM20	Cy 3 - AF 555	600
Astrocytes/GFAP	Cy 5 - AF 647	1000
Neurons /MAP2	Cy 5 - AF 647	900
Cell nucleus/DAPI	DAPI - 355	40

2.10 Image analysis

2.10.1 ROI selection and image formatting

The images taken with the VS 120 slide scanner microscope were saved as .vsi and .ets files and had to be formatted into smaller sized images in order to be opened by the image analysis software FIJI (version 1.54f, 2023). Therefore, QuPath (v.0.4.3, 2023) was used to both select the region of interest (ROI) and transform the images into .tif files. Three ROIs with the size of 500x500 µm were selected per image based on the presence of cells in the astrocyte or neuronal channel (see Table 7, above). The mitochondrial channel was turned off during the ROI selection process to prevent me from subconsciously selecting cells/regions with high/low mitochondrial density. Each ROI was then saved as a 16-bit image and transformed into a .tif file with a size of approx. 700 MB. The images were size calibrated to ensure accurate distance and area measurements. For more detailed image formatting protocol, see Appendix III.

In total, 270 images with the dimension of 500 x 500 µm were made from the scanned sections. 11 of the mouse tissue images were removed after inspection due to the images being out of focus, presence of folds and cuts in the tissue sections or missing staining of cells. See appendix IV for exclusion reasons of the specific images. In the end, 259 images were used in the final analysis giving a total analysed tissue area of 64 750 000 μm^2. The images were created from 5 z-slices, as described below (paragraph 2.10.2 creating z-stacks), meaning that the same area was imaged at 5 different depths and added together in the final two-dimensional image (Figure 10).

2.10.2 Creating z-stacks

The first step of the image analysis in ImageJ/FIJI included making z-projections of the images. Z-projections are used to collapse all the information in different z-slices into a single 2D image. This is done by applying the same operation on all the x- and y-values along the z-axis (depth) of the images. The operations applied depend on which type of z-projection is selected.

Two different z-projections were made, one using only the neuron/astrocyte channel and one using the mitochondrial channel. For the astrocyte and neuronal channels, a maximum z-projection was used. This only included the maximum x- and y-value along each z-axis and it was selected based upon that it showed the clearest difference between cell staining and background noise. A maximum projection returns a 2D image projection based on only one intensity value and therefore doesn't give a clear measure of the intensity of the stain through the section. However, for the cell channels it was more important to find the outlines of the cell areas then to record the actual pixel intensities and therefore the maximum intensity projection was evaluated as the best option. For the mitochondrial channel, an average projection was applied. This takes all the x- and y-values along the z-axis into account and calculates the mean of these values. This projection is a more accurate reflection of the pixel intensities found along the z-axis of the image and can be used for further fluorescence intensity quantification.

Although each image contained 13 z-slices, not all of the slices portrayed cells that were in focus. Therefore, a series of 5 slices were selected per image to make the z-stacks. This was done by scrolling through the z-slices of the neuron or astrocyte channel and selecting the range of z-slices where the cells were the most in focus. The z-projection of the mitochondrial channel was made using the exact same 5 z-slices.

2.10.3 Thresholding for cell detection

After making a z-projection of the cell channels, image thresholding was performed to get rid of any background noise. Thresholding creates a binary image from a chosen pixel intensity value as a threshold. Everything below that value will get assigned the pixel intensity = 0 and everything above will get a pixel intensity = 1. The threshold of each image was set manually by evaluating which threshold excluded the most background noise while also including the most cell staining.

Before thresholding the astrocyte channel, the “find edges” command was applied. This creates lines in the image where there is a steep increase or decrease in pixel intensity, like at the edges of stained cells. This was applied to outline the astrocytes and separate the cells from each other. The “find edges” command was however not used for the neuron channel, this was due to the neurons mainly not appearing as whole cells, but as fragmented fractions of cell body, dendrites and axons (Figure 9). The find edges command would only increase the fragmentation of the cells and was therefore not included.

2.10.4 Creating cell ROIs

The thresholded cells created the basis for the area where the mitochondrial density would be measured. Therefore, each cell was turned into a region of interest (ROI) which was applied to the mitochondria channel for specifying the area of measurement. The ROIs were created by using the “Analyze particles” command. When the command is applied to a binary image, it considers all the connected pixels with intensity = 1 as one particle and saves this particle as a ROI. For the cell channels, the command was set to only include particles over 5 μm^2 to exclude small cell fractions and noise. ROIs that clearly were not cells were manually removed from the images.

2.10.5 Auto and manual cell selection

Two different cell selection methods were used: The auto selection of cells and the manual selection of cells.

The automated cell selection made one combined ROI from all the particles that had been saved through the “Analyse particles” command. This means that it created a ROI of all the cells in an image. However, not all the saved particles might be cells, but could be structures like erythrocytes or capillaries that had strong fluorescent intensities. The risk of including too much noise in the automated cell selection process, created the base for using a manual cell selection method. In the manual method, 3 cells were manually selected from each image by identifying cells by eye. These cells were saved as separate ROIs. It was not always possible to identify three cells in an image and therefore some images only have 1 or 2 manually selected cells. In total, 757 cells were manually selected from all images.

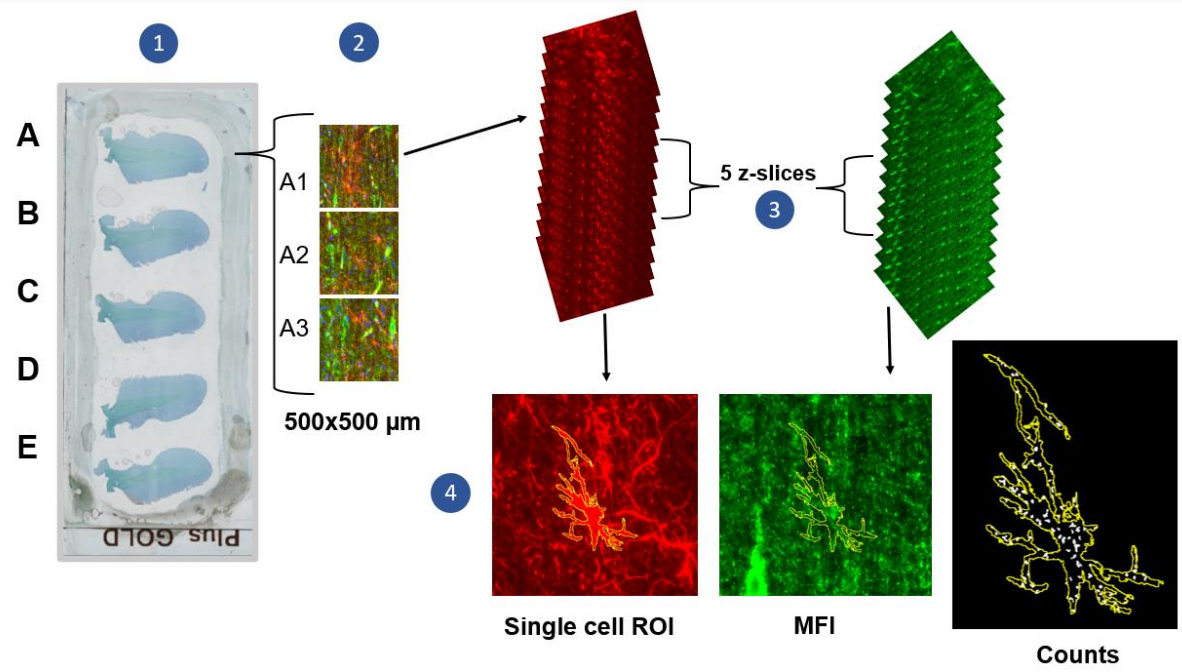

Figure 10. Schematic representation of the steps in image analysis. 1) Sections of hooded seal visual cortex on a microscope slide were labelled A-E. 2) Three images of 500x500 µm were analysed per section. 3) Z-projections were created from the neuron/astrocyte channel (red) and the mitochondrial channel (green) using 5 of the z-slices. 4) Cell regions of interest (ROIs) were created and applied to the mitochondrial channel to measure mean fluorescence intensities (MFI) and to the thresholded/filtered mitochondrial channel to obtain mitochondrial counts.

2.10.6 Measuring mean fluorescence intensities (MFI)

To measure the mean fluorescence intensity (MFI) of mitochondria in astrocytes and neurons, the ROIs created from the cell channels by the auto and manual cell selection method, were laid over the mitochondrial z-projection. Thereby only the intensities inside the detected cells were recorded. The mean fluorescence intensities were adjusted by removing the background mean fluorescence intensities:

$$adjusted\ MFI = measured\ MFI - background\ MFI$$

The background MFI (bMFI) values were obtained from the negative control sections that were incubated only with secondary antibody.

2.10.7 Measuring mitochondrial counts

The method to count the mitochondria in astrocytes and neurons was developed based on descriptions by Song et al. (2008) and Shihan et al. (2021). The whole process was automated

by creating macros (Appendix VI) which significantly reduced the time of image analysis and made sure that all of the images were analysed using the same settings.

First, a median filter subtraction was applied to the z-projection of the mitochondrial channel based on the method by Song et al. (2008). This imaging processing step applies a median filter to the z-projection created from the mitochondrial channel. The filter takes the median of the pixel values inside a chosen pixel radius and applies this value to all the pixels inside the radius. The result is a picture consisting of median values and therefore a more blurred version of the original. The filtered image is then subtracted from the original unfiltered image, which will result in an image containing only the lowest and highest pixel intensity values of the original. This is a method of separating the mitochondria from each other and from the background noise so that they can be recognized by further applying a thresholding application.

A radius of 4 pixels was used as pixel radius for median filtering. This was selected by comparing different pixels radius sizes and their effect on the final thresholded image. A lower pixel radius would result in smaller particles and a lower detection of mitochondria. A larger pixel radius would result in larger particles that could float together, thus reducing resolution. The pixel radius = 4 gave the most promising detection of mitochondria (Figure 11).

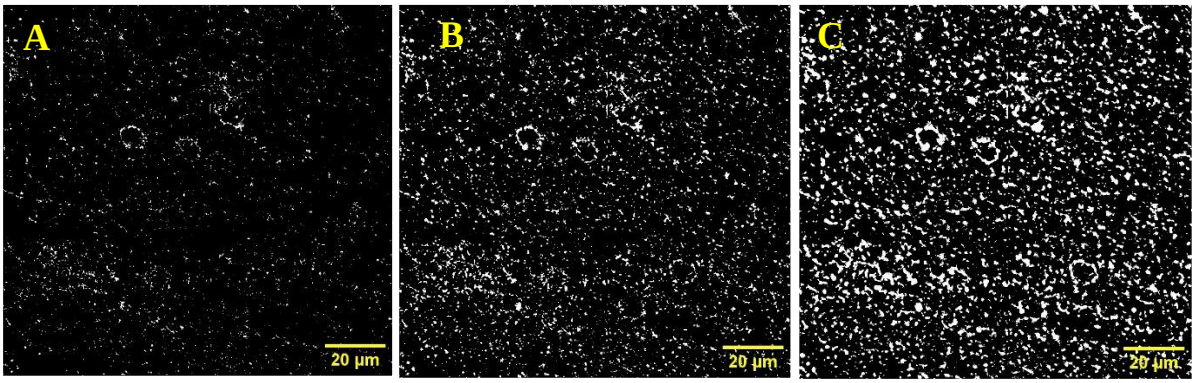

Figure 11. Otsu thresholded image (50,65535) of mitochondrial stain average z-projection, illustrating that a median filter radius of 4 pixels gave the most optimal detection of mitochondria. Median filter settings A) Radius = 2 pixels, B) radius = 4 pixels, C) radius = 8 pixels.

Further, the image was thresholded using *Otsu* based on the method by Shihan et al. (2021). Otsu thresholding divides the pixels into two separate groups based on the threshold that gives the lowest variance within each of the pixel groups (Otsu, 1979). After thresholding, the "watershed" command was applied to the image. This separates particles that are aggregated

together (like adjacent mitochondria) by using the local lowest pixel intensity values (Schindelin et al., 2012).

The mitochondria where then counted by overlaying the cell ROIs (to make sure to only count mitochondria within the detected cells) and applying the "Analyze particles" command. This would count and record the sizes of all the detected within each cell ROI. All particles with an area below 0.4 μm^2 were excluded as these were regarded as pixel noise.

2.11 Statistical analysis

To compare mitochondrial density across cell types (neuron, astrocyte) and animal groups (adult seal, juvenile seal, mouse), I used a generalised linear mixed model (GLMM) with Poisson distribution. This type of model can analyse grouped data with fixed explanatory variables that also have several random "nested" explanatory variables. In my data, *Animal-ID*, *Section-ID* and *Image-ID* are the nested random variables that can explain some of the variation found in cell types or animal groups. The Poisson distribution was used for the mitochondrial density model because mitochondrial count (a discrete variable) was used as a response variable. The offset of the cell area (log-transformed) and the interaction of cell type and animal group were included as explanatory variables. *Section-ID* nested in *Animal-ID* was included as random term to correct for potential autocorrelation of images belonging to a given section of a given animal. The GLMM was run separately for auto and manually selected cells. For the manually selected cells, *Image-ID* was additionally nested and included as a random term to correct for possible autocorrelations found in the cells selected from the same image.

To compare adjusted mitochondrial mean fluorescence intensity (aMFI) across cell types and animal groups, I used a linear mixed model (LMM) with Gaussian distribution. This model can analyse grouped data with fixed and random "nested" explanatory variables where the response variable is normally distributed. The interaction of cell type and animal group was included as fixed effect, and *Section-ID* nested in *Animal-ID* was used as random structure. A sperate model was run for the auto selected and manually selected cells. In the manually selected cells, *Image-ID* was additionally nested and included in the random structure. The same model was used for comparing mean mitochondrial sizes across all cell types and animal groups.

All analyses were done in RStudio (version 4.3.1, 2023). I used the R-package *glmmTMB* (Brooks et al., 2017) for modelling. For pairwise post-hoc comparisons of all combinations of cell types and animal groups, I used the R-package *emmeans* (Lenth et al., 2023).

3 Results

3.1 Recorded cell area

A total brain tissue area of 64 750 000 μm^2 was analysed. This area was screened for stained cells and the automated cell selection method detected 1 951 884.2 μm^2 of astrocytes and 3 822 875.2 μm^2 of neuronal cell area over all animal groups.

3.1.1 Automated selection method

In the auto selected cells, the neurons accounted for a higher percentage of the total tissue in all animal groups (Table 8). The highest cell detection was in juvenile seals where 14.79 % of the tissue was detected as neurons and 8.86 % was detected as astrocytes. Adult seals had lower cell detection percentages than juvenile seals. In mice, the percentage of cells detected was significantly lower than in the seals for both astrocytes and neurons. Only 1.79 % of the area analysed in mice was recorded as astrocytes and 8.69 % was recorded as neurons. The automated method of cell selection took all the thresholded cell area of an image into account and gave much higher values of cell area than the manual selection of cells (Table 8).

3.1.2 Manual selection method

The manually selected cells only accounted for between 0.19 – 0.46 % of the total analysed tissue area (Table 8). The highest percentage of selected cells per tissue was in the adult seals, while the lowest was, similar to the auto selection method, in mice. The manually selected cells however, had a more even representation of area between astrocytes and neurons. The most even representation was found in adult seals where neurons accounted for 0.46 % and astrocytes for 0.44 % of the total area. In juvenile seals the astrocytes accounted for 0.39 % of the tissue area, whereas the neurons only accounted for 0.27 % of the area.

Table 8. Total tissue area analysed in auto and manually selected astrocytes and neurons in the visual cortex of adult hooded seals, juvenile hooded seals, and adult mice. "% cell area" indicates how much cell area was detected in percentage of the total tissue area.

Animal group	Cell type	Total tissue area (µm²)	Auto selected cells		Manually selected cells	
			Total cell area (µm²)	% cell area	Total cell area (µm²)	% cell area
Adult seal	Astrocytes	11250000	793445.11	7.05	49 026.07	0.44
	Neurons	11250000	1224438.91	10.88	51 199.45	0.46
Juvenile seal	Astrocytes	11250000	997022.56	8.86	44 083.22	0.39
	Neurons	11250000	1664111.77	14.79	30 674.59	0.27
Mouse	Astrocytes	9000000	161416.51	1.79	17 300.50	0.19
	Neurons	10750000	934324.52	8.69	27 210.25	0.25

3.2 Mitochondrial density

3.2.1 Total counts

Mitochondria were automatically counted within the whole detected cell area of astrocytes and neurons in the automated method and within single selected cells with the manual selection method. These counts do not represent the density of mitochondria but give an overview of the number analysed mitochondria. In total, 865 501 mitochondria were counted over all animals and cell types. With the automated method, the highest count of mitochondria (n = 342 842) was in the neurons of juvenile seals, whereas the lowest counts were made in the astrocytes of mice (n = 20 901) (Table 9).

The automated cell selection method obviously gave much higher total counts of mitochondria than the manually selected cells, considering the difference in detected cell area between the methods. Similar to the detected cell area, the counts of mitochondria were more disproportional between astrocytes and neurons when analysed with the automated cell selection method. The distribution of mitochondrial counts between cell types was more even when the manual selection method was used.

Table 9. Total mitochondrial count in auto and manually selected neurons and astrocytes of the visual cortex of adult hooded seals, juvenile hooded seals, and adult mice.

	Auto selected cells		Manually selected cells	
Animal group	**Astrocytes** (n mitochondria)	**Neurons** (n mitochondria)	**Astrocytes** (n mitochondria)	**Neurons** (n mitochondria)
Adult seal	95 721	113 930	5271	5224
Juvenile seal	146 917	342 842	6172	6154
Mouse	20 901	145 190	2721	4312

3.2.2 Variability in density between sections

The density of mitochondria was calculated by dividing the number of counts by cell area. A section wise density was estimated by the taking the mean of the total number of images that were analysed per section (Appendix IV). For the automated cell selection there was only one recording of cells within the entire image which was then used to calculate the section average. As for the manual cell selection, all the cells selected per image per section (Appendix IV) were used in calculating the section average.

There was a higher section-wise variability in mice compared to seals (figure 12). The seals had the highest variability of mitochondrial density in neurons. In comparison, the mice showed higher variability of mitochondrial density in the astrocytes than in neurons. The auto selected cells had a lower variation in mitochondrial density per section than the quantification that was based on manually selected cells. In all but a few exceptions, the two selection methods had a similar median mitochondrial density per section. There was also relatively low variation between the sections from the same animal. One visible trend is that section E usually had a lower recorded density than the other sections, regardless of species and cell type.

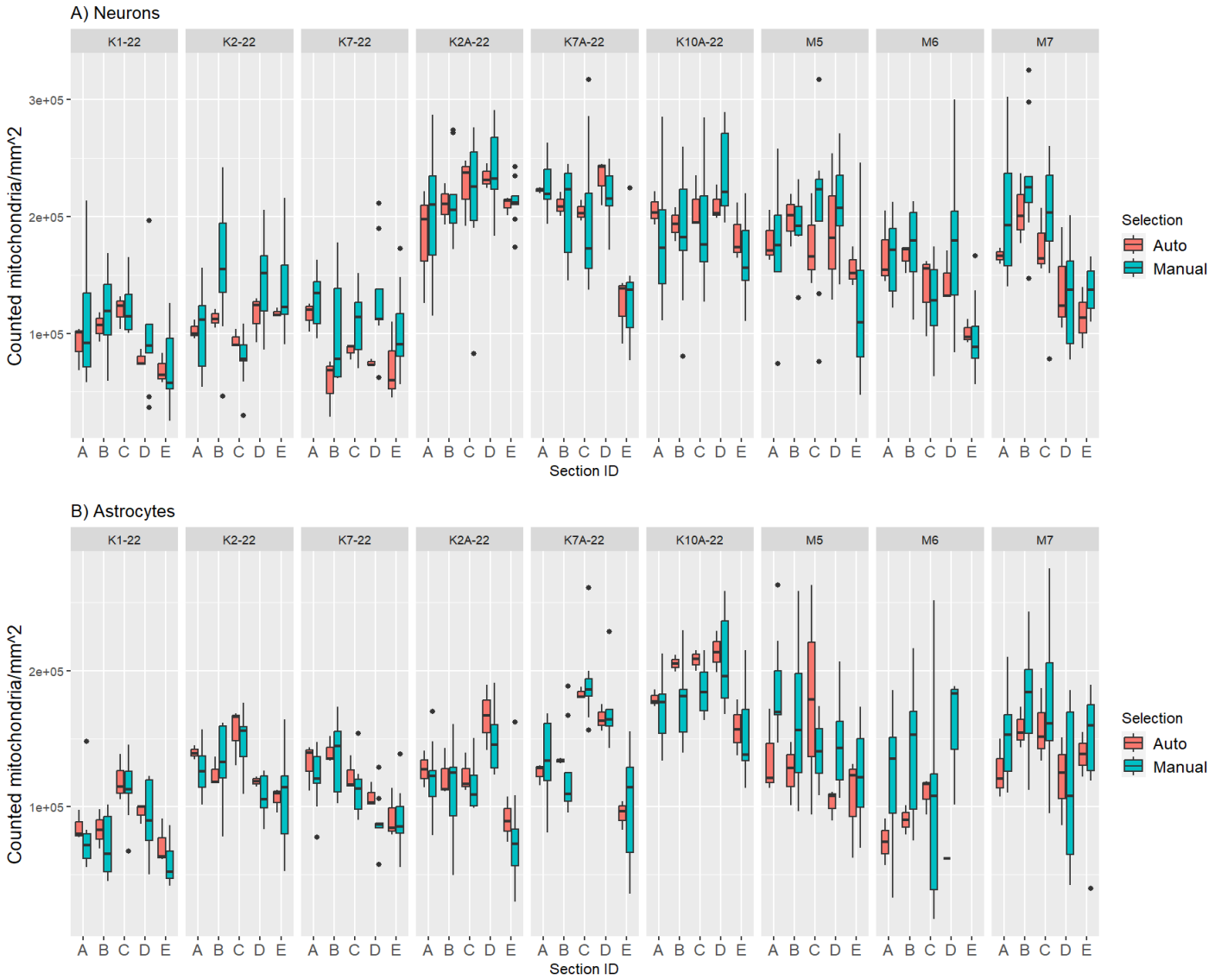

Figure 12. Counted mitochondria per mm^2 of cell area in A) neurons and B) astrocytes of the visual cortex sections A-E. Selection indicates the cell selection method: "Auto" = automated selection of all cells per image, "Manual" = manual selections of up to 3 cells per image. Adult hooded seals: K1-22, K2-22, K7-22. Juvenile hooded seals: K2A-22, K7A-22, K10A-22. Adult mice: M5, M6, M7. The middle line of the boxplots shows the median, while the upper and lower end of the boxes show the 25th and 75th percentile. The whiskers indicate the lowest and highest value, within 1.5 x the length of the closest percentile. The dots outside the boxes are outliers.

3.2.3 Mitochondrial density in neurons and astrocytes

The mitochondrial density varied with cell type and animal group for both the automated and manual cell selection method (GLMM, Table 10, Appendix V).

In the auto selected cells, the highest mitochondrial density was found in the juvenile seal neurons and the lowest density in the adult seal neurons (figure 13A). The mitochondrial density in neurons was significantly different between adult seals, juvenile seals and mice (all $p < 0.004$). The difference in density in astrocytes between animals was only significant between juvenile and adult seals ($p = 0.002$), whereas the mouse astrocytes had similar mitochondrial density to both juvenile ($p = 0.121$) and adult seals ($p = 0.793$). The density in astrocytes and neurons were all significantly different within the same animal group (all $p < 0.001$). In juvenile seals and mice, the neurons had a higher mitochondrial density than the astrocytes, while in adult seal, the neurons had lower mitochondrial density than the astrocytes (Figure 13A).

In the manually selected cells, the highest mitochondrial density was again found in the juvenile seal neurons (figure 13B). The lowest mitochondrial density was found in the adult seal astrocytes. The mitochondrial density in adult seal neurons was significantly lower than in the juvenile seal and mouse neurons ($p < 0.001$). The density in the neurons of juvenile seals and mice were not significantly different ($p = 0.0712$). The adult seal astrocytes also had significantly lower mitochondrial density than the juvenile and mouse astrocytes ($p < 0.0104$). However, the juvenile seal and mouse astrocytes showed a high similarity in mitochondrial density. Within each animal group, there was less significant difference in mitochondrial density between astrocytes and neurons than found in the auto selected cells (Figure 13).

Mitochondrial density of the manually selected astrocytes and neurons of adult seals and mice did not show a significant difference ($p = 0.999$ and $p = 0.112$ respectively). There was, however, still a significantly different mitochondrial density between the two cell types in juvenile seals ($p < 0.001$).

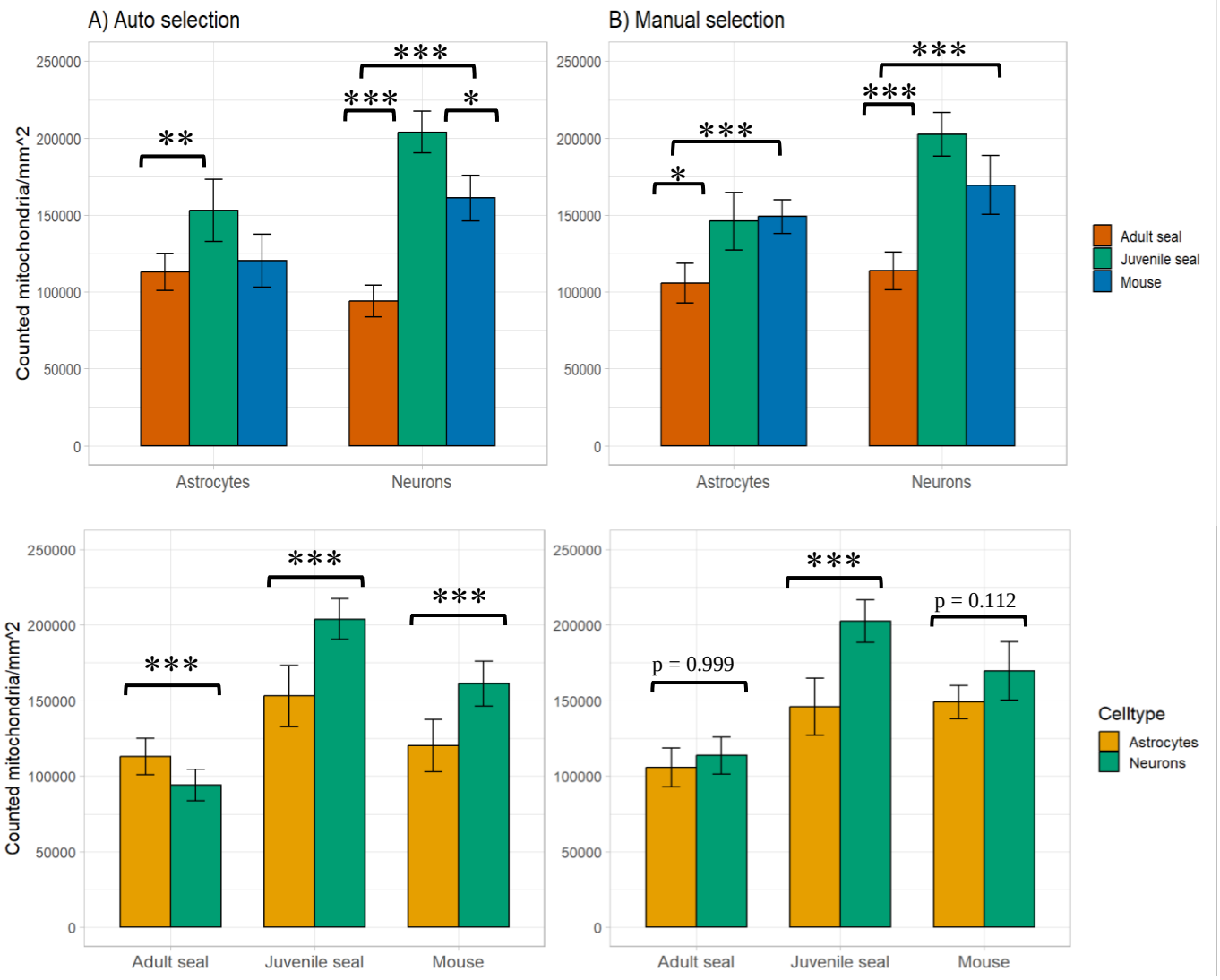

Figure 13. Mean density of mitochondria per mm^2 in A) auto and B) manually selected neurons and astrocytes of the visual cortex in each animal group. Each bar is based on number of sections in each animal group (n = 15) for all except in mouse astrocytes (n = 14). Error bars show the 95% confidence interval. Significance codes: * p < 0.05, **p < 0.01, ***p < 0.001.

Table 10. Summary of the generalized linear mixed models (GLMMs) used to model the variation in mitochondrial density in neurons and astrocytes (cell type) in adult seal, juvenile seal, and mouse (animal group), for automated and manual cell selection. Intercept = Species (adult seal).

Method	Predictor	Estimate	Std. Error	z value	P
Automated	(Intercept)	-2.195656	0.049401	-44.45	< 0.001
	Species (juv seal)	0.266211	0.069824	3.81	< 0.001
	Species (mouse)	0.090142	0.070147	1.29	0.199
	Cell type (neuro)	-0.189556	0.004587	-41.33	< 0.001
	Species(juv seal):Cell type(neuro)	0.524388	0.005594	93.73	< 0.001
	Species(mouse):Cell type(neuro)	0.445258	0.009183	48.49	< 0.001
Manual	(Intercept)	-2.265306	0.059808	-37.88	< 0.001
	Species (juv seal)	0.283461	0.084461	3.36	< 0.001
	Species (mouse)	0.352444	0.086265	4.09	< 0.001
	Cell type (neuro)	0.008539	0.020647	0.41	0.679
	Species(juv seal):Cell type(neuro)	0.365434	0.027893	13.1	< 0.001
	Species(mouse):Cell type(neuro)	0.065413	0.035658	1.83	0.067

3.3 Mitochondrial fluorescence intensities

The mitochondrial adjusted mean fluorescence intensity (aMFI = MFI – background MFI) was estimated for each cell type and section of the nine animals. In the auto selected cells the average aMFI was based on the intensities of the images (for n see Appendix IV) for each section. As for the manual cell selection, first an average of the selected cells was calculated for each image which was then used in calculating the average aMFI per section.

3.3.1 Adjusted MFI variability between sections

The astrocytes had a higher section wise variation in aMFI in the mice than in hooded seals (Figure 14 B). The section wise variation in aMFI in neurons was however more similar over all animal groups (figure 14 A). The auto selected cells generally showed less variation in aMFI in both neurons and astrocytes, compared to the manually selected cells. The mean aMFI for both selection methods was however similar in most sections. The sections (n=5) of the same animal also had a largely similar mean aMFI, although there are a few outliers. The same trend was found here as in the mitochondrial density measurements, where section E tended to have lower aMFI values than the other sections.

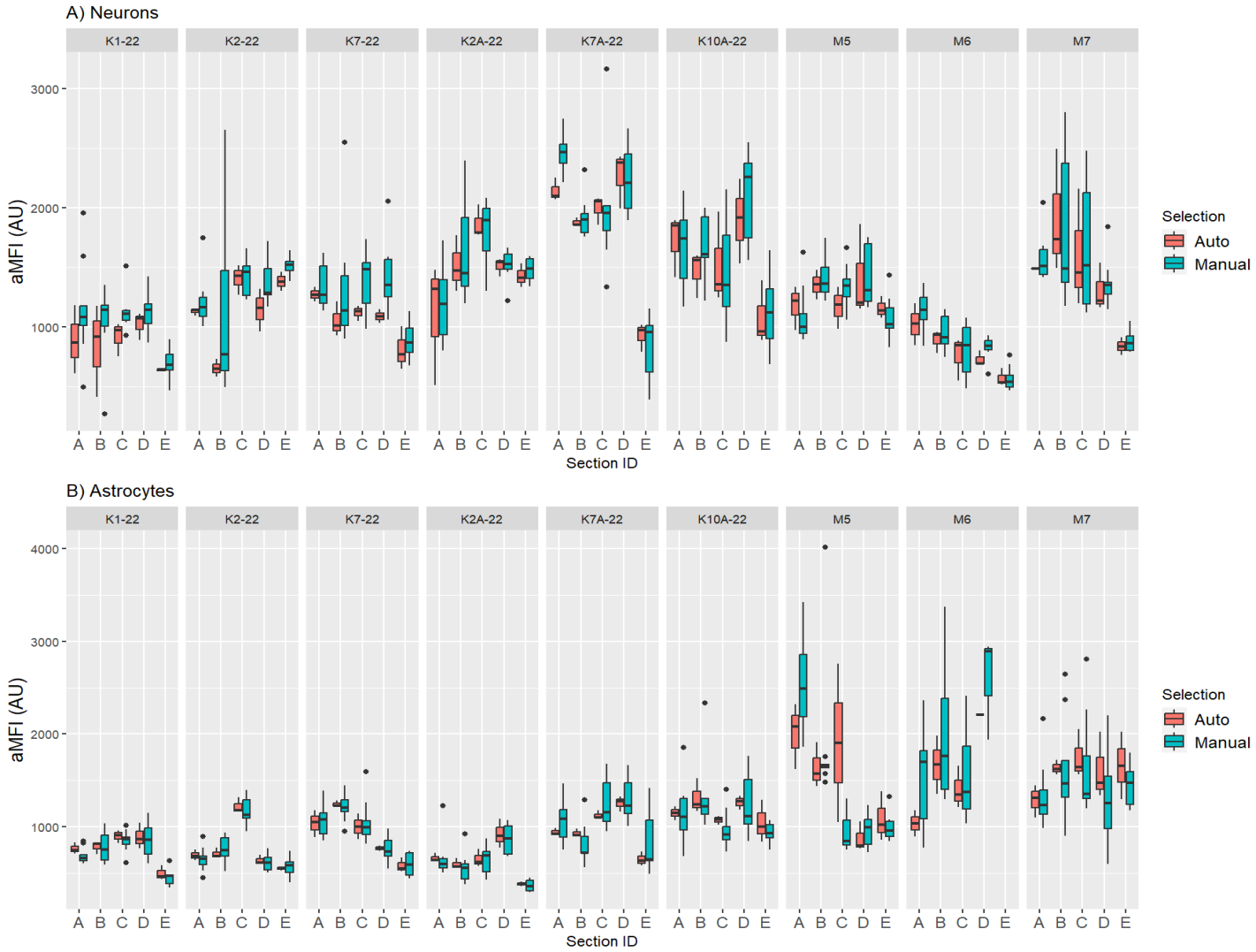

Figure 14. Boxplot of the adjusted mean fluorescence intensity (aMFI = MFI – background MFI) of the mitochondrial stain in A) neurons and B) astrocytes of the visual cortex sections A-E, adjusted by subtracting the background mean fluorescence intensity. AU = arbitrary units. Selection indicates the cell selection method: "Auto" = automated selection of all cells per image, "Manual" = manual selections of up to 3 cells per image. Adult hooded seals: K1-22, K2-22, K7-22. Juvenile hooded seals: K2A-22, K7A-22, K10A-22. Adult mice: M5, M6, M7. The middle line of the boxplots shows the median, while the upper and lower end of the boxes show the 25th and 75th percentile. The whiskers indicate the lowest and highest value, within 1.5 x the length of the closest percentile. The points outside the boxes are outliers.

3.3.2 Adjusted MFI in neurons and astrocytes

The average aMFI for each section was used in calculating an average for neurons and astrocytes in adult seal, juvenile seal, and mouse (LMM, Table 11, Appendix V). The auto selected cells showed similar values of aMFI to the manually selected cells (figure 15). The only notable difference between selection methods was that the difference between the adult seal astrocytes and neurons was not as distinct in the auto selected cells compared to the manually selected cells. However, the difference was still significant ($p = 0.008$).

In the auto selected cells, the highest mean aMFI was found in the neurons of juvenile seals and the lowest mean aMFI was found in the adult seal astrocytes (Figure 15). The aMFI in juvenile seal neurons was significantly higher than the aMFI of adult seal ($p < 0.001$) and mouse neurons ($p = 0.004$). The mouse and adult seal neurons however, showed no significant difference in aMFI ($p = 0.885$). The aMFI in mouse astrocytes was significantly higher than both in the adult seal and juvenile seal astrocytes (both $p < 0.001$), while the adult seal and juvenile seal had similar aMFI in the astrocytes ($p = 0.947$). The neurons of adult seal had significantly higher values of aMFI than the astrocytes of adult seal ($p = 0.008$). The same significant distribution was observed in the juvenile seal astrocytes and neurons ($p < 0.001$). In mouse however, the astrocytes had significantly higher values of aMFI than the neurons ($p < 0.001$).

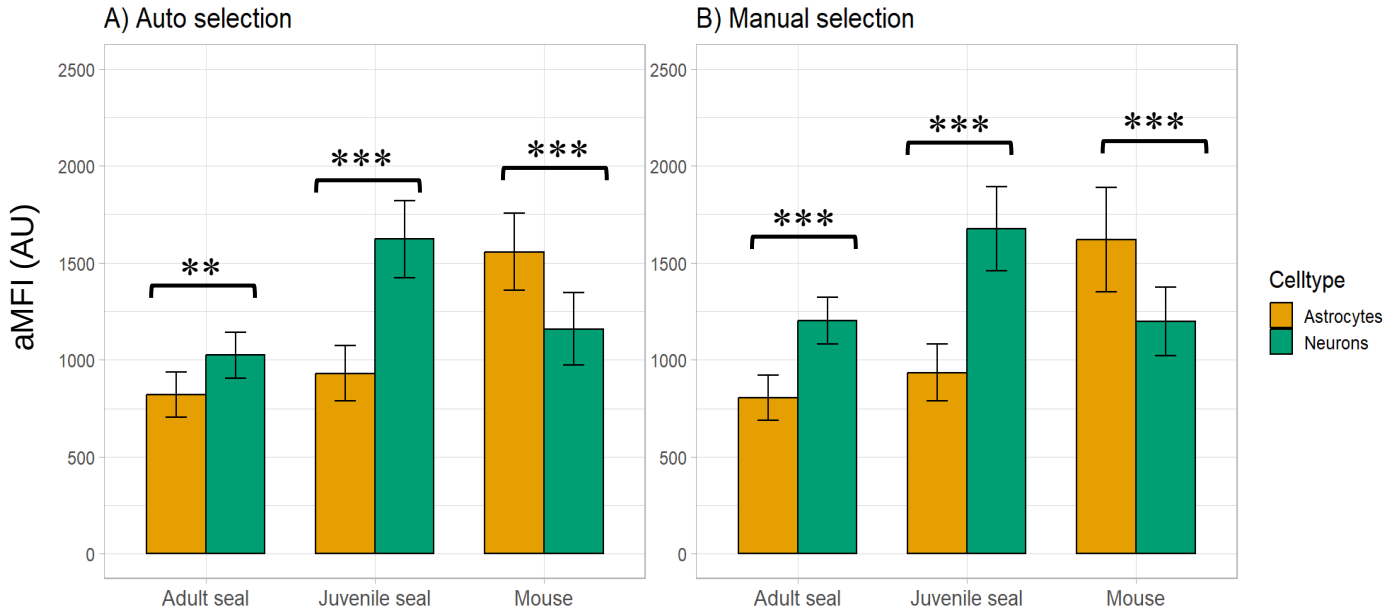

Figure 15. Mean aMFI of the mitochondrial stain in A) auto and B) manually selected neurons and astrocytes of the visual cortex in each animal group. MFI was adjusted by subtracting the background mean fluorescence intensity. AU = arbitrary units. Each bar is based on total number of sections in each animal group (n = 15) for all except in Mouse Astrocytes (n = 14). Error bars show the 95% confidence interval. Significance codes: * $p < 0.05$, ** $p < 0.01$, *** $p < 0.001$.

Table 11. Summary of the linear mixed models (LMMs) used to model the variation in mitochondrial adjusted mean fluorescence intensity (aMFI) in neurons and astrocytes (cell type) in adult seal, juvenile seal, and mouse (animal group), for automated and manual cell counts. Intercept = Species (adult seal).

Method	Predictor	Estimate	Std. Error	z value	P
Automated	(Intercept)	819.33	87.72	9.340	< 0.001
	Species (juv seal)	111.46	124.06	0.898	0.369
	Species (mouse)	653.33	126.41	5.168	< 0.001
	Cell type (neuro)	204.81	59.17	3.461	< 0.001
	Species(juv seal):Cell type(neuro)	485.80	83.68	5.806	< 0.001
	Species(mouse):Cell type(neuro)	-517.65	87.74	-5.900	< 0.001
Manual	(Intercept)	805.75	78.01	10.328	< 0.001
	Species (juv seal)	128.54	110.33	1.165	0.244
	Species (mouse)	718.03	112.72	6.370	< 0.001
	Cell type (neuro)	409.45	44.30	9.243	< 0.001
	Species(juv seal):Cell type(neuro)	331.56	62.26	5.325	< 0.001
	Species(mouse):Cell type(neuro)	-737.47	67.47	-10.931	< 0.001

3.4 Correlation of mitochondrial density and adjusted MFI

To measure the correlation between mitochondrial counts and aMFI, the Pearson correlation was estimated for the auto selected cells in all images (n = 259). The Pearson correlation is a linear correlation that returns a correlation coefficient (R) that ranges from -1 to 1. A $R > 0$ indicates a positive correlation, whereas a $R < 0$ indicates a negative correlation between the variables. If the coefficient = 0, there is no correlation between the measurements, and if the coefficient = +/- 1 there is a perfect correlation between the two measurements. Generally a R between 0 and 0.3 is said to have a weak correlation, a R between 0.3 and 0.5 a moderate correlation and a R between 0.5 and 1 a strong correlation (Turney, 2023).

There is a positive correlation between mitochondrial density and aMFI, with an overall Pearson correlation coefficient of 0.62 (Figure 16). The highest correlation is found in juvenile seals (R = 0.85), whereas there is almost no correlation between these measurements in adult seal (R = 0.26). Mouse also has a poor correlation between mitochondrial density and aMFI (R = 0.34).

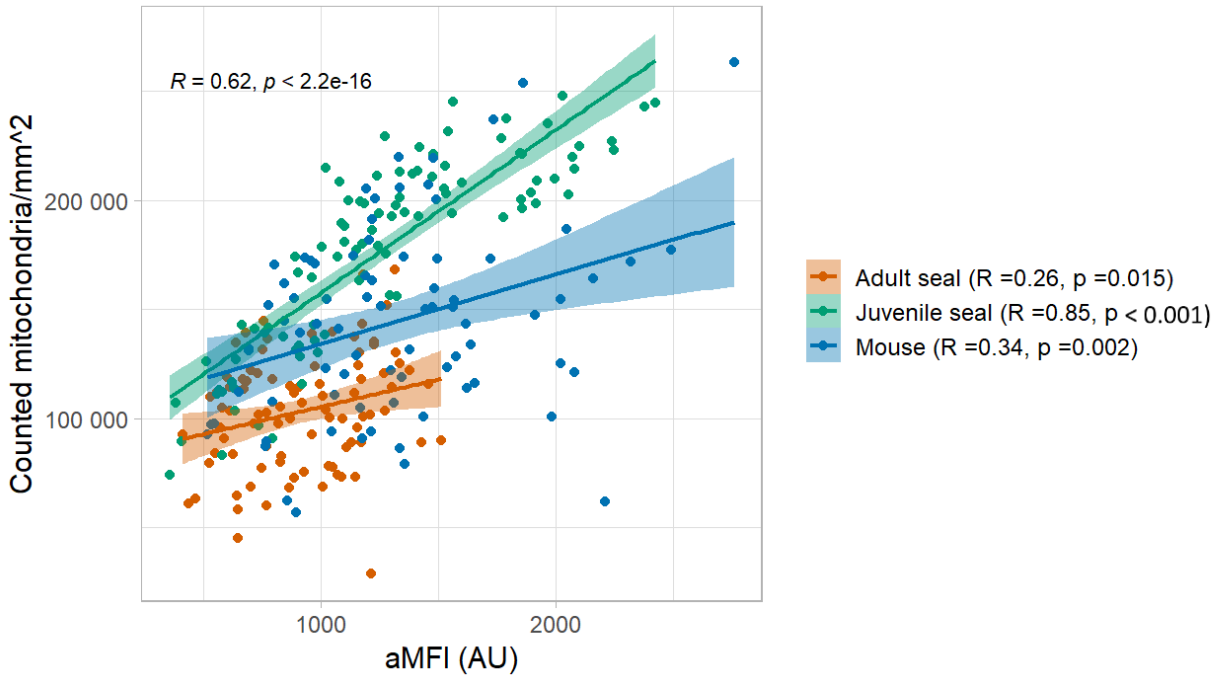

Figure 16. Pearson correlation of mitochondrial density and mean fluorescence intensities in auto selected neurons and astrocytes in adult hooded seal, juvenile hooded seal, and adult mouse. One point represents the one image (n=259). Estimated Pearson correlation coefficient is displayed as R values. P-values show the significance of the estimated Pearson correlation coefficient from a R = 0.

3.5 Mitochondrial size

3.5.1 Average sizes

The size of each of the counted mitochondria (n = 865 501) was recorded and used in estimating a mean for neurons and astrocytes in each animal group (LMM, Table 12, Appendix V).

The auto selected cells had similar mitochondrial sizes to the manually selected cells (Figure 17). One notable difference between the selection methods was that the auto selected adult seal astrocytes had significantly larger sizes of mitochondria compared to the adult seal neurons ($p < 0.001$). The manually selected cells had no significant difference between the adult seal astrocytes and neurons ($p = 0.063$). Another difference is that the adult seal and mouse neurons had similar mitochondrial sizes in the manually selected cells ($p = 0.623$), while in the auto selected cells, the mouse neurons had significantly larger sizes of mitochondria ($p < 0.001$).

For the auto cell selection method, the largest average sizes of mitochondria were found in juvenile seal astrocytes, juvenile seal neurons and in mouse astrocytes (Figure 17). There was

also not found any significant difference in mitochondrial size between these cell groups. The smallest average sizes of mitochondria were found in the adult seal neurons. The mitochondrial sizes in the juvenile seal neurons were significantly larger than in the neurons of adult seal and mouse (both $p < 0.001$). The mitochondrial sizes in adult seal astrocytes were significantly smaller than in the juvenile seal ($p = 0.002$) and mouse astrocytes ($p = 0.023$). However, there was no significant difference in mean mitochondrial sizes in the astrocytes of juvenile seals and mice ($p = 0.976$). When comparing the cell types within the same animal group, there were significantly larger mitochondria in the astrocytes compared to the neurons of mouse ($p < 0.001$). Significantly larger mitochondria were also found in adult seal astrocytes compared to neurons ($p < 0.001$). In comparison, there was not found any difference in mean mitochondrial sizes between the neurons and astrocytes of juvenile seal ($p = 0.999$).

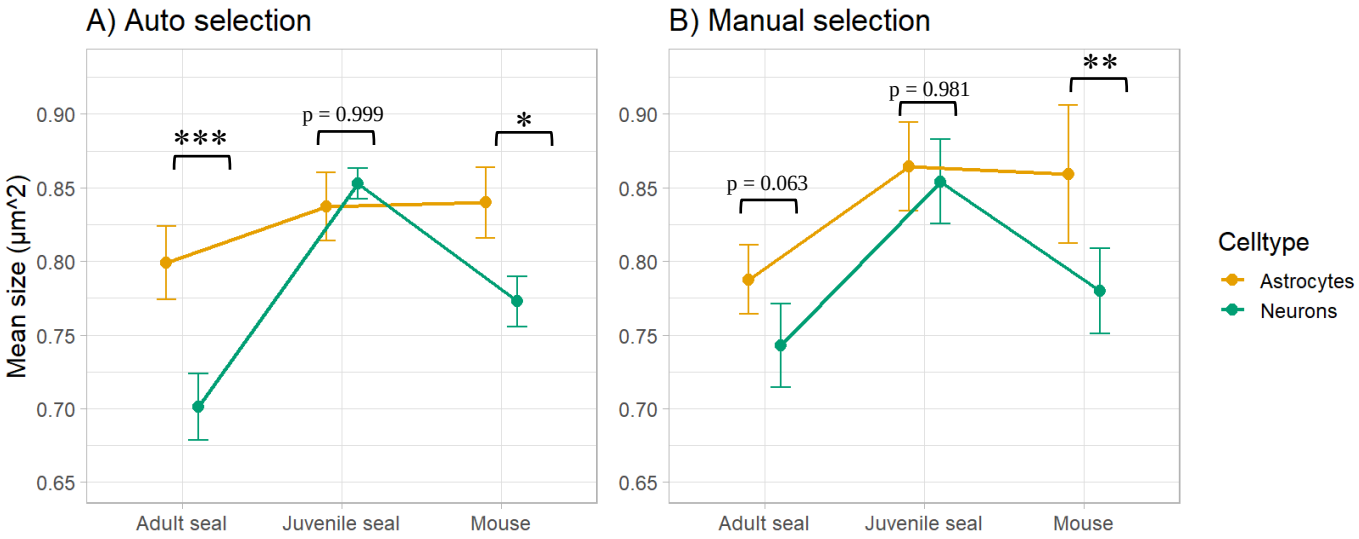

Figure 17. Mean size of mitochondria (µm^2) in A) auto and B) manually selected neurons and astrocytes in adult hooded seal, juvenile hooded seal and adult mouse. Error bars show the 95% confidence interval.

Table 12. Summary of the linear mixed models (LMMs) used to model the variation in mean mitochondrial size in neurons and astrocytes (cell type) in adult seal, juvenile seal and mouse (species), for automated and manual cell counts. Intercept = Species (adult seal)

Method	Predictor	Estimate	Std. Error	z value	P
Automated	(Intercept)	0.776717	0.012644	61.43	< 0.001
	Species (juv seal)	0.070073	0.017881	3.92	< 0.001
	Species (mouse)	0.056492	0.018292	3.09	0.002
	Cell type (neuro)	-0.077966	0.009888	-7.88	< 0.001
	Species(juv seal):Cell type(neuro)	0.080783	0.013984	5.78	< 0.001
	Species(mouse):Cell type(neuro)	0.017235	0.014604	1.18	0.238

3.5.2 Size distributions

The average mitochondrial sizes were small and varied between 0.79-0.86 µm^2 for astrocytes and 0.70 – 0.85 µm^2 for neurons. When looking at the distribution of mitochondria in specific size ranges, 35 – 48 % of all the counted mitochondria were in the lowest size range; 0.4 – 0.6 µm^2 (Figure 18). In adult seal, 48 % of the mitochondria in neurons where within the lowest size range, while only 38 % of the mitochondria found in astrocytes were in the same size range. In mice, similar proportions of mitochondria were in the smallest size range in neurons (39 %) and astrocytes (37 %). There was a similar ratio in the 0.4 – 0.6 µm^2 size range between astrocytes (35 %) and neurons (34 %) in juvenile seals.

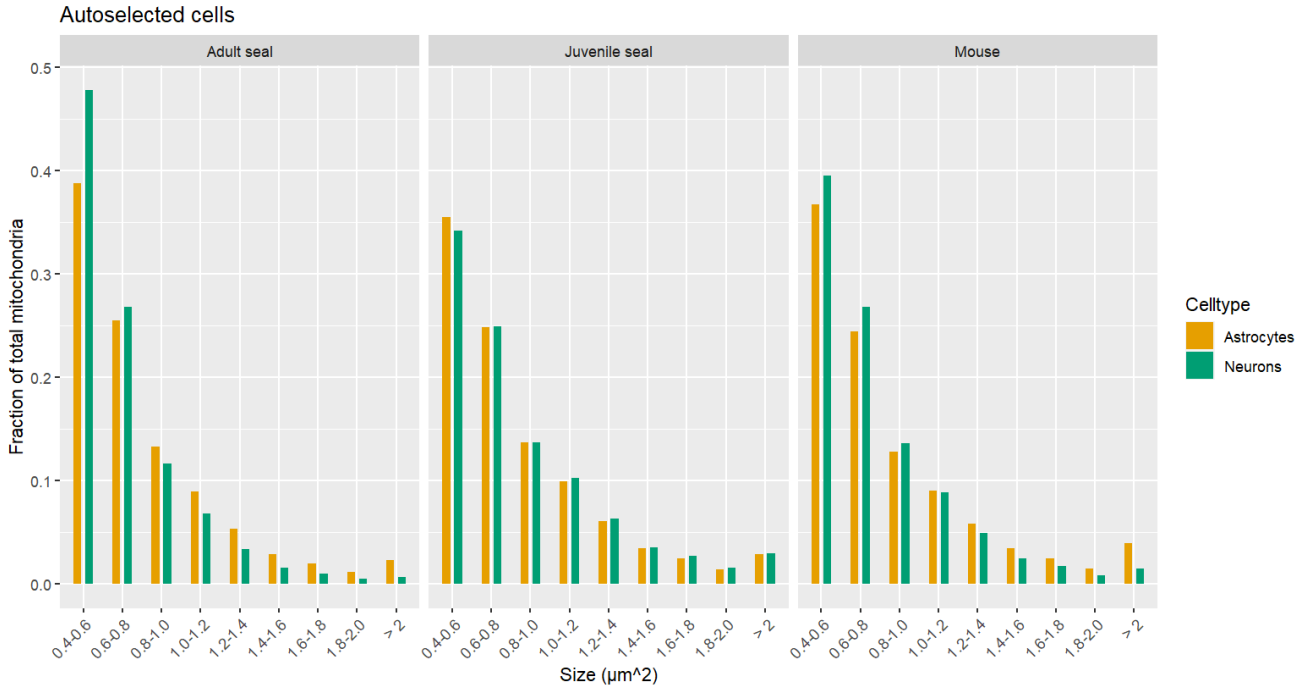

Figure 18. Distribution of mitochondria within specific size intervals in auto selected neurons and astrocytes for the three animal groups. Fraction of total mitochondria = number of mitochondria within size range / total number of mitochondria.

3.5.3 Distribution of large mitochondria

The recorded sizes of mitochondria ranged from 0.42 - 7.43 µm^2 in astrocytes and 0.42 – 11.49 µm^2 in neurons. However, only a small percentage of the mitochondria had a size above 2 µm^2 (Figure 19). The astrocytes had higher ratios of mitochondria above 2 µm^2 than the neurons over all the three animal groups. In astrocytes, the highest percentage of mitochondria above that size level was found in mice (3.9 %), whereas juvenile seals (2.9 %) and adult seals (2.3 %) both had lower percentages. In neurons, the highest percentages of mitochondria above 3 µm^2 were found in juvenile seals (2.9 %), while the lowest was in adult seals (0.7 %).

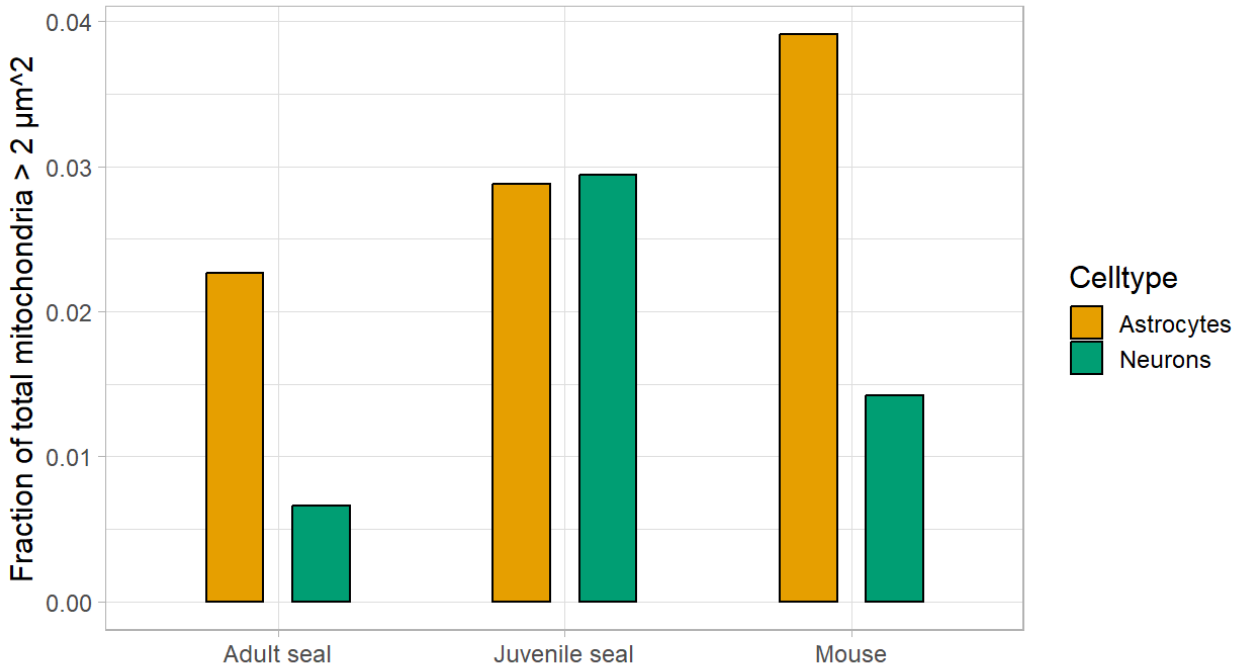

Figure 19. Fraction of mitochondria above 2 µm^2 in auto selected neurons and astrocytes in adult hooded seal, juvenile hooded seal and adult mouse. Fraction of total mitochondria = number of mitochondria within size range / total number of mitochondria.

4 Discussion

4.1 Mitochondrial density

In this section, mitochondrial density is evaluated and described based on the mitochondrial counts (number of counted mitochondria per area), which, according to my observations, is a better measurement of mitochondrial density compared to "mitochondrial mean fluorescence intensity (MFI)", as will be discussed in section *4.4.*.

Mitochondrial density is related to the efficiency of aerobic metabolism in a cell, where cells of higher respiratory capacity, like mouse neurons, have a higher mitochondrial density than cells of low metabolic capacity, like mouse astrocytes (Harris et al., 2012; Wong-Riley, 1989).

4.1.1 Mitochondrial densities in astrocytes and neurons

My findings show that mice neurons have a higher mitochondrial density compared to mice astrocytes (Figure 13). This is consistent with previous studies on mitochondrial density in the mouse brain (Wong-Riley 1989, Alano et al. 2007), and thereby supports the validity of my chosen method of mitochondrial quantification.

In hooded seals, there was a different mitochondrial density distribution between juveniles (i.e., ~15 months old) and adults (Figure 13). Similar to mice, the juvenile seals had a significantly higher mitochondrial density in the neurons compared to the astrocytes. However, the adult seals had a significantly higher (auto selected cells) or similar (manually selected cells) mitochondrial density in the astrocytes compared to the neurons. The observed mitochondrial densities in adult seals support my hypothesis, that astrocytes have higher mitochondrial densities than neurons of hooded seals, and could indicate that the astrocytes in hooded seals might indeed, have a higher capacity for oxidative metabolism as suggested by Mitz et al. (2009). The observed mitochondrial density in juvenile seals, however, also suggests that mitochondrial density is an age dependent trait in hooded seals.

4.1.2 Mitochondrial densities between species

The neurons of mice had significantly higher mitochondrial densities than the neurons of adult hooded seals (Figure 13). This supports the suggestions made by Mitz et al. (2009), that the neurons of hooded seals rely less on aerobic metabolism than they do in non-diving

species. However, the astrocytes of mice also had significantly higher (manually selected cells) or similar (auto selected cells) mitochondrial densities as the astrocytes of adult hooded seals. This is contrary to my hypothesis of hooded seals having higher mitochondrial densities in the astrocytes as mice.

My hypothesis was based on the reverse-ANLS hypothesis suggested by Mitz et al. (2009) who observed a stronger fluorescent staining for neuroglobin and cytochrome c in hooded seal astrocytes than in the neurons. It is, however, important to note that the concentration of cytochrome c in a cell does not necessarily reflect the numbers of mitochondria. Cytochrome c is part of the electron transport chain on the inner mitochondrial membrane, and its presence is correlated to cytochrome c oxidase activity which serves as a proxy for the mitochondria metabolic state (Gulyás et al., 2006; Wong-Riley, 2012). Mitochondria with a higher capacity of oxidative metabolism with a well-developed and organized inner mitochondrial membrane (Kristián et al., 2006b), could have higher concentrations of electron transport chain proteins and alas higher concentrations of cytochrome c. In mitochondria with lower oxidative metabolic capacity the concentration of cytochrome c could be lower. This means that although I observed lower mitochondrial densities in the hooded seal astrocytes compared to mouse astrocytes, the hooded seal astrocytes could still have mitochondria with a higher oxidative capacity and therefore high levels of cytochrome c (Mitz et al. 2009).

Overall, the mitochondrial density in adult seals was lower in both astrocytes and neurons compared to juvenile seals and mice. A lower mitochondrial density could indicate that adult seals rely less on aerobic cerebral metabolism. A transcriptomic study on isolated adult hooded seal neurons, showed that they have a reduced expression of genes connected to synaptic transmission (Geßner et al., 2022). Since synaptic activity is the main determinant of energy expenditure in the brain (Harris et al., 2012), this could indicate that the potential for energy conversion in the hooded seal brain is low, which could explain the observed lower densities of mitochondria in adult tissue. The same study however, also measured an increased expression of genes connected to aerobic metabolism and “mitochondrial envelope” in hooded seal neurons compared to mouse neurons (Geßner et al., 2022). This would, instead, suggest a higher density of mitochondria in hooded seal neurons which is contrary to my observations. Further research on this topic is required to explain the differences in the findings of these studies.

4.1.3 Mitochondrial densities in juveniles

Juvenile seals had significantly higher mitochondrial densities in the astrocytes than the adults and similar densities to the astrocytes of mice (Figure 13). The juvenile seal neurons also had significantly higher (manually selected cells), or similar (auto selected cells) mitochondrial densities compared to the neurons of mice. This could indicate an elevated aerobic metabolic capacity in both neurons and astrocytes at young age in seals. This is contrary to what has been observed in mice, where the mitochondrial density in the brain increases with age, being lowest at birth and highest in adults (Blomgren & Hagberg, 2006).

4.2 Mitochondrial size

Mitochondrial size is typically positively correlated with cytochrome c oxidase activity, indicating that cells with larger mitochondria have a higher capacity of oxidative phosphorylation (Mjaatvedt & Wong-Riley, 1988; Wong-Riley, 1989).

4.2.1 Mitochondrial sizes in astrocytes vs. neurons

Mitochondrial sizes are commonly reported to range between 0.75 – 3 μm^2 (Bereiter-Hahn, 1990; Wiemerslage & Lee, 2016), but recent imaging studies have recorded that a large proportion of the mitochondria in neurons and astrocytes are below 0.75 μm^2 (Fogo et al., 2021; Quintana et al., 2019). Adult seals had significantly larger average mitochondrial sizes in the astrocytes compared to in the neurons (Figure 17). 48 % of the mitochondria in adult seal neurons were in the size range of 0.4 – 0.6 μm^2, meaning that they had a very high proportion of small mitochondria (Figure 18). In adult seal astrocytes only 38 % of the mitochondria were in this lower size range. The proportion of large mitochondria (area above 2 μm^2) was also higher in the astrocytes compared to in the neurons of adult seals (Figure 19). This indicates that adult seals have a higher density of small mitochondria in neurons and a higher density of large mitochondria in the astrocytes. My hypothesis saying that there are larger mitochondria in astrocytes compared to neurons in hooded seals, is thereby supported by these findings and could imply that astrocytes have a higher capacity of aerobic metabolism than the neurons in hooded seal, as was proposed by Mitz et al. (2009).

However, a similar mitochondrial size distribution was found in mice: the astrocytes of mice had a significantly higher mean mitochondrial size compared to the neurons (Figure 17). The proportion of small mitochondria (0.4 – 0.6 μm^2) was similar between the astrocytes and neurons of mice, but the proportion of large mitochondria (area above 2 μm^2) was higher in the astrocytes compared to the neurons. Since mouse neurons mainly rely on oxidative

metabolism and astrocytes predominantly produce energy anaerobically (Bélanger et al., 2011; Hyder et al., 2006) it would be expected that the mitochondrial sizes in neurons would be larger than the mitochondrial sizes of astrocytes. However, little research has been done on the comparison of mitochondrial sies between astrocytes and neurons in mice. Therefore, further research is needed to explain and validate my findings.

4.2.2 Mitochondrial sizes between species

When comparing the mean mitochondrial sizes between species, adult seal neurons had significantly smaller mitochondrial sizes than mouse neurons in auto selected cells (Figure 17). This would seem to be in accordance with the theory of a lower aerobic metabolism in the neurons of adult hooded seal compared to the neurons in mice (Mitz et al., 2009), since small mitochondria associate with lower aerobic capacity (Mjaatvedt & Wong-Riley, 1988; Wong-Riley, 1989). In the manually selected cells there was however no significant difference found in mean mitochondrial sizes between adult seal and mouse neurons, showing some important differences in the method of cell selection that are further discussed below (section 4.5).

A finding that contradicts my hypothesis, expecting larger mitochondria in hooded seal astrocytes than in mice astrocytes, is that adult seals had a significantly smaller mean mitochondrial size in the astrocytes compared to that of astrocytes in mice. This would imply that adult seal astrocytes have a decreased capacity for aerobic metabolism compared to the mouse astrocytes. A capacity of enhanced aerobic metabolism in hooded seal astrocytes was proposed to be one of the mechanisms behind the observed high hypoxia-tolerance of the hooded seal brain (Mitz et al. 2009). My findings, showing that the seal astrocytes could even have lower aerobic capacities than mouse astrocytes, would seem to contradict this. However, the overall metabolism might be supressed in the hooded seal brain (Geßner et al., 2022; Harris et al., 2012), and the weight specific metabolism of mouse brains might be higher (as will be discussed in section 4.3.2), which could explain the lower metabolic capacity of hooded seal astrocytes compared to mice. Therefore, the comparison between species might not be as important – and relevant – as the comparison of astrocytes vs. neurons within the same species. As mentioned, the mean mitochondrial sizes in adult seals was significantly larger in the astrocytes compared to in the neurons, which could support the suggested switch in aerobic metabolism between these cells in hooded seal (Mitz et al. 2009).

4.2.3 Mitochondrial sizes in juveniles

There was no significant difference in average mitochondrial size between neurons and astrocytes in juvenile hooded seals, and there was also a similar distribution of small mitochondria and large mitochondria between astrocytes and neurons (Figure 17, 18, 19). The juvenile seal astrocytes had significantly larger mitochondria than adult seal astrocytes. There was however no significant difference in mean mitochondrial size in juvenile seal astrocytes compared to mouse astrocytes, indicating no difference in aerobic metabolic capacity between them. The mean mitochondrial sizes in juvenile seal neurons were however larger than both in the mouse and adult seal neurons. This would indicate that juvenile seal astrocytes have a higher metabolic capacity than adult seal astrocytes, and that juvenile seal neurons have an even higher aerobic metabolic capacity than mouse neurons. This is another indication of that mitochondrial morphology and density and thereby also aerobic metabolic capacity is age dependent in hooded seals.

4.2.4 The use of mitochondrial size as a proxy for respiratory rate

There are multiple factors that can influence mitochondrial sizes, which therefore question the use of mitochondrial size as proxy for the respiratory rate of a cell. Mitochondria are constantly changing through fission and fusion (Lewis & Lewis, 1915). The size of the mitochondria can however not go beyond the size of its cellular compartment, and cellular compartments with small diameters in astrocytes and neurons have been seen to contain smaller-sized mitochondria (Derouiche et al., 2015; Hollenbeck & Saxton, 2005). Therefore, the mitochondrial sizes observed in this project might be influenced by the sizes of the recorded cell compartments. To account for this, further analysis of the images, taking the size of cell bodies and smaller cellular appendixes, like axons and dendrites in neurons or end feet in astrocytes, into account would need to be investigated.

The rate at which mitochondria can drive oxidative phosphorylation is highly dependent on the structure of the electron transport chain. The electron transport chain is however dependent on the organization of the inner mitochondrial membrane (Kristián et al., 2006b), which indicates that mitochondrial ultrastructure is important and that size alone is not enough to give the full picture of the mitochondrial oxidative capacity.

4.3 Functional implications of my findings

The metabolic roles of astrocytes and neurons in a diving brain vs. non-diving brain

4.3.1 Support of a metabolic switch between astrocytes and neurons

Several of my observations support that there might be a shift in oxidative metabolism between neurons and astrocytes in the hooded seal brain: astrocytes of adult seals have a higher mitochondrial density and larger mitochondrial sizes than in the neurons. This could imply that astrocytes in hooded seals might have a different role in brain metabolism compared to the astrocytes of non-diving mammals (e.g.,mice), like hypothesized by Mitz et al. (2009). Studies on other hypoxia-tolerant species, like freshwater turtles, have shown that astrocytes may play an important role during hypoxia (Kesaraju et al., 2009; Larson et al., 2014). My observations on mitochondrial densities give additional indications of the importance of astrocytes in a diving brain.

4.3.2 Support of adaptations to hypoxia

The overall observed lower mitochondrial density (compared to juveniles and mice) could indicate that adult hooded seals have enhanced mechanisms for anaerobic ATP production. This could explain how their brain could meet its metabolic demands during dives when the oxygen supply is low (Larson et al., 2014).

Transcriptomic analysis on adult hooded seal neurons however showed that there was no higher expression of glycolytic genes in seals compared to mice (Geßner et al., 2022). However, since there is evidence of a supressed synaptic activity, both functionally (Geiseler et al., 2016) and molecularly (Geßner et al., 2022), the overall energy requirement of the hooded seal brain might be low. Together with diving adaptations like metabolic depression and selective brain cooling (Blix et al., 2010; Thompson & Fedak, 1993; Blix 2018), the low density of observed mitochondria might be sufficient to meet their brains metabolic needs, without having to resort to high-capacity anaerobic glycolysis during dives.

A reduction in the number of mitochondria could also have a neuroprotective effect. Being the main source of reactive oxygen species (ROS) lowering mitochondrial density will also lower the amount of ROS produced (Elsner et al., 1998; Halliwell, 2006). ROS productions is known to be elevated during tissue reoxygenation (Epstein & McCord, 1985), a condition which seals are routinely exposed to when re-surfacing after dives. Transcriptomic studies have however shown that hooded seal neurons have a higher expression of genes linked to

antioxidant defence than the neurons of mice (Geßner et al., 2022). Together with this increased antioxidant defence, and brain hypometabolism during diving, the decreased mitochondrial density may be another adaptation that help protect neurons against the harmful damage from ROS after reoxygenation.

There are some reservations in comparing mitochondrial densities between species with large differences in body mass, like mice and seals. Kleiber's law on metabolic scaling, states that larger animals have a lower metabolic rate per body mass than smaller animals (Wang et al., 2001). Although debated, this metabolic scaling has shown to be true for many species including humans and mice. In these species, the law also applies to the weight specific metabolic rate of specific organs, like the brain (Wang et al., 2001). Mouse brains have shown a 3-fold higher weight specific energy expenditure at rest than the brains of humans (Kummitha et al., 2014). Giving the difference in brain size between hooded seals and mice, the mouse brain may have a higher weight specific resting metabolism and alas, a higher density of mitochondria compared to hooded seals. However, an observation that would contradict this metabolic scaling issue is that juvenile seals have similar or even higher mitochondrial densities than mice. Although juveniles may have smaller brains than adult seals, they are still many times larger than the brains of mice.

4.3.3 Mitochondrial size and densities change with age in hooded seals.

The 15-month-old seals (juveniles) used in this study, had different mitochondrial densities and sizes compared to the adult seals. Specifically, the overall mitochondrial density and mitochondrial sizes were significantly higher in juvenile seals compared to the adults. This differs from the observations in rats which showed that the mitochondrial sizes in the brain stay the same through a rat's life stages (Pysh 1970). An explanation of this difference could be that juvenile seals might not have a suppressed synaptic transmission like observed in adult hooded seals by Geßner et al., (2022). Therefore, juvenile seals might have a higher overall metabolic rate in the brain and an increased need of mitochondria compared to the adults. In addition, the neurons of juveniles had significantly higher mitochondrial densities compared to the astrocytes, indicating that the neurons have a higher oxidative capacity. This suggests that the possible metabolic shift between astrocytes and neurons might yet not be developed in juvenile seals. It is however important to note that developing brains have a presumably high metabolic activity in relation to synapse formation and learning (Kalil, 1989; Kennedy,

2016). Juvenile seals might therefore still have a high energy expenditure connected to synaptic formation in their developing brain.

An increased oxidative metabolism in juvenile seals can be explained by several factors. If hooded seals have a similar early brain development as humans, the brain will reach its full size before sexual maturation (Hill et al., 2016). Since other organs of the body are still not fully developed before sexual maturation, the brain of juveniles will account for a higher fraction of the total body metabolism. This could explain why the oxidative metabolic capacity is increased in juvenile seal brain compared to the brain of adult seals and would indicate that mitochondrial density and sizes are traits that develop when seals reach the age of sexual maturation. In addition, the decrease in overall energy requirements and a potential switch in oxidative metabolism between astrocytes and neurons might be an adaptation to diving in hooded seals. Juvenile seals have substantially smaller blood oxygen stores than adults (Burns et al., 2007) and their diving behaviour consists of shorter dives and to shallower depths (Folkow et al., 2010), which suggests that their diving abilities are still not fully developed. Therefore, mitochondrial density and size might be traits that develop parallelly to the diving abilities of hooded seals. It is however important to note that the juvenile seals used in this study have been captive since birth and have never had the possibility to dive in the free. The observed mitochondrial distribution may therefore differ from a wild juvenile hooded seal.

4.4 Comparing mitochondrial counts and MFI

Mean fluorescence intensity is calculated by summing up all the pixel intensities within a region of interest (ROI) and dividing this by the number of pixels inside the ROI. The mitochondrial MFI is therefore a measurement of the average intensity of the mitochondrial stain within a cell. This would mean that an increase in mitochondrial stain will give an increase in MFI. It is expected that mitochondrial stain is correlated with the number of mitochondria within a cell, since a higher number of mitochondria would result in a higher number of TOMM20 receptors which the primary antibody can bind to during the staining process. However, a poor correlation of these measurements within adult seals and mice suggests otherwise.

Adult seals have significantly higher aMFI in the neurons compared to the astrocytes, whereas mice have significantly higher aMFI in the astrocytes compared to the neurons (Figure 15). However, the mitochondrial counts show the opposite (Figure 13). Only the juvenile seals have a distribution of aMFI in astrocytes and neurons similar to the mitochondrial counts. Since both the counts and the aMFI should be proxies for mitochondrial densities, they should also be closely correlated. There is a positive correlation between these two measurements over all animals and cell types (Figure 16). However, the highest correlation is in juvenile seals (R=0.85), while mice and adult seals have a correlation coefficient closer to zero, indicating a poor correlation between mitochondrial counts and aMFI. This raises the question as to why these measurements are not always strongly correlated and why they show contradictive results to the mitochondrial counts in neurons and astrocytes for mice and adult seals.

Mean fluorescence intensity could be more influenced by "noise" (i.e. artefacts) than mitochondrial counts. Noise in the mitochondrial stain could be caused by autofluorescence from blood vessels and erythrocytes in my samples. If some of these structures lay inside a ROI, they will influence the MFI of that ROI. Since the MFI measurement is sensitive to outliers, a few structures with high fluorescence intensities could influence the overall measured mean of the ROI. In comparison, the mitochondrial count does not take into account the difference in pixel intensities in the same way. The median filter subtraction creates outlines of particles based on the aggregation of pixel intensities regardless of intensity values, meaning that particles with low fluorescence intensities will be included as much as particles with higher fluorescence intensities. The thresholding of the particles gives all of them the same pixel value, which means that particles of higher and lower intensities will have the same weight. If a structure creating noise through high fluorescence intensity lays within an ROI, the structure would be counted similarly to the other particles and will therefore have the same impact on the overall measurement.

The aMFI measured in mice indicate contradictive results to previous studies on mitochondrial densities in mice astrocytes and neurons (Alano et al., 2007; Wong-Riley, 1989), which further supports my reservations against using aMFI as a proxy for mitochondrial density. Based on these reasons, I would suggest that mitochondrial counts and not aMFI, more accurately reflects the mitochondrial density. However, the substantial differences between the results of these measurement methods need further investigation.

4.5 Manual cell selection vs. Auto cell selection

The neurons and astrocytes were selected using two different methods: auto selection (taking all detected cell area in an image into account) and manual selection (manually selecting only 3 cells per image). The manually selected cells had, obviously, a lower recorded total cell area and lower total mitochondrial counts than the auto selected cells (Table 8 and 9). The manually selected cells also generally showed a greater section-wise variation in mitochondrial measurements (Figure 12 and 14). This could be explained by that the manually selected cell measurements were based on less recorded cell area and number of mitochondria and therefore any outliers in the data might have a higher influence on the result, compared to the auto selected cells. However, when looking at aMFI and mitochondrial counts per area across species, most results showed a high similarity between the auto selected and the manually selected cells (Figure 12 and 14). There were however some important differences in the findings, suggesting that the selection method of the cells could have an influence on the data obtained.

The mitochondrial density was generally higher in manually selected neurons compared to the auto selected neurons. This especially changed the ratio of mitochondrial density between astrocytes and neurons in adult hooded seals (Figure 13). In the auto selected cells, the astrocytes had a significantly lower mitochondrial density, whereas in the manually selected cells there was no significant difference. Although this doesn't influence my conclusions on mitochondrial density much, since (in the manually selected cells) the mitochondrial density ratio between astrocytes and neurons in adult seals, still differed much from those observed in mice and juvenile seals, it is obvious that the selection method influenced the results. One reason for the different observed mitochondrial densities in neurons between the auto and manually selected cells, is that the cell body of neurons might be overrepresented in the manual selection method. The neurons were very fragmented (Figure 9) and therefore their cell bodies were mostly selected when selecting cells manually. The axons and dendrites were also visible, but as separate units (separate ROIs). The automated counting, which would include cell bodies, as well as axons and dendrites, could therefore give a better representation of the whole cell. This may explain the difference in the observed mitochondrial counts in neurons between the two selection methods.

There are some methodological considerations that should be mentioned in relation to the two different selection methods. As described previously in my methods, the manual selected cell

selection method was included based on the notion that the auto selected method would include more non-cellular artefacts and therefore more "noise". The similarity between the results of the two selection methods, however, indicate that the noise included in the auto selection method might have had an insignificant effect on the results. Since the auto selection method detects a larger cell area, the resulting ratio of noise to cell area might be relatively small. There are several methodological advantages with the auto selection method, especially concerning repeatability of the measurements and selection bias, suggesting that this might be a superior method for cell selection. An overview of pros and cons of the two selection methods is given in Table 13.

Table 13. Comparison of pros and cons of the two cell selection methods used in image analysis for detecting astrocytes and neurons in brain tissue.

Auto selection	**Manual selection**
• Fast • No selection bias • Repeatable • Includes more noise • Measures more cell area	• Time consuming • Selection bias • Difficult to repeat • Includes less noise • Measures less cell area

4.6 Other methodological considerations

4.6.1 Methodological advantages

The method developed for immunostaining and fluorescence microscopy of fixed hooded seal brain tissue for this thesis, has proven to be a promising method for mitochondrial quantification. There are several advantages of this method:

<u>It can be applied to fixed tissue and there is therefore no need of cell cultures.</u>

There are so far no published studies that have successfully managed to culture astrocytes and neurons of hooded seals, although investigation into this field is currently being done (Ciccone, unpublished). Creating cell cultures from "exotic species" that rarely get sampled or live in difficult sampling environments can be challenging. The fixing of tissue samples (e.g. with PFA fixatives) is however much more convenient and allows the samples to be preserved for long periods (month to years) for further analysis. Fixed tissue samples, especially from wild animals, are therefore usually more readily available for research. The

use of animal tissue also gives a more accurate reflection of the actual processes inside an animal. Some cellular processes found in tissue might not be reflected in cell cultures, since components and interactions of cells that are found in real tissue are missing in cell cultures. Thus, for example mitochondrial densities and sizes which could be closely related to the astrocyte-neuron metabolic coupling, might not be the same in cell cultures as in brain tissue. Studying the brain tissue might therefore give the "real image" of cellular processes and traits within an animal.

Mitochondria can be measured in individual cells.

The imaging method used allows us to quantify mitochondria in individual cells. Several methods for protein quantifications like western blots or enzyme-linked immunosorbent assay (ELISA) only give cell population estimates and cannot show the distribution of mitochondria between individual cells. The imaging method developed for this thesis allows the selection of individual cells in brain tissue and the quantification of mitochondria therein.

4.6.2 Methodological limitations

4.6.2.1 Limitations in animal and tissue sampling

Juvenile seals were not able to dive deep in captivity.

The seals were held captive from birth and although they had access to two 40 000 L pools in the animal facilities at UiT, they did not have the possibility to dive down to the depths usually recorded for wild seals at this age (Folkow et al., 2010). There was also no data on their diving behaviour including lengths and frequency of their dives, in captivity. As I have suggested earlier, the mitochondrial densities and sizes might be affected by the seals diving capabilities which could be different in captive and wild juvenile seals.

Different concentrations of PFA were used for fixing the tissue.

The adult hooded seals were sampled in March 2022 and fixed with a 4% PFA fixative. The mice and juvenile seals where however sampled in spring 2023 and fixed with a 8% PFA fixative. All the tissue for the final experiment was immunostained and imaged in September 2023. The adult seal tissue was therefore both stored for a longer period before analysis and fixed with a different PFA concentration. The quality of PFA fixed tissue samples has been seen to diminish when stored over longer time (Likhithaswamy et al., 2022). There were

however no visible difference in tissue quality between adult seal and juvenile seal brain tissue.

4.6.2.2 Limitations in sectioning and staining

The sections might have been too thick.

The sections cut with the cryostat for this project had a thickness of 20 µm. This was chosen in order *a)* to get as much of the cell volume as possible, and *b)* since the only other staining tests were done on 40 µm tissue sections that resulted in noisy images. When refining the protocol for image analysis, it was discovered that even though 13 z-slices were imaged thorough 12 µm of the tissue volume, only about 5 of the z-slices showed in-focus cells and mitochondria. Therefore, only 4 µm of the tissue thickness was actually taken into account for the analysis. The blurry images found in the remaining z-slices could be due to that the widefield microscope detects much of the out-of-focus light in tissue sections of this thickness. It would be reasonable to decrease the tissue section thickness to see if it would decrease the amount of noise throughout the tissue volume. This could lead to more in-focus z-slices, which – paradoxically – means that a thinner section thickness could actually give a higher volume of imaged tissue area.

There was a difference in tissue quality between seals and mice.

None of the seal images were excluded from the analysis, whereas 11 images were excluded for the mouse tissue (Appendix IV). The images of seal tissue showed generally a higher tissue quality upon inspection, having a lower presence of cuts, folds and wrinkles in the section. In some white matter mouse tissue sections, there was also not found any cell staining and the images had to be excluded due to astrocytes not being present. One of the reasons for differences in tissue quality could be due to improper mounting of the sections due to the differences in section sizes. The mouse tissue sections which had a size of about 1 mm^2 were difficult to handle due to their small size. This could have caused wrinkles and folds when mounting them on the slides. The seal sections which had a size of about 1.5 cm^2 could more smoothly be mounted on the microscopy slides.

GFAP is not present in all compartments of astrocytes.

Recently it was discovered that astrocytes do not act as uniform cells, but as compartmentalized units with distribution of different functions and metabolic pathways between the cell compartments (Derouiche et al., 2015). Particularly, the peripheral astrocyte process, a compartment is involved in glutamate uptake from the synaptic cleft, has a high

density of small mitochondria (Derouiche et al., 2015). This compartment does not, however, contain GFAP, the protein targeted for immunostaining of astrocytes in this project. Therefore, this compartment was probably not included in my measurements, and the observed mitochondrial density might therefore not fully reflect the real mitochondrial density of the studied astrocytes.

4.6.2.3 Limitations in image analysis

Median filter subtraction might influence mitochondrial size.

The filtering of the images to remove background noise (median filter subtraction), could have an impact on the recorded mitochondrial sizes. The filter could have removed some of the mitochondrial area, making them smaller than their actual sizes, or the filter could have included some of the background noise and thereby making the mitochondrial sizes larger. Small adjustments of the median filter subtraction had large implications on mitochondrial size, as seen in Figure 11. The same filtering settings were used for all the images which means that the area added or subtracted from the actual mitochondrial size would be the same for all mitochondria across species and cell types. Therefore, the mitochondrial sizes can still be compared to each other in this study but might not be comparable to the mitochondrial sizes found by other studies using different methods of filtering or image analysis.

Outliers like “Section E” might influence the estimated average.

No extreme data points were removed from the data analysis, even though some outliers are visible when plotting the variability within sections (Figure 12 and 14). The reasons for not cleaning the data was the high number of observations: 259 images, 757 selected cells, 865 501 counted mitochondria. The large sample size was therefore expected to minimize the influence of outliers. However, there was observed a generally lower aMFI and mitochondrial counts in section E. This section was positioned closest to the labelling field on all of the microscope slides. This indicates that there might have been factors in the staining process (e.g. uneven antibody distribution, increased quenching) or in the imaging process (e.g. uneven illumination from the microscope) that could have affected the quality of this section. Since this section might be a probable outlier that overall lowers the mitochondrial measurements, it could be a good option to remove it from the data set.

4.7 Further analysis

4.7.1 Gathering more evidence for the reverse ANLS theory

Although my findings on mitochondrial sizes and densities may support the theory of a reverse ANLS in hooded seals (Mitz et al. 2009), more research is needed. An increased mitochondrial density might indicate a higher capacity for aerobic metabolism in astrocytes, but it does not give direct evidence about a reverse shuttling of lactate from neurons to astrocytes (Mitz et al. 2009). Previous research on lactate dehydrogenase isoenzymes (LDH) has shown that LDHB, the enzyme mostly responsible for converting lactate into pyruvate, is highly co-localized with GFAP in the hooded seal brain (Hoff et al., 2016), which is in support of a lactate-fueled metabolism in the astrocytes. Further, investigating monocarboxylate transporters (MCTs) that transport lactated in and out of cells, could help to shed more light onto this topic. Different types of MCTs are associated with cells that predominantly receive lactate and cells that predominantly release lactate (Beard et al., 2022; Pierre & Pellerin, 2005). Finding out which MCTs are associated with astrocytes and neurons in the hooded seal brain is currently being investigated (Folkow & Jensen, unpublished) and could give new insights into the shuttling of lactate between these cells. Further investigations into mitochondrial morphology in neurons and astrocytes could give additional insight into their metabolic roles. Several samples in this thesis were fixed for the use in CLEM and TEM (Table 2), which are methods that can be used in investigating the organisation of the inner mitochondrial membrane and thus the respiratory capacity of mitochondria in astrocytes and neurons (Kristián et al., 2006b).

4.7.2 Categorizing brain regions

I have imaged three different areas of the visual cortex: grey matter with high densities of neuronal cell bodies, grey matter with mostly neuropil (consisting of unmyelinated axons and dendrites) and white matter. Neurons detected in all these regions have been grouped together when quantifying mitochondrial densities in this thesis. However, neurons are heterogenous cell types that differ in their metabolism and function between different brain areas. It has also been found differences in mitochondrial densities and sizes between different intracellular compartments like dendrites, soma and axon terminals in neurons of mice and primates (Faitg et al., 2021; Wong-Riley, 1989). Further analysis could be done through categorising the images based on the different tissue areas. This could give an insight on how neuronal mitochondrial densities differ between different regions of the visual cortex, and between different neuronal intracellular regions.

To shed light on the metabolic coupling between astrocytes and neurons it would be especially interesting to have specific mitochondrial density measurements in neurons of white matter, where the highest density of astrocytes was observed. Very few astrocytes were found in the grey matter of hooded seal visual cortex and therefore only white matter regions were used in measuring the mitochondrial density of astrocytes. This results in a split of regions of mitochondrial density quantification between astrocytes and neurons in this analysis. Although white matter regions also were included in the neuronal mitochondrial density measurements, many of the images analysed for neurons were of grey matter regions, where astrocyte mitochondrial density was not measured.

4.7.3 Mitochondrial networks

When recording the mitochondrial counts, the x- and y-coordinates for the centroid (middle point) of each mitochondrion was recorded. This data could be used in analysing how fragmented or aggregated the mitochondria are in the cells, and if this differs between the different cell types between the species. It is known that mitochondria can form large, interconnected networks, and that these networks especially are formed in respiratory active cells. In contrast, cells that display less oxidative respiration tend to have smaller and more fragmented mitochondria (Westerman 2012). For hooded seals, particularly adults, it could be hypothesized that the possibly more oxidatively active astrocytes, would have more densely aggregated mitochondrial networks, while the mitochondria in neurons might be more fragmented. While the opposite would be expected for the astrocytes and neurons in mice. Recently developed machine learning techniques, have been used in classification of neuronal mitochondrial networks based on their shape and size (Fogo et al., 2021) which could give increased insights into cell metabolism. Analysis of such data was beyond the scope of this thesis, due to time constraints, but could represent an opportunity for further research.

4.7.4 Mitochondrial changes during hypoxia

My observations suggest that mitochondrial sizes and densities might not stay constant through the life stages of hooded seals. However, the mitochondrial sizes and densities might not even stay constant from hour to hour. Lewis & Lewis already observed in 1915 that the sizes and numbers of mitochondria in cell cultures change significantly within minutes. The sizes and numbers might constantly change with small changes in metabolic needs or if the cells are exposed to any stressors (Collins et al., 2002; Westermann, 2012). Therefore, the recording of mitochondria through live cell imaging over a longer period of time might give a

better understanding of how mitochondrial sizes and densities differ between cells and species. It would also be interesting to see how mitochondrial sizes in cells of hooded seals are affected by hypoxia, by designing hypoxia experiments for tissue sections or cell cultures. In this context, hypoxia and re-oxygenation has already been observed to have significant effects on the mitochondrial sizes in mouse astrocytes (Quintana et al., 2019).

4.8 Future prospects

My findings have shown that astrocytes might have an enhanced metabolic role in hooded seals, a hypoxia-tolerant species. The metabolic role of astrocytes might be part of the mechanisms against hypoxia-induced brain tissue damage. The development of clinical treatments that enhance the metabolic roles of astrocytes, could therefore be useful in the treatment of patients with stroke or other diseases that impair the oxygen supply to the brain.

5 Conclusion

The visual cortex of adult seals has higher mitochondrial densities and larger mitochondrial sizes in astrocytes compared to the neurons. This could mean that astrocytes have a higher capacity for aerobic metabolism than neurons in hooded seals, which supports the theory for a metabolic switch between astrocytes and neurons, as presented by Mitz et al. (2009). The overall mitochondrial density is lower in adult seals than in mice and juvenile seals, which could be related to a suppression of synaptic activity (Geiseler et al., 2016; Geßner et al., 2022) and a cerebral metabolic depression during diving (Larson et al., 2014; Ramirez et al., 2007). Juvenile hooded seal brains, however, do have higher mitochondrial densities in the neurons than in the astrocytes, and their overall mitochondrial densities are elevated compared to those of adult seals. This could imply that the metabolic switch between astrocytes and neurons and the suppressed synaptic transmission and cerebral hypometabolism, is age dependent and related to the development of diving capacity (Folkow et al., 2010).

The use of immunostaining, fluorescence microscopy and image analysis has proven to be a promising method for mitochondrial quantification in fixed brain tissue. There were, however, substantial differences in the two measurement methods, mitochondrial mean fluorescence intensity and mitochondrial counts. The increased sensitivity to noise and opposing results to previous studies in mice, suggest that mitochondrial mean fluorescence intensity might not be a reliable proxy of mitochondrial density, whereas direct mitochondrial counts are more reliable. Several methodological considerations however suggests that the method for estimating mitochondrial densities needs further consideration and research development.

References

Alano, C. C., Tran, A., Tao, R., Ying, W., Karliner, J. S., & Swanson, R. A. (2007). Differences among cell types in NAD+ compartmentalization: A comparison of neurons, astrocytes, and cardiac myocytes. *Journal of Neuroscience Research*, *85*(15). https://doi.org/10.1002/jnr.21479

Alle, H., Roth, A., & Geiger, J. R. P. (2009). Energy-efficient action potentials in hippocampal mossy fibers. *Science*. https://doi.org/10.1126/science.1174331

Allen, N. J., Káradóttir, R., & Attwell, D. (2005). A preferential role for glycolysis in preventing the anoxic depolarization of rat hippocampal area CA1 pyramidal cells. *Journal of Neuroscience*, *25*(4). https://doi.org/10.1523/JNEUROSCI.4157-04.2005

Attwell, D., & Laughlin, S. B. (2001). An energy budget for signaling in the grey matter of the brain. In *Journal of Cerebral Blood Flow and Metabolism* (Vol. 21, Issue 10). https://doi.org/10.1097/00004647-200110000-00001

Beard, E., Lengacher, S., Dias, S., Magistretti, P. J., & Finsterwald, C. (2022). Astrocytes as Key Regulators of Brain Energy Metabolism: New Therapeutic Perspectives. In *Frontiers in Physiology* (Vol. 12). https://doi.org/10.3389/fphys.2021.825816

Bélanger, M., Allaman, I., & Magistretti, P. J. (2011). Brain energy metabolism: Focus on Astrocyte-neuron metabolic cooperation. In *Cell Metabolism* (Vol. 14, Issue 6). https://doi.org/10.1016/j.cmet.2011.08.016

Bereiter-Hahn, J. (1990). Behavior of Mitochondria in the Living Cell. *International Review of Cytology*, *122*(C). https://doi.org/10.1016/S0074-7696(08)61205-X

Birrell, G. B., Hedberg, K. K., & Griffith, O. H. (1987). Pitfalls of immunogold labeling: analysis by light microscopy, transmission electron microscopy, and photoelectron microscopy. *The Journal of Histochemistry and Cytochemistry : Official Journal of the Histochemistry Society*, *35*(8). https://doi.org/10.1177/35.8.2439584

Bittar, P. G., Charnay, Y., Pellerin, L., Bouras, C., & Magistretti, P. J. (1996). Selective distribution of lactate dehydrogenase isoenzymes in neurons and astrocytes of human brain. *Journal of Cerebral Blood Flow and Metabolism*, *16*(6), 1079–1089. https://doi.org/10.1097/00004647-199611000-00001/ASSET/IMAGES/LARGE/10.1097_00004647-199611000-00001-FIG6.JPEG

Blix, A. S. (2005). *Arctic animals and their adaptations to life on the edge*. Tapir Academic Press.

Blix, A. S. (2018). Adaptations to deep and prolonged diving in phocid seals. In *Journal of Experimental Biology* (Vol. 221, Issue 12). Company of Biologists Ltd. https://doi.org/10.1242/JEB.182972

Blix, A. S., Elsner, R., & Kjekshus, J. K. (1983). Cardiac output and its distribution through capillaries and A-V shunts in diving seals. *Acta Physiologica Scandinavica*, *118*(2). https://doi.org/10.1111/j.1748-1716.1983.tb07250.x

Blix, A. S., Walløe, L., Messelt, E. B., & Folkow, L. P. (2010). Selective brain cooling and its vascular basis in diving seals. *Journal of Experimental Biology*, *213*(15). https://doi.org/10.1242/jeb.040345

Blomgren, K., & Hagberg, H. (2006). Free radicals, mitochondria, and hypoxia-ischemia in the developing brain. In *Free Radical Biology and Medicine* (Vol. 40, Issue 3). https://doi.org/10.1016/j.freeradbiomed.2005.08.040

Bolaños, J. P., Peuchen, S., Heales, S. J. R., Land, J. M., & Clark, J. B. (1994). Nitric oxide-mediated inhibition of the mitochondrial respiratory chain in cultured astrocytes. *Journal of Neurochemistry*, *63*(3). https://doi.org/10.1046/j.1471-4159.1994.63030910.x

Bouvier, M., Szatkowski, M., Amato, A., & Attwell, D. (1992). The glial cell glutamate uptake carrier countertransports pH-changing anions. *Nature*, *360*(6403).

https://doi.org/10.1038/360471a0
Bowen, W. D., Oftedal, O. T., & Boness, D. J. (1985). Birth to weaning in 4 days: remarkable growth in the hooded seal, Cystophora cristata. *Canadian Journal of Zoology*, *63*(12). https://doi.org/10.1139/z85-424
Bron, K. M., Murdaugh, H. V., Millen, J. E., Lenthall, R., Raskin, P., & Robin, E. D. (1966). Arterial Constrictor Response in a Diving Mammal. *Science*, *152*(3721), 540–543. https://doi.org/10.1126/SCIENCE.152.3721.540
Brooks, M. E., Kristensen, K., van Benthem, K. J., Magnusson, A., Berg, C. W., Nielsen, A., Skaug, H. J., Mächler, M., & Bolker, B. M. (2017). glmmTMB balances speed and flexibility among packages for zero-inflated generalized linear mixed modeling. *R Journal*, *9*(2). https://doi.org/10.32614/rj-2017-066
Brown, A. M. (2004). Brain glycogen re-awakened. *Journal of Neurochemistry*, *89*(3), 537–552. https://doi.org/10.1111/J.1471-4159.2004.02421.X
Burmester, T., & Hankeln, T. (2009). Commentary what is the function of neuroglobin? *Journal of Experimental Biology*, *212*(10). https://doi.org/10.1242/jeb.000729
Burmester, T., Welch, B., Reinhardt, S., & Hankeln, T. (2000). A verteblrate globin expressed in the brain. *Nature*, *407*(6803). https://doi.org/10.1038/35035093
Burns, J. M., Lestyk, K. C., Folkow, L. P., Hammill, M. O., & Blix, A. S. (2007). Size and distribution of oxygen stores in harp and hooded seals from birth to maturity. *Journal of Comparative Physiology B: Biochemical, Systemic, and Environmental Physiology*, *177*(6), 687–700. https://doi.org/10.1007/s00360-007-0167-2
Bussolati, G., & Radulescu, R. T. (2011). Blocking endogenous peroxidases in immunohistochemistry: A mandatory, yet also subtle measure. In *Applied Immunohistochemistry and Molecular Morphology* (Vol. 19, Issue 5). https://doi.org/10.1097/PAI.0b013e318219a6e6
Chance, B., & Williams, G. R. (1956). The respiratory chain and oxidative phosphorylation. In *Advances in Enzymology and Related Subjects of Biochemistry* (Vol. 17). https://doi.org/10.1002/9780470122624.ch2
Chang, D. T. W., Honick, A. S., & Reynolds, I. J. (2006). Mitochondrial trafficking to synapses in cultured primary cortical neurons. *Journal of Neuroscience*, *26*(26). https://doi.org/10.1523/JNEUROSCI.1012-06.2006
Chryssanthopoulos, C., Williams, C., Nowitz, A., & Bogdanis, G. (2004). Skeletal muscle glycogen concentration and metabolic responses following a high glycaemic carbohydrate breakfast. *Journal of Sports Sciences*, *22*(11–12). https://doi.org/10.1080/02640410410001730007
Collins, T. J., Berridge, M. J., Lipp, P., & Bootman, M. D. (2002). Mitochondria are morphologically and functionally heterogeneous within cells. *EMBO Journal*, *21*(7). https://doi.org/10.1093/emboj/21.7.1616
Cruz, N. F., & Dienel, G. A. (2002). High glycogen levels in brains of rats with minimal environmental stimuli: Implications for metabolic contributions of working astrocytes. *Journal of Cerebral Blood Flow and Metabolism*, *22*(12). https://doi.org/10.1097/01.WCB.0000034362.37277.C0
Curti, D., Giangare, M. C., Redolfi, M. E., Fugaccia, I., & Benzi, G. (1990). Age-related modifications of cytochrome c oxidase activity in discrete brain regions. *Mechanisms of Ageing and Development*, *55*(2). https://doi.org/10.1016/0047-6374(90)90024-A
Czech-Damal, N. U., Geiseler, S. J., Hoff, M. L. M., Schliep, R., Ramirez, J. M., Folkow, L. P., & Burmester, T. (2014). The role of glycogen, glucose and lactate in neuronal activity during hypoxia in the hooded seal (Cystophora cristata) brain. *Neuroscience*, *275*, 374–383. https://doi.org/10.1016/J.NEUROSCIENCE.2014.06.024
De Boer, P., Hoogenboom, J. P., & Giepmans, B. N. G. (2015). Correlated light and electron

microscopy: Ultrastructure lights up! In *Nature Methods* (Vol. 12, Issue 6). https://doi.org/10.1038/nmeth.3400
Dehmelt, L., & Halpain, S. (2005). The MAP2/Tau family of microtubule-associated proteins. In *Genome Biology* (Vol. 6, Issue 1). https://doi.org/10.1186/gb-2004-6-1-204
Derouiche, A., Haseleu, J., & Korf, H. W. (2015). Fine Astrocyte Processes Contain Very Small Mitochondria: Glial Oxidative Capability May Fuel Transmitter Metabolism. *Neurochemical Research*, *40*(12). https://doi.org/10.1007/s11064-015-1563-8
Duka, T., Anderson, S. M., Collins, Z., Raghanti, M. A., Ely, J. J., Hof, P. R., Wildman, D. E., Goodman, M., Grossman, L. I., & Sherwood, C. C. (2014). Synaptosomal lactate Dehydrogenase Isoenzyme composition is shifted toward aerobic forms in primate brain evolution. *Brain, Behavior and Evolution*, *83*(3). https://doi.org/10.1159/000358581
Elsner, R., Øyasæter, S., Almaas, R., & Saugstad, O. D. (1998). Diving seals, ischemia-reperfusion and oxygen radicals. *Comparative Biochemistry and Physiology - A Molecular and Integrative Physiology*, *119*(4). https://doi.org/10.1016/S1095-6433(98)00012-9
Eng, L. F., Ghirnikar, R. S., & Lee, Y. L. (2000). Glial Fibrillary Acidic Protein: GFAP-Thirty-One Years (1969-2000). *Neurochemical Research*, *25*(9–10). https://doi.org/10.1023/a:1007677003387
Epstein, F. H., & McCord, J. M. (1985). Oxygen-Derived Free Radicals in Postischemic Tissue Injury. *New England Journal of Medicine*, *312*(3). https://doi.org/10.1056/nejm198501173120305
Erecińska, M., & Silver, I. A. (2001). Tissue oxygen tension and brain sensitivity to hypoxia. *Respiration Physiology*, *128*(3), 263–276. https://doi.org/10.1016/S0034-5687(01)00306-1
Faitg, J., Lacefield, C., Davey, T., White, K., Laws, R., Kosmidis, S., Reeve, A. K., Kandel, E. R., Vincent, A. E., & Picard, M. (2021). 3D neuronal mitochondrial morphology in axons, dendrites, and somata of the aging mouse hippocampus. *Cell Reports*, *36*(6). https://doi.org/10.1016/j.celrep.2021.109509
Fogo, G. M., Anzell, A. R., Maheras, K. J., Raghunayakula, S., Wider, J. M., Emaus, K. J., Bryson, T. D., Bukowski, M. J., Neumar, R. W., Przyklenk, K., & Sanderson, T. H. (2021). Machine learning-based classification of mitochondrial morphology in primary neurons and brain. *Scientific Reports*, *11*(1). https://doi.org/10.1038/s41598-021-84528-8
Folkow, L. P., & Blix, A. S. (1995). Distribution and diving behaviour of hooded seals. *Developments in Marine Biology*, *4*(C). https://doi.org/10.1016/S0163-6995(06)80023-5
Folkow, L. P., & Blix, A. S. (1999). Diving behaviour of hooded seals (Cystophora cristata) in the Greenland and Norwegian Seas. *Polar Biology*, *22*(1), 61–74. https://doi.org/10.1007/s003000050391
Folkow, L. P., Nordøy, E. S., & Blix, A. S. (2010). Remarkable development of diving performance and migrations of hooded seals (Cystophora cristata) during their first year of life. *Polar Biology*, *33*(4). https://doi.org/10.1007/s00300-009-0718-y
Folkow, L. P., Ramirez, J. M., Ludvigsen, S., Ramirez, N., & Blix, A. S. (2008). Remarkable neuronal hypoxia tolerance in the deep-diving adult hooded seal (Cystophora cristata). *Neuroscience Letters*, *446*(2–3). https://doi.org/10.1016/j.neulet.2008.09.040
Geiseler, S. J., Larson, J., & Folkow, L. P. (2016). Synaptic transmission despite severe hypoxia in hippocampal slices of the deep-diving hooded seal. *Neuroscience*, *334*. https://doi.org/10.1016/j.neuroscience.2016.07.034
Geßner, C., Krüger, A., Folkow, L. P., Fehrle, W., Mikkelsen, B., & Burmester, T. (2022). Transcriptomes Suggest That Pinniped and Cetacean Brains Have a High Capacity for Aerobic Metabolism While Reducing Energy-Intensive Processes Such as Synaptic Transmission. *Frontiers in Molecular Neuroscience*, *15*.

https://doi.org/10.3389/fnmol.2022.877349
Gulyás, A. I., Buzsáki, G., Freund, T. F., & Hirase, H. (2006). Populations of hippocampal inhibitory neurons express different levels of cytochrome c. *European Journal of Neuroscience*, *23*(10). https://doi.org/10.1111/j.1460-9568.2006.04814.x
Halassa, M. M., Fellin, T., Takano, H., Dong, J. H., & Haydon, P. G. (2007). Synaptic islands defined by the territory of a single astrocyte. *Journal of Neuroscience*, *27*(24). https://doi.org/10.1523/JNEUROSCI.1419-07.2007
Halim, N. D., Mcfate, T., Mohyeldin, A., Okagaki, P., Korotchkina, L. G., Patel, M. S., Jeoung, N. H., Harris, R. A., Schell, M. J., & Verma, A. (2010). Phosphorylation status of pyruvate dehydrogenase distinguishes metabolic phenotypes of cultured rat brain astrocytes and neurons. *GLIA*, *58*(10). https://doi.org/10.1002/glia.20996
Halliwell, B. (2006). Oxidative stress and neurodegeneration: Where are we now? In *Journal of Neurochemistry* (Vol. 97, Issue 6). https://doi.org/10.1111/j.1471-4159.2006.03907.x
Hammill, M. O., & Stenson, G. B. (2000). Estimated prey consumption by harp seals (phoca groenlandica), hooded seals (cystophora cristata), grey seals (halichoerus grypus) and harbour seals (phoca vitulina) in Atlantic Canada. *Journal of Northwest Atlantic Fishery Science*, *26*. https://doi.org/10.2960/J.v26.a1
Hansen, A. J., & Nedergaard, M. (1988). Brain ion homeostasis in cerebral ischemia. *Neurochemical Pathology*, *9*(1). https://doi.org/10.1007/BF03160362
Harris, J. J., Jolivet, R., & Attwell, D. (2012). Synaptic Energy Use and Supply. In *Neuron*. https://doi.org/10.1016/j.neuron.2012.08.019
Haug, T., Nilssen, K. T., & Lindblom, L. (2004). Feeding habits of harp and hooded seals in drift ice waters along the east coast of Greenland in summer and winter. *Polar Research*, *23*(1). https://doi.org/10.1111/j.1751-8369.2004.tb00127.x
Hauksson, E., & Bogason, V. (1997). Comparative feeding of grey (Halichoerus grypus) and common seals (Phoca vitulina) in coastal waters of Iceland, with a note on the diet of hooded (Cystophora cristata) and harp seals (Phoca groenlandica). *Journal of Northwest Atlantic Fishery Science*, *22*. https://doi.org/10.2960/J.v22.a11
Hill, R. W., Wyse, G. A., & Anderson, M. (2016). *Animal Physiology* (Fourth edi). Sinauer Associates, Inc. Publishers.
Hoff, M. L. M., Fabrizius, A., Folkow, L. P., & Burmester, T. (2016). An atypical distribution of lactate dehydrogenase isoenzymes in the hooded seal (Cystophora cristata) brain may reflect a biochemical adaptation to diving. *Journal of Comparative Physiology B: Biochemical, Systemic, and Environmental Physiology*, *186*(3), 373–386. https://doi.org/10.1007/s00360-015-0956-y
Hollenbeck, P. J., & Saxton, W. M. (2005). The axonal transport of mitochondria. *Journal of Cell Science*, *118*(23). https://doi.org/10.1242/jcs.02745
Hyder, F., Patel, A. B., Gjedde, A., Rothman, D. L., Behar, K. L., & Shulman, R. G. (2006). Neuronal-glial glucose oxidation and glutamatergic-GABAergic function. In *Journal of Cerebral Blood Flow and Metabolism* (Vol. 26, Issue 7). https://doi.org/10.1038/sj.jcbfm.9600263
Hyder, F., Rothman, D. L., & Bennett, M. R. (2013). Cortical energy demands of signaling and nonsignaling components in brain are conserved across mammalian species and activity levels. *Proceedings of the National Academy of Sciences of the United States of America*, *110*(9), 3549–3554. https://doi.org/10.1073/PNAS.1214912110/SUPPL_FILE/PNAS.201214912SI.PDF
ICES. (2019). ICES/NAFO/NAMMCO Working Group on Harp and Hooded Seals (WGHARP). *ICES Scientific Reports*, *1*(72).
Jefferson, T. A., Webber, M. A., & Pitman, R. L. (2015). Pinnipeds. *Marine Mammals of the World*, 358–522. https://doi.org/10.1016/B978-0-12-409542-7.50005-6

Kalil, R. E. (1989). Synapse formation in the developing brain. *Scientific American*, *261*(6). https://doi.org/10.1038/scientificamerican1289-76

Katayama, Y., Kawamata, T., Tamura, T., Hovda, D. A., Becker, D. P., & Tsubokawa, T. (1991). Calcium-dependent glutamate release concomitant with massive potassium flux during cerebral ischemia in vivo. *Brain Research*, *558*(1). https://doi.org/10.1016/0006-8993(91)90730-J

Katsura, K., Kristian, T., & Siesjo, B. K. (1994). Energy metabolism, ion homeostasis, and cell damage in the brain. *Biochemical Society Transactions*, *22*(4), 991–996. https://doi.org/10.1042/bst0220991

Kennedy, M. B. (2016). Synaptic signaling in learning and memory. *Cold Spring Harbor Perspectives in Biology*, *8*(2). https://doi.org/10.1101/cshperspect.a016824

Kesaraju, S., Schmidt-Kastner, R., Prentice, H. M., & Milton, S. L. (2009). Modulation of stress proteins and apoptotic regulators in the anoxia tolerant turtle brain. *Journal of Neurochemistry*, *109*(5). https://doi.org/10.1111/j.1471-4159.2009.06068.x

Khan, A. A., Wang, Y., Sun, Y., Xiao, O. M., Xie, L., Miles, E., Graboski, J., Chen, S., Ellerby, L. M., Jin, K., & Greenberg, D. A. (2006). Neuroglobin-overexpressing transgenic mice are resistant to cerebral and myocardial ischemia. *Proceedings of the National Academy of Sciences of the United States of America*, *103*(47). https://doi.org/10.1073/pnas.0607497103

Kimelberg, H. K., & Norenberg, M. D. (1989). Astrocytes. In *Scientific American*. https://doi.org/10.1038/scientificamerican0489-66

Kovacs, K. M., & Lavigne, D. M. (1986). *Cystophora cristata. Mammalian Species*.

Kristián, T., Hopkins, I. B., McKenna, M. C., & Fiskum, G. (2006a). Isolation of mitochondria with high respiratory control from primary cultures of neurons and astrocytes using nitrogen cavitation. *Journal of Neuroscience Methods*, *152*(1–2), 136–143. https://doi.org/10.1016/j.jneumeth.2005.08.018

Kristián, T., Hopkins, I. B., McKenna, M. C., & Fiskum, G. (2006b). Isolation of mitochondria with high respiratory control from primary cultures of neurons and astrocytes using nitrogen cavitation. *Journal of Neuroscience Methods*, *152*(1–2), 136–143. https://doi.org/10.1016/J.JNEUMETH.2005.08.018

Kummitha, C. M., Kalhan, S. C., Saidel, G. M., & Lai, N. (2014). Relating tissue/organ energy expenditure to metabolic fluxes in mouse and human: Experimental data integrated with mathematical modeling. *Physiological Reports*, *2*(9). https://doi.org/10.14814/phy2.12159

Larson, J., Drew, K. L., Folkow, L. P., Milton, S. L., & Park, T. J. (2014). No oxygen? No problem! intrinsic brain tolerance to hypoxia in vertebrates. In *Journal of Experimental Biology* (Vol. 217, Issue 7). https://doi.org/10.1242/jeb.085381

Lenth, R. V., Bolker, B., Buerkner, P., Giné-Vázquez, l., Herve, M., Jung, M., Love, J., Miguez, F., Riebl, H., & Singmann, H. (2023). Package "emmeans." In *American Statistician* (Vol. 34, Issue 4).

Lewis, M. R., & Lewis, W. H. (1915). Mitochondria (and other cytoplasmic structures) in tissue cultures. *American Journal of Anatomy*, *17*(3). https://doi.org/10.1002/aja.1000170304

Likhithaswamy, H. R., Madhushankari, G. S., Selvamani, M., Mohan Kumar, K. P., Kokila, G., & Mahalakshmi, S. (2022). Assessing the quality of long-term stored tissues in formalin and in paraffin-embedded blocks for histopathological analysis. *Journal of Microscopy and Ultrastructure*, *10*(1). https://doi.org/10.4103/JMAU.JMAU_53_20

Ludvigsen, S. (2010). Neuronal hypoxia tolerance in diving endotherms. *Dissertation Thesis*.

Magistretti, P. J., & Allaman, I. (2015). *Review A Cellular Perspective on Brain Energy Metabolism and Functional Imaging*. https://doi.org/10.1016/j.neuron.2015.03.035

Magistretti, P. J., & Chatton, J. Y. (2005). Relationship between L-glutamate-regulated intracellular Na+ dynamics and ATP hydrolysis in astrocytes. *Journal of Neural Transmission*, *112*(1), 77–85. https://doi.org/10.1007/s00702-004-0171-6

Mamczur, P., Borsuk, B., Paszko, J., Sas, Z., Mozrzymas, J., Wiśniewski, J. R., Gizak, A., & Rakus, D. (2015). Astrocyte-neuron crosstalk regulates the expression and subcellular localization of carbohydrate metabolism enzymes. *GLIA*, *63*(2). https://doi.org/10.1002/glia.22753

Medawar, P. B. (1941). III.—THE RATE OF PENETRATION OF FIXATIVES. *Journal of the Royal Microscopical Society*, *61*(1–2). https://doi.org/10.1111/j.1365-2818.1941.tb00884.x

Meir, J. U., Champagne, C. D., Costa, D. P., Williams, C. L., & Ponganis, P. J. (2009). Extreme hypoxemic tolerance and blood oxygen depletion in diving elephant seals. *American Journal of Physiology - Regulatory Integrative and Comparative Physiology*, *297*(4). https://doi.org/10.1152/ajpregu.00247.2009

Meldrum, B. S. (2000). Glutamate as a neurotransmitter in the brain: Review of physiology and pathology. *Journal of Nutrition*, *130*(4 SUPPL.). https://doi.org/10.1093/jn/130.4.1007s

Mink, J. W., Blumenschine, R. J., & Adams, D. B. (1981). Ratio of central nervous system to body metabolism in vertebrates: its constancy and functional basis. *Https://Doi.Org/10.1152/Ajpregu.1981.241.3.R203*, *10*(2), 203–212. https://doi.org/10.1152/AJPREGU.1981.241.3.R203

Mitz, S. A., Reuss, S., Folkow, L. P., Blix, A. S., Ramirez, J. M., Hankeln, T., & Burmester, T. (2009). When the brain goes diving: glial oxidative metabolism may confer hypoxia tolerance to the seal brain. *Neuroscience*, *163*(2), 552–560. https://doi.org/10.1016/j.neuroscience.2009.06.058

Mjaatvedt, A. E., & Wong-Riley, M. T. T. (1988). Relationship between synaptogenesis and cytochrome oxidase activity in Purkinje cells of the developing rat cerebellum. *Journal of Comparative Neurology*, *277*(2). https://doi.org/10.1002/cne.902770202

Odell, I. D., & Cook, D. (2013). Immunofluorescence techniques. *Journal of Investigative Dermatology*, *133*(1). https://doi.org/10.1038/jid.2012.455

Otsu, N. (1979). THRESHOLD SELECTION METHOD FROM GRAY-LEVEL HISTOGRAMS. *IEEE Trans Syst Man Cybern*, *SMC-9*(1). https://doi.org/10.1109/tsmc.1979.4310076

Pellerin, L., & Magistretti, P. J. (1994). Glutamate uptake into astrocytes stimulates aerobic glycolysis: A mechanism coupling neuronal activity to glucose utilization (glutamate transporter/Na+/K+-ATPase/2-deoxyglucose/positron-embsson tomography/magnetic resonance imaging). In *Proc. Natd. Acad. Sci. USA* (Vol. 91).

Phelps, C. H. (1972). Barbiturate-induced glycogen accumulation in brain. An electron microscopic study. *Brain Research*, *39*(1). https://doi.org/10.1016/0006-8993(72)90797-4

Pierre, K., & Pellerin, L. (2005). Monocarboxylate transporters in the central nervous system: Distribution, regulation and function. In *Journal of Neurochemistry* (Vol. 94, Issue 1). https://doi.org/10.1111/j.1471-4159.2005.03168.x

Pysh, J. J. (1970). Mitochondrial changes in rat inferior colliculus during postnatal development: An electron microscopic study. *Brain Research*, *18*(2). https://doi.org/10.1016/0006-8993(70)90332-X

Quintana, D. D., Garcia, J. A., Sarkar, S. N., Jun, S., Engler-Chiurazzi, E. B., Russell, A. E., Cavendish, J. Z., & Simpkins, J. W. (2019). Hypoxia-reoxygenation of primary astrocytes results in a redistribution of mitochondrial size and mitophagy. *Mitochondrion*, *47*. https://doi.org/10.1016/j.mito.2018.12.004

Qvist, J., Hill, R. D., Schneider, R. C., Falke, K. J., Liggins, G. C., Guppy, M., Elliot, R. L., Hochachka, P. W., & Zapol, W. M. (1986). Hemoglobin concentrations and blood gas tensions of free-diving Weddell seals. *Journal of Applied Physiology*, *61*(4), 1560–1569. https://doi.org/10.1152/jappl.1986.61.4.1560

Ramirez, J. M., Folkow, L. P., & Blix, A. S. (2007). Hypoxia tolerance in mammals and birds: From the wilderness to the clinic. In *Annual Review of Physiology* (Vol. 69). https://doi.org/10.1146/annurev.physiol.69.031905.163111

Rothstein, J. D., Dykes-Hoberg, M., Pardo, C. A., Bristol, L. A., Jin, L., Kuncl, R. W., Kanai, Y., Hediger, M. A., Wang, Y., Schielke, J. P., & Welty, D. F. (1996). Knockout of glutamate transporters reveals a major role for astroglial transport in excitotoxicity and clearance of glutamate. *Neuron*. https://doi.org/10.1016/S0896-6273(00)80086-0

Schindelin, J., Arganda-Carreras, I., Frise, E., Kaynig, V., Longair, M., Pietzsch, T., Preibisch, S., Rueden, C., Saalfeld, S., Schmid, B., Tinevez, J. Y., White, D. J., Hartenstein, V., Eliceiri, K., Tomancak, P., & Cardona, A. (2012). Fiji: An open-source platform for biological-image analysis. In *Nature Methods* (Vol. 9, Issue 7). https://doi.org/10.1038/nmeth.2019

Schneuer, M., Flachsbarth, S., Czech-Damal, N. U., Folkow, L. P., Siebert, U., & Burmester, T. (2012). Neuroglobin of seals and whales: Evidence for a divergent role in the diving brain. *Neuroscience*, *223*. https://doi.org/10.1016/j.neuroscience.2012.07.052

Schurr, A., West, C. A., & Rigor, B. M. (1988). Lactate-supported synaptic function in the rat hippocampal slice preparation. *Science Science*, *240*(4857). https://doi.org/10.1126/science.3375817

Shihan, M. H., Novo, S. G., Le Marchand, S. J., Wang, Y., & Duncan, M. K. (2021). A simple method for quantitating confocal fluorescent images. *Biochemistry and Biophysics Reports*, *25*. https://doi.org/10.1016/j.bbrep.2021.100916

Song, W., Bossy, B., Martin, O. J., Hicks, A., Lubitz, S., Knott, A. B., & Bossy-Wetzel, E. (2008). Assessing mitochondrial morphology and dynamics using fluorescence wide-field microscopy and 3D image processing. *Methods*, *46*(4). https://doi.org/10.1016/j.ymeth.2008.10.003

Thompson, D., & Fedak, M. A. (1993). Cardiac responses of grey seals during diving at sea. *The Journal of Experimental Biology*, *174*. https://doi.org/10.1242/jeb.174.1.139

Turney, S. (2023). *Pearson Correlation Coefficient (r) | Guide & Examples. Scribbr.* https://www.scribbr.com/statistics/pearson-correlation-coefficient/

Vacquie-Garcia, J., Lydersen, C., Biuw, M., Haug, T., Fedak, M. A., & Kovacs, K. M. (2017). *Hooded seal Cystophora cristata foraging areas in the Northeast Atlantic Ocean-Investigated using three complementary methods*. https://doi.org/10.1371/journal.pone.0187889

Vaishnavi, S. N., Vlassenko, A. G., Rundle, M. M., Snyder, A. Z., Mintun, M. A., & Raichle, M. E. (2010). Regional aerobic glycolysis in the human brain. *Proceedings of the National Academy of Sciences of the United States of America*, *107*(41). https://doi.org/10.1073/pnas.1010459107

Walz, W., & Mukerji, S. (1988). Lactate release from cultured astrocytes and neurons: A comparison. *Glia*, *1*(6). https://doi.org/10.1002/glia.440010603

Wang, Z., O'Connor, T. P., Heshka, S., & Heymsfield, S. B. (2001). The reconstruction of Kleiber's law at the organ-tissue level. *Journal of Nutrition*, *131*(11). https://doi.org/10.1093/jn/131.11.2967

Waniewski, R. A., & Martin, D. L. (1986). Exogenous Glutamate Is Metabolized to Glutamine and Exported by Rat Primary Astrocyte Cultures. *Journal of Neurochemistry*, *47*(1). https://doi.org/10.1111/j.1471-4159.1986.tb02863.x

Webster, P., & Webster, A. (2014). Cryosectioning fixed and cryoprotected biological

material for immunocytochemistry. *Methods in Molecular Biology*, *1117*. https://doi.org/10.1007/978-1-62703-776-1_13
Westermann, B. (2012). Bioenergetic role of mitochondrial fusion and fission. *Biochimica et Biophysica Acta - Bioenergetics*, *1817*(10). https://doi.org/10.1016/j.bbabio.2012.02.033
Whittington, N. C., & Wray, S. (2017). Suppression of Red Blood Cell Autofluorescence for Immunocytochemistry on Fixed Embryonic Mouse Tissue. *Current Protocols in Neuroscience*, *81*(1). https://doi.org/10.1002/cpns.35
WHO GHE. (2020). Leading causes of death and disability. The top 10 causes of death. *WHO Reports*, *December*.
Wiemerslage, L., & Lee, D. (2016). Quantification of mitochondrial morphology in neurites of dopaminergic neurons using multiple parameters. *Journal of Neuroscience Methods*, *262*. https://doi.org/10.1016/j.jneumeth.2016.01.008
Wong-Riley, M. T. T. (1989). Cytochrome oxidase: an endogenous metabolic marker for neuronal activity. In *Trends in Neurosciences* (Vol. 12, Issue 3). https://doi.org/10.1016/0166-2236(89)90165-3
Wong-Riley, M. T. T. (2012). Bigenomic regulation of cytochrome c oxidase in neurons and the tight coupling between neuronal activity and energy metabolism. *Advances in Experimental Medicine and Biology*, *748*. https://doi.org/10.1007/978-1-4614-3573-0_12
Yano, M., Kanazawa, M., Terada, K., Takeya, M., Hoogenraad, N., & Mori, M. (1998). Functional analysis of human mitochondrial receptor Tom20 for protein import into mitochondria. *Journal of Biological Chemistry*, *273*(41). https://doi.org/10.1074/jbc.273.41.26844
Yeon, J. H., Ryu, H. R., Chung, M., Hu, Q. P., & Jeon, N. L. (2012). In vitro formation and characterization of a perfusable three-dimensional tubular capillary network in microfluidic devices. *Lab on a Chip*, *12*(16). https://doi.org/10.1039/c2lc40131b
Zapol, W. M., Liggins, G. C., Schneider, R. C., Qvist, J., Snider, M. T., Creasy, R. K., & Hochachka, P. W. (1979). Regional blood flow during simulated diving in the conscious Weddell seal. *Journal of Applied Physiology Respiratory Environmental and Exercise Physiology*, *47*(5). https://doi.org/10.1152/jappl.1979.47.5.968
Zhang, S., Hulver, M. W., McMillan, R. P., Cline, M. A., & Gilbert, E. R. (2014). The pivotal role of pyruvate dehydrogenase kinases in metabolic flexibility. In *Nutrition and Metabolism* (Vol. 11, Issue 1). https://doi.org/10.1186/1743-7075-11-10

Appendixes

Appendix I

Tokuyasu sections - Immunostaining protocol

Based on standardized staining procedures at the Core Facility of Advanced Microscopy (KAM) at UiT.

The tissue sections were attached on poly-L-lysine coated circular coverslips before staining.

1. Wash with room temperature ddH2O 2x10 min.
    a. Place the coverslips in filled petri dishes with the tissue downwards to the liquid.
2. Wash with 37C ddH2O 1x10 min.
3. Incubate with blocking solution (0.8 % cwFSG + 0.1% BSA) for 15 min at room temperature.
4. Dilute primary antibodies in blocking solution to the desired concentrations
5. Incubate with primary antibody (40 ul drops) for 20 min at room temperature.
6. Wash with PBS 5x2 min
7. Dilute secondary antibodies in blocking solution to the desired concentrations
8. Incubate with secondary antibody (40 ul drops) for 15 min at room temperature.
9. Wash with PBS 5x2min
10. Incubate with DAPI (conc?) in PBS for 2 min at room temperature.
11. Wash with ddH2O 3x1min
12. Mount on microscope slide using 10 ul mowiol. Let sit until next day.
13. Store slides in the dark at 4C.

Notes

- When washing the coverslips in ddH2O: Place the coverslips in filled petri dishes with the tissue facing the liquid. The coverslips should float on the water surface.
- The incubations and PBS washes are done with drops on parafilm. The desired amount of liquid is placed as a series of drops on the parafilm and the coverslips are moved with tweezers between the drops
- When moving the coverslips, lift the slide towards the side using a tweezer to minimize the amount of liquid transferred from drop to drop.
- When the incubation time is long, place a petri dish over the coverslips to avoid evaporation.
- Keep the coverslips in the dark after applying secondary antibodies. Turn off the light and cover with aluminum foil boxes.

Appendix II

Staining protocol – cryostat sections

Cut tissue sections (20-40 um) in cryostat

- Immerse tissue blocks in 30% sucrose in PBS overnight (or until they sink)
- Embed tissue block in OCT and cut around it to have a small cutting surface
- Pick up the slices in cryoprotective fluid or directly in PBS
- Wash with PBS 3x2 min
- Transfer to microscopy slides using a paintbrush and drop of dH20 -> soak up fluid with tissue paper
- Store the slides in an airtight container at 4℃

Staining day 1 (ca. 4 hours)

- Dry slides at 50℃ for 30 min
- Draw circle around with a hydro-pen
- Right after drying -> drops of 4% PFA in PBS for 20 min
- Wash with PBS 3x5min
- Antigen retrieval= Citrate buffer at 80℃ for 30 min
- Let cool down to RT
- Wash with PBS 2x5min
- Autofluorescence reduction = 3%H2O2 + 10% MeOH in PBS for 10 min
- Wash with PBS 3x5min
- Draw circle around with a hydro-pen
- Block with BS-T: 0.2 %Triton X in 0.8%cwFSG + 0.1% BSA (100 ul) for 30 min
- Incubate with primary antibody in BS-T (100 ul) over night at 4C

Staining day 2 (ca. 4,5 hours)

- Wash with PBS 3x10min
- Incubate with secondary antibody in BS-T (100 ul) for 90 min at RT
- Wash with PBS 3x10min
- Drops (100 ul) of DAPI (1ul/ml) in PBS for 15 min
- Wash with PBS 2x5 min
- Quenching with True Black: 20x diluted in 70% ethanol -> Immerse in box for 30 seconds
- Wash with PBS 3x10 min
- Wash with dH20 1x2 min
- Mount coverslips on slides with DABCO anti-fade solution and nail polish
- Store slides in the dark at 4℃

Appendix III

QuPath - Image formatting and ROI selection guide.

Based on Christine Labnos Guide "Managing Olympus VS200 Slide Scanner Files in QuPath" University of Chicago, Integrated Light Microscopy Core, 2019.

https://bpb-us-w2.wpmucdn.com/voices.uchicago.edu/dist/c/2275/files/2019/04/Managing-VS200-files-in-QuPath.pdf

The slide scanner creates one .vsi file as well as a folder with .ets files per scanned microscope slide. The following steps were used to transform the images into smaller .tif files that can be used in ImageJ/FIJI for analysis.

1. Start QuPath-0.4.3
2. Open the .vsi file.
    a. The .vsi file has to be in the same folder as the .ets images folder.
    b. All the images for a single slide will show up, but it is only possible to select one at a time. For transforming multiple images per slide, the same .vsi file has to be opened again.
3. Deselect the mitochondrial channel, making only the DAPI and either the neuron or astrocyte channel visible.
4. Scroll through the Z-stacks to find a stack in-focus.
5. Create ROIs
    a. Objects > Annotations > specify annotations..
    b. Set the dimensions to 500 x 500 um and click "create"
    c. Move the ROIs to the preferred regions by marking them in the "Annotations" tab
    d. Save as.. to save the ROIs to the image
6. Send regions to imageJ
    a. Choose "Select all" in the Annotations tab to select all the ROIs
    b. Go to Extensions > ImageJ > send regions to ImageJ
    c. Choose the following options to not change the properties of the image and to include all the z-slices:

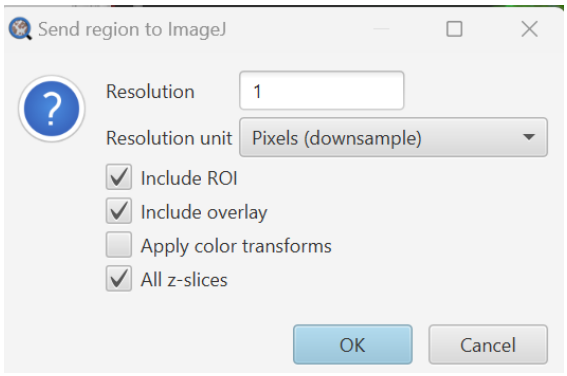

7. Save as .tif file
    a. Wait until image has opened in ImageJ/FIJI. This can take up to 2 minutes.
    b. Go to File > Save as.. > Tiff

Appendix IV

Table Appendix. Overview of *images included and excluded from the analysis* and total *number of manually selected cells*, per cell type and section for each animal. Total number of images included in analysis = 259. Excluded images = 11. Total number of manually selected cells included in analysis = 757.

Animal group	Animal ID	Cell type	Number of images	Number of manually selected cells	Section ID	Number of images per section	Number of manually selected cells per section	Excluded images (n=11) and reasons for exclusion
Adult seal	K1-22	Astrocytes	15	45	A	3	9	M5 astro_C2 = no astrocytes detected M6 astro_A2 = no astrocytes detected M6 astro_B2 = no astrocytes detected M6 astro_D2 = wrinkles in tissue M6 astro_D3 = wrinkles in tissue M6 astro_E1 + E2 + E3 = whole section E was removed due to it being wrinkled and out of focus. M7 astro_E1 = tissue overlapping on section. M7 neuro_A2 = uneven illumination/staining M7 neuro_E3 = crack in the tissue creating a strong stained edge effect.
					B	3	9	
					C	3	9	
					D	3	9	
					E	3	9	
		Neurons	15	40	A	3	9	
					B	3	7	
					C	3	6	
					D	3	9	
					E	3	9	
	K2-22	Astrocytes	15	45	A	3	9	
					B	3	9	
					C	3	9	
					D	3	9	
					E	3	9	
		Neurons	15	45	A	3	9	
					B	3	9	
					C	3	9	
					D	3	9	
					E	3	9	
	K7-22	Astrocytes	15	45	A	3	9	
					B	3	9	
					C	3	9	
					D	3	9	
					E	3	9	
		Neurons	15	45	A	3	9	
					B	3	9	
					C	3	9	
					D	3	9	
					E	3	9	
Juvenile seal	K2A-22	Astrocytes	15	45	A	3	9	
					B	3	9	
					C	3	9	
					D	3	9	
					E	3	9	
		Neurons	15	45	A	3	9	
					B	3	9	
					C	3	9	
					D	3	9	
					E	3	9	
	K7A-22	Astrocytes	15	45	A	3	9	
					B	3	9	
					C	3	9	
					D	3	9	
					E	3	9	
		Neurons	15	45	A	3	9	
					B	3	9	
					C	3	9	
					D	3	9	
					E	3	9	
	K10A-22	Astrocytes	15	45	A	3	9	
					B	3	9	

					C	3	9	
					D	3	9	
					E	3	9	
		Neurons	15	45	A	3	9	
					B	3	9	
					C	3	9	
					D	3	9	
					E	3	9	
Mouse	M5	Astrocytes	14	33	A	3	7	
					B	3	9	
					C	2	3	
					D	3	8	
					E	3	6	
		Neurons	15	41	A	3	8	
					B	3	6	
					C	3	9	
					D	3	9	
					E	3	9	
	M6	Astrocytes	8	22	A	2	6	
					B	2	6	
					C	3	7	
					D	1	3	
					E	Excluded	Excluded	
		Neurons	15	45	A	3	9	
					B	3	9	
					C	3	9	
					D	3	9	
					E	3	9	
	M7	Astrocytes	14	42	A	3	9	
					B	3	9	
					C	3	9	
					D	3	9	
					E	2	6	
		Neurons	13	39	A	2	6	
					B	3	9	
					C	3	9	
					D	3	9	
					E	2	6	

Appendix V

Statistical models:

Mitochondrial counts – Auto selection of cells

```
> summary(MDens_mod4)


 Family: poisson  ( log )
Formula:
Count ~ offset(log(Area)) + Species * Celltype + (1 | AnimalID/SectionID)
Data: MFI_aut

     AIC      BIC   logLik deviance df.resid
 22109.5  22137.9 -11046.7  22093.5      251

Random effects:

Conditional model:
 Groups             Name        Variance Std.Dev.
 SectionID:AnimalID (Intercept) 0.024217 0.15562
 AnimalID           (Intercept) 0.002439 0.04939
Number of obs: 259, groups:  SectionID:AnimalID, 45; AnimalID, 9

Conditional model:
                              Estimate Std. Error z value Pr(>|z|)
(Intercept)                  -2.195656   0.049401  -44.45  < 2e-16 ***
Speciesjuv seal               0.266211   0.069824    3.81 0.000138 ***
Speciesmouse                  0.090142   0.070147    1.29 0.198777
Celltypeneuro                -0.189556   0.004587  -41.33  < 2e-16 ***
Speciesjuv seal:Celltypeneuro 0.524388   0.005594   93.73  < 2e-16 ***
Speciesmouse:Celltypeneuro    0.445258   0.009183   48.49  < 2e-16 ***
---
Signif. codes:  0 ‘***’ 0.001 ‘**’ 0.01 ‘*’ 0.05 ‘.’ 0.1 ‘ ’ 1
> plot_model(MDens_mod4, type="int")
```

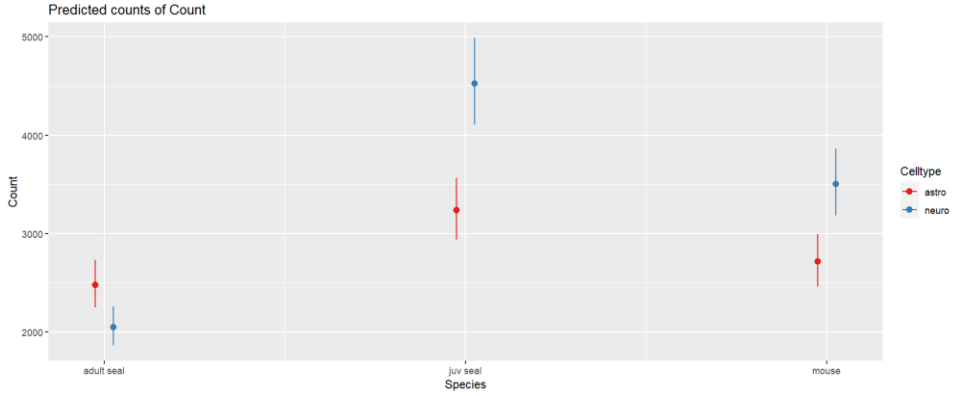


```
> ## pairwise comparison
> lsm.count <- lsmeans(MDens_mod4, c("Species","Celltype"))
> cld(lsm.count, Letters=letters, details = TRUE)
$emmeans
 Species    Celltype lsmean     SE  df asymp.LCL asymp.UCL .group
 adult seal neuro      7.63 0.0494 Inf      7.53      7.72  a
 adult seal astro      7.82 0.0494 Inf      7.72      7.91   b
 mouse      astro      7.91 0.0498 Inf      7.81      8.00   bc
 juv seal   astro      8.08 0.0493 Inf      7.99      8.18    cd
 mouse      neuro      8.16 0.0493 Inf      8.07      8.26     d
 juv seal   neuro      8.42 0.0493 Inf      8.32      8.51      e

Results are given on the log (not the response) scale.
Confidence level used: 0.95
P value adjustment: tukey method for comparing a family of 6 estimates
significance level used: alpha = 0.05
NOTE: If two or more means share the same grouping symbol,
      then we cannot show them to be different.
      But we also did not show them to be the same.

$comparisons
 contrast                              estimate      SE  df z.ratio p.value
 adult seal astro - adult seal neuro     0.1896 0.00459 Inf  41.327  <.0001
 mouse astro - adult seal neuro          0.2797 0.07012 Inf   3.989  0.0009
 mouse astro - adult seal astro          0.0901 0.07015 Inf   1.285  0.7934
 juv seal astro - adult seal neuro       0.4558 0.06980 Inf   6.530  <.0001
 juv seal astro - adult seal astro       0.2662 0.06982 Inf   3.813  0.0019
 juv seal astro - mouse astro            0.1761 0.07011 Inf   2.511  0.1207
 mouse neuro - adult seal neuro          0.5354 0.06980 Inf   7.671  <.0001
 mouse neuro - adult seal astro          0.3458 0.06983 Inf   4.953  <.0001
 mouse neuro - mouse astro               0.2557 0.00796 Inf  32.141  <.0001
 mouse neuro - juv seal astro            0.0796 0.06979 Inf   1.141  0.8642
 juv seal neuro - adult seal neuro       0.7906 0.06976 Inf  11.332  <.0001
 juv seal neuro - adult seal astro       0.6010 0.06979 Inf   8.612  <.0001
 juv seal neuro - mouse astro            0.5109 0.07008 Inf   7.291  <.0001
 juv seal neuro - juv seal astro         0.3348 0.00320 Inf 104.537  <.0001
 juv seal neuro - mouse neuro            0.2552 0.06975 Inf   3.659  0.0035

Results are given on the log (not the response) scale.
P value adjustment: tukey method for comparing a family of 6 estimates
```

Mitochondrial counts – Manual selection of cells

```
> summary(MDens_man5)
 Family: poisson  ( log )
Formula:
Count ~ offset(log(Area)) + Species * Celltype + (1 | AnimalID/SectionID/ImageID)
Data: MFI_man

     AIC      BIC   logLik deviance df.resid
  6158.5   6200.2  -3070.3   6140.5      748

Random effects:

Conditional model:
 Groups                      Name        Variance Std.Dev.
 ImageID:SectionID:AnimalID (Intercept) 0.016304 0.12769
 SectionID:AnimalID         (Intercept) 0.023819 0.15433
 AnimalID                   (Intercept) 0.004263 0.06529
Number of obs: 757, groups:
ImageID:SectionID:AnimalID, 135; SectionID:AnimalID, 45; AnimalID, 9

Conditional model:
                            Estimate Std. Error z value Pr(>|z|)
(Intercept)                -2.265306   0.059808  -37.88  < 2e-16 ***
Speciesjuv seal             0.283461   0.084461    3.36  0.00079 ***
Speciesmouse                0.352444   0.086265    4.09  4.4e-05 ***
Celltypeneuro               0.008539   0.020647    0.41  0.67917
Speciesjuv seal:Celltypeneuro  0.365434   0.027893   13.10  < 2e-16 ***
Speciesmouse:Celltypeneuro     0.065413   0.035658    1.83  0.06659 .
---
Signif. codes:  0 ‘***’ 0.001 ‘**’ 0.01 ‘*’ 0.05 ‘.’ 0.1 ‘ ’ 1
> plot_model(MDens_man5, type="int")
```

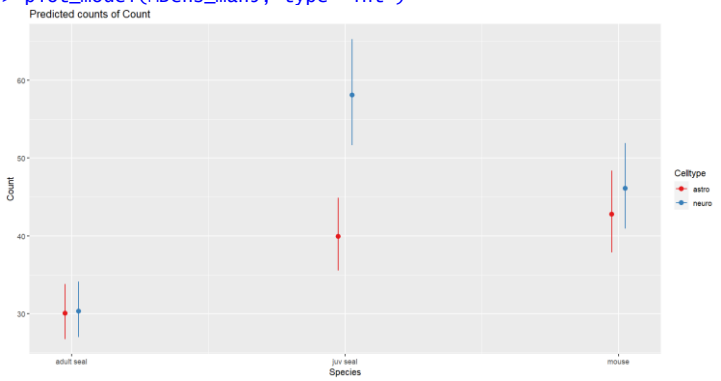


```
> ## pairwise comparison
> lsm.count.man <- lsmeans(MDens_man5, c("Species","Celltype"))
> cld(lsm.count.man, Letters=letters, details = TRUE)
$emmeans
 Species    Celltype lsmean     SE  df asymp.LCL asymp.UCL .group
 adult seal astro      3.40 0.0598 Inf      3.29      3.52  a
 adult seal neuro      3.41 0.0599 Inf      3.30      3.53  a
 juv seal   astro      3.69 0.0596 Inf      3.57      3.80   b
 mouse      astro      3.76 0.0622 Inf      3.63      3.88   b
 mouse      neuro      3.83 0.0605 Inf      3.71      3.95   bc
 juv seal   neuro      4.06 0.0596 Inf      3.95      4.18    c

Results are given on the log (not the response) scale.
Confidence level used: 0.95
P value adjustment: tukey method for comparing a family of 6 estimates
significance level used: alpha = 0.05
NOTE: If two or more means share the same grouping symbol,
      then we cannot show them to be different.
      But we also did not show them to be the same.

$comparisons
 contrast                          estimate     SE  df z.ratio p.value
 adult seal neuro - adult seal astro  0.00854 0.0206 Inf   0.414  0.9985
 juv seal astro - adult seal astro    0.28346 0.0845 Inf   3.356  0.0103
 juv seal astro - adult seal neuro    0.27492 0.0845 Inf   3.252  0.0146
 mouse astro - adult seal astro       0.35244 0.0863 Inf   4.086  0.0006
 mouse astro - adult seal neuro       0.34390 0.0863 Inf   3.983  0.0010
 mouse astro - juv seal astro         0.06898 0.0861 Inf   0.801  0.9675
 mouse neuro - adult seal astro       0.42640 0.0851 Inf   5.011  <.0001
 mouse neuro - adult seal neuro       0.41786 0.0852 Inf   4.907  <.0001
 mouse neuro - juv seal astro         0.14294 0.0850 Inf   1.682  0.5436
 mouse neuro - mouse astro            0.07395 0.0291 Inf   2.543  0.1117
 juv seal neuro - adult seal astro    0.65743 0.0844 Inf   7.789  <.0001
 juv seal neuro - adult seal neuro    0.64890 0.0845 Inf   7.681  <.0001
 juv seal neuro - juv seal astro      0.37397 0.0188 Inf  19.933  <.0001
 juv seal neuro - mouse astro         0.30499 0.0861 Inf   3.542  0.0053
 juv seal neuro - mouse neuro         0.23104 0.0849 Inf   2.721  0.0712

Results are given on the log (not the response) scale.
P value adjustment: tukey method for comparing a family of 6 estimates
```

Adjusted MFI = (MFI-background) – Auto selection of cells

```
> summary(MFI_mod2)
 Family: gaussian  ( identity )
Formula:          Mean_adj ~ Species * Celltype + (1 | AnimalID/SectionID)
Data: MFI_aut

     AIC      BIC   logLik deviance df.resid
  3737.4   3769.4  -1859.7   3719.4      250

Random effects:

Conditional model:
 Groups              Name        Variance Std.Dev.
 SectionID:AnimalID (Intercept) 35952    189.6
 AnimalID           (Intercept) 10644    103.2
 Residual                       78774    280.7
Number of obs: 259, groups:  SectionID:AnimalID, 45; AnimalID, 9

Dispersion estimate for gaussian family (sigma^2): 7.88e+04

Conditional model:
                             Estimate Std. Error z value Pr(>|z|)
(Intercept)                    819.33      87.72   9.340  < 2e-16 ***
Speciesjuv seal                111.46     124.06   0.898 0.368938
Speciesmouse                   653.33     126.41   5.168 2.36e-07 ***
Celltypeneuro                  204.81      59.17   3.461 0.000537 ***
Speciesjuv seal:Celltypeneuro  485.80      83.68   5.806 6.42e-09 ***
Speciesmouse:Celltypeneuro    -517.65      87.74  -5.900 3.63e-09 ***
---
Signif. codes:  0 ‘***’ 0.001 ‘**’ 0.01 ‘*’ 0.05 ‘.’ 0.1 ‘ ’ 1
> plot_model(MFI_mod2, type="int")
```

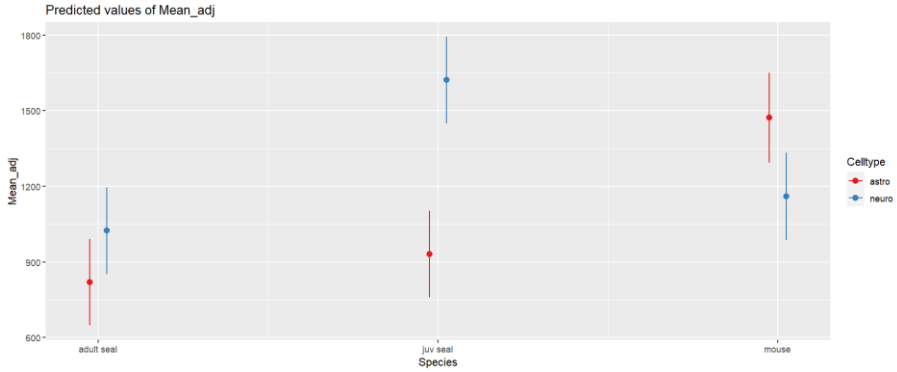


```
> ## pairwise comparison
> lsm.MFI <- lsmeans(MFI_mod2, c("Species","Celltype"))
> cld(lsm.MFI, Letters=letters, details = TRUE)
$emmeans
 Species    Celltype lsmean   SE  df lower.CL upper.CL .group
 adult seal astro       819 87.7 250      647      992  a
 juv seal   astro       931 87.7 250      758     1104  ab
 adult seal neuro      1024 87.7 250      851     1197   b
 mouse      neuro      1160 88.3 250      986     1334  ab
 mouse      astro      1473 91.0 250     1293     1652    c
 juv seal   neuro      1621 87.7 250     1449     1794    c

Confidence level used: 0.95
P value adjustment: tukey method for comparing a family of 6 estimates
significance level used: alpha = 0.05
NOTE: If two or more means share the same grouping symbol,
      then we cannot show them to be different.
      But we also did not show them to be the same.

$comparisons
 contrast                            estimate    SE  df t.ratio p.value
 juv seal astro - adult seal astro      111.5 124.1 250   0.898  0.9466
 adult seal neuro - adult seal astro    204.8  59.2 250   3.461  0.0082
 adult seal neuro - juv seal astro       93.3 124.1 250   0.752  0.9750
 mouse neuro - adult seal astro         340.5 124.4 250   2.736  0.0718
 mouse neuro - juv seal astro           229.0 124.4 250   1.840  0.4418
 mouse neuro - adult seal neuro         135.7 124.4 250   1.090  0.8850
 mouse astro - adult seal astro         653.3 126.4 250   5.168  <.0001
 mouse astro - juv seal astro           541.9 126.4 250   4.287  0.0004
 mouse astro - adult seal neuro         448.5 126.4 250   3.548  0.0061
 mouse astro - mouse neuro              312.8  64.8 250   4.829  <.0001
 juv seal neuro - adult seal astro      802.1 124.1 250   6.465  <.0001
 juv seal neuro - juv seal astro        690.6  59.2 250  11.672  <.0001
 juv seal neuro - adult seal neuro      597.3 124.1 250   4.814  <.0001
 juv seal neuro - mouse neuro           461.6 124.4 250   3.709  0.0035
 juv seal neuro - mouse astro           148.7 126.4 250   1.177  0.8476

P value adjustment: tukey method for comparing a family of 6 estimates
```

Adjusted MFI = (MFI-background) – Manual selection of cells

```
> summary(MFI_man3)


 Family: gaussian  ( identity )
Formula:
Mean_adj ~ Species * Celltype + (1 | AnimalID/SectionID/ImageID)
Data: MFI_man

     AIC      BIC   logLik deviance df.resid
 11208.4  11254.7  -5594.2  11188.4      747

Random effects:

Conditional model:
 Groups                    Name        Variance Std.Dev.
 ImageID:SectionID:AnimalID (Intercept)  11425   106.9
 SectionID:AnimalID         (Intercept)  47778   218.6
 AnimalID                   (Intercept)   5070    71.2
 Residual                                129241   359.5
Number of obs: 757, groups:
ImageID:SectionID:AnimalID, 135; SectionID:AnimalID, 45; AnimalID, 9

Dispersion estimate for gaussian family (sigma^2): 1.29e+05

Conditional model:
                            Estimate Std. Error z value Pr(>|z|)
(Intercept)                   805.75      78.01  10.328  < 2e-16 ***
Speciesjuv seal               128.54     110.33   1.165    0.244
Speciesmouse                  718.03     112.72   6.370 1.89e-10 ***
Celltypeneuro                 409.45      44.30   9.243  < 2e-16 ***
Speciesjuv seal:Celltypeneuro 331.56      62.26   5.325 1.01e-07 ***
Speciesmouse:Celltypeneuro   -737.47      67.47 -10.931  < 2e-16 ***
---
Signif. codes:  0 ‘***’ 0.001 ‘**’ 0.01 ‘*’ 0.05 ‘.’ 0.1 ‘ ’ 1
> plot_model(MFI_man3, type="int")
```

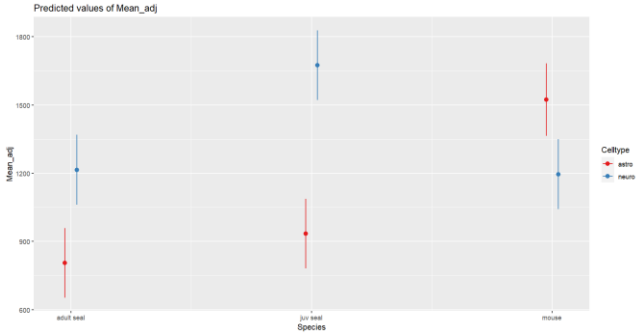


```
> ## pairwise comparison
> lsm.MFI.man <- lsmeans(MFI_man3, c("Species","Celltype"))
> cld(lsm.MFI.man, Letters=letters, details = TRUE)
$emmeans
 Species    Celltype lsmean   SE  df lower.CL upper.CL .group
 adult seal astro       806 78.0 747      653      959  a
 juv seal   astro       934 78.0 747      781     1087  ab
 mouse      neuro      1196 78.7 747     1041     1350   b
 adult seal neuro      1215 78.3 747     1061     1369   bc
 mouse      astro      1524 81.4 747     1364     1684    cd
 juv seal   neuro      1675 78.0 747     1522     1828     d

Confidence level used: 0.95
P value adjustment: tukey method for comparing a family of 6 estimates
significance level used: alpha = 0.05
NOTE: If two or more means share the same grouping symbol,
      then we cannot show them to be different.
      But we also did not show them to be the same.

$comparisons
 contrast                              estimate    SE  df t.ratio p.value
 juv seal astro - adult seal astro        128.5 110.3 747   1.165  0.8533
 mouse neuro - adult seal astro           390.0 110.8 747   3.520  0.0061
 mouse neuro - juv seal astro             261.5 110.8 747   2.360  0.1719
 adult seal neuro - adult seal astro      409.4  44.3 747   9.243  <.0001
 adult seal neuro - juv seal astro        280.9 110.5 747   2.541  0.1137
 adult seal neuro - mouse neuro            19.4 111.0 747   0.175  1.0000
 mouse astro - adult seal astro           718.0 112.7 747   6.370  <.0001
 mouse astro - juv seal astro             589.5 112.7 747   5.230  <.0001
 mouse astro - mouse neuro                328.0  50.9 747   6.446  <.0001
 mouse astro - adult seal neuro           308.6 112.9 747   2.732  0.0702
 juv seal neuro - adult seal astro        869.5 110.3 747   7.881  <.0001
 juv seal neuro - juv seal astro          741.0  43.8 747  16.935  <.0001
 juv seal neuro - mouse neuro             479.5 110.8 747   4.328  0.0002
 juv seal neuro - adult seal neuro        460.1 110.5 747   4.162  0.0005
 juv seal neuro - mouse astro             151.5 112.7 747   1.344  0.7602

P value adjustment: tukey method for comparing a family of 6 estimates
```

Mitochondrial size – Auto selection of cells – Average sizes

```
> summary(Size_mod1)


 Family: gaussian  ( identity )
Formula:          Mean_size ~ Species * Celltype + (1 | AnimalID/SectionID)
Data: MFI_aut

     AIC      BIC   logLik deviance df.resid
  -795.5   -763.5    406.8   -813.5      250

Random effects:

Conditional model:
 Groups              Name        Variance  Std.Dev.
 SectionID:AnimalID (Intercept) 0.0003089 0.01757
 AnimalID           (Intercept) 0.0002712 0.01647
 Residual                       0.0022001 0.04691
Number of obs: 259, groups:  SectionID:AnimalID, 45; AnimalID, 9

Dispersion estimate for gaussian family (sigma^2): 0.0022

Conditional model:
                             Estimate Std. Error z value Pr(>|z|)
(Intercept)                  0.776717   0.012644   61.43  < 2e-16 ***
Speciesjuv seal              0.070073   0.017881    3.92 8.90e-05 ***
Speciesmouse                 0.056492   0.018292    3.09  0.00201 **
Celltypeneuro               -0.077966   0.009888   -7.88 3.16e-15 ***
Speciesjuv seal:Celltypeneuro  0.080783   0.013984    5.78 7.62e-09 ***
Speciesmouse:Celltypeneuro     0.017235   0.014604    1.18  0.23792
---
Signif. codes:  0 ‘***’ 0.001 ‘**’ 0.01 ‘*’ 0.05 ‘.’ 0.1 ‘ ’ 1
> plot_model(Size_mod1, type="int")
```

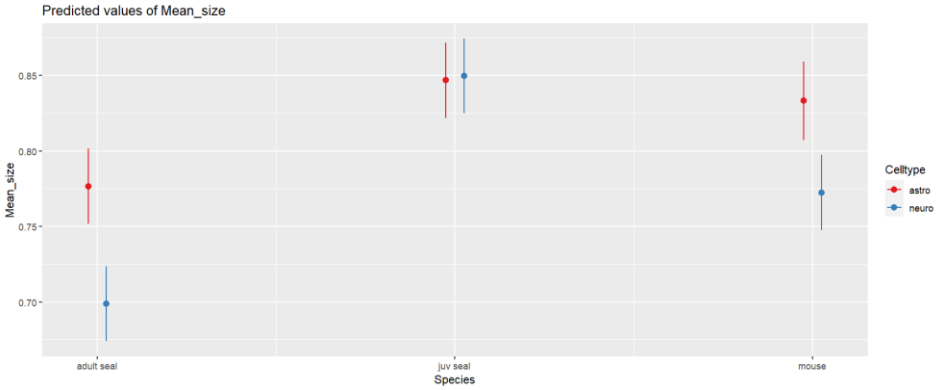


```
> ## pairwise comparison
> lsm.size.aut <- lsmeans(Size_mod1, c("Species","Celltype"))
> cld(lsm.size.aut, Letters=letters, details = TRUE)
$emmeans
 Species    Celltype lsmean     SE  df lower.CL upper.CL .group
 adult seal neuro     0.699 0.0126 250    0.674    0.724  a
 mouse      neuro     0.772 0.0127 250    0.747    0.798   b
 adult seal astro     0.777 0.0126 250    0.752    0.802   b
 mouse      astro     0.833 0.0132 250    0.807    0.859    c
 juv seal   astro     0.847 0.0126 250    0.822    0.872    c
 juv seal   neuro     0.850 0.0126 250    0.825    0.875    c

Confidence level used: 0.95
P value adjustment: tukey method for comparing a family of 6 estimates
significance level used: alpha = 0.05
NOTE: If two or more means share the same grouping symbol,
      then we cannot show them to be different.
      But we also did not show them to be the same.

$comparisons
 contrast                              estimate      SE  df t.ratio p.value
 mouse neuro - adult seal neuro         0.07373 0.01795 250   4.107  0.0008
 adult seal astro - adult seal neuro    0.07797 0.00989 250   7.885  <.0001
 adult seal astro - mouse neuro         0.00424 0.01795 250   0.236  0.9999
 mouse astro - adult seal neuro         0.13446 0.01829 250   7.350  <.0001
 mouse astro - mouse neuro              0.06073 0.01075 250   5.651  <.0001
 mouse astro - adult seal astro         0.05649 0.01829 250   3.088  0.0269
 juv seal astro - adult seal neuro      0.14804 0.01788 250   8.279  <.0001
 juv seal astro - mouse neuro           0.07431 0.01795 250   4.140  0.0007
 juv seal astro - adult seal astro      0.07007 0.01788 250   3.919  0.0016
 juv seal astro - mouse astro           0.01358 0.01829 250   0.742  0.9764
 juv seal neuro - adult seal neuro      0.15086 0.01788 250   8.437  <.0001
 juv seal neuro - mouse neuro           0.07713 0.01795 250   4.296  0.0004
 juv seal neuro - adult seal astro      0.07289 0.01788 250   4.076  0.0009
 juv seal neuro - mouse astro           0.01640 0.01829 250   0.896  0.9471
 juv seal neuro - juv seal astro        0.00282 0.00989 250   0.285  0.9997

P value adjustment: tukey method for comparing a family of 6 estimates
```

Mitochondrial size – Manual selection of cells – average sizes

```
> summary(Size_man1)
 Family: gaussian  ( identity )
Formula:          Mean_size ~ Species * Celltype + (1 | AnimalID/SectionID/ImageID)
Data: MFI_man

     AIC      BIC   logLik deviance df.resid
 -1231.3  -1185.0    625.7  -1251.3      747

Random effects:

Conditional model:
 Groups                     Name        Variance  Std.Dev.
 ImageID:SectionID:AnimalID (Intercept) 0.0013010 0.03607
 SectionID:AnimalID         (Intercept) 0.0008672 0.02945
 AnimalID                   (Intercept) 0.0002351 0.01533
 Residual                               0.0097321 0.09865
Number of obs: 757, groups:
ImageID:SectionID:AnimalID, 135; SectionID:AnimalID, 45; AnimalID, 9

Dispersion estimate for gaussian family (sigma^2): 0.00973

Conditional model:
                             Estimate Std. Error z value Pr(>|z|)
(Intercept)                   0.77734    0.01540   50.47  < 2e-16 ***
Speciesjuv seal               0.07685    0.02178    3.53 0.000418 ***
Speciesmouse                  0.06485    0.02266    2.86 0.004209 **
Celltypeneuro                -0.03373    0.01216   -2.77 0.005528 **
Speciesjuv seal:Celltypeneuro 0.04227    0.01709    2.47 0.013367 *
Speciesmouse:Celltypeneuro   -0.03052    0.01848   -1.65 0.098546 .
---
Signif. codes:  0 ‘***’ 0.001 ‘**’ 0.01 ‘*’ 0.05 ‘.’ 0.1 ‘ ’ 1
> plot_model(Size_man1, type="int")
```

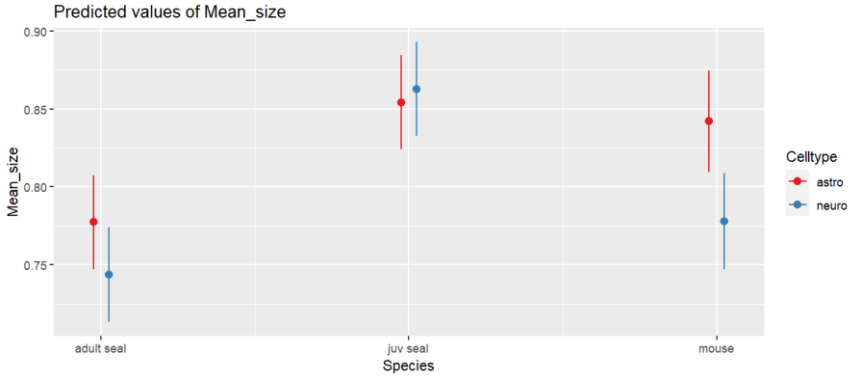


```
> ## pairwise comparison
> lsm.size.man <- lsmeans(Size_man1, c("Species","Celltype"))
> cld(lsm.size.man, Letters=letters, details = TRUE)
$emmeans
 Species    Celltype lsmean     SE  df lower.CL upper.CL .group
 adult seal neuro     0.744 0.0155 747    0.713    0.774  a
 adult seal astro     0.777 0.0154 747    0.747    0.808  a
 mouse      neuro     0.778 0.0157 747    0.747    0.809  a
 mouse      astro     0.842 0.0166 747    0.810    0.875   b
 juv seal   astro     0.854 0.0154 747    0.824    0.884   b
 juv seal   neuro     0.863 0.0154 747    0.832    0.893   b

Confidence level used: 0.95
P value adjustment: tukey method for comparing a family of 6 estimates
significance level used: alpha = 0.05
NOTE: If two or more means share the same grouping symbol,
      then we cannot show them to be different.
      But we also did not show them to be the same.

$comparisons
 contrast                          estimate     SE  df t.ratio p.value
 adult seal astro - adult seal neuro 0.033732 0.0122 747   2.775  0.0627
 mouse neuro - adult seal neuro      0.034325 0.0220 747   1.557  0.6269
 mouse neuro - adult seal astro      0.000593 0.0220 747   0.027  1.0000
 mouse astro - adult seal neuro      0.098581 0.0227 747   4.335  0.0002
 mouse astro - adult seal astro      0.064849 0.0227 747   2.862  0.0493
 mouse astro - mouse neuro           0.064256 0.0139 747   4.616  0.0001
 juv seal astro - adult seal neuro   0.110582 0.0219 747   5.058  <.0001
 juv seal astro - adult seal astro   0.076850 0.0218 747   3.529  0.0059
 juv seal astro - mouse neuro        0.076257 0.0220 747   3.473  0.0072
 juv seal astro - mouse astro        0.012001 0.0227 747   0.530  0.9950
 juv seal neuro - adult seal neuro   0.119122 0.0219 747   5.449  <.0001
 juv seal neuro - adult seal astro   0.085391 0.0218 747   3.921  0.0013
 juv seal neuro - mouse neuro        0.084798 0.0220 747   3.862  0.0017
 juv seal neuro - mouse astro        0.020542 0.0227 747   0.907  0.9448
 juv seal neuro - juv seal astro     0.008541 0.0120 747   0.711  0.9806

P value adjustment: tukey method for comparing a family of 6 estimates
```

Appendix VI

Example of image analysis macro

```
open("filepath");

run("Split Channels");


//Select the astrocyte channel = C3

run("Z Project...", "start=6 stop=10 projection=[Max Intensity]");

run("Find Edges");


//run("Threshold...") and manually adjust it

setAutoThreshold("Otsu dark");

setOption("BlackBackground", true);

run("Convert to Mask");


//Select ROIs

run("Analyze Particles...", "size=5-Infinity display include summarize add
composite");

roiManager("Show All with labels");


//Clean ROIs - Manually remove ROIs that are clearly not cells

roiManager("Select", 855);

roiManager("Delete");

Table.deleteRows(855, 855);

roiManager("Select", 104);

roiManager("Delete");

Table.deleteRows(104, 104);

roiManager("Show All without labels");


//Save astrocyte measurements

saveAs("filepath ");

run("Clear Results");
```

```
//Manually select and rename 3 cells
roiManager("Select", 676);
roiManager("Rename", "c1");
roiManager("Select", 158);
roiManager("Rename", "c2");
roiManager("Select", 704);
roiManager("Rename", "c3");
//Combine all the ROIs to a single ROI
roiManager("Select",);
run("Select All");
roiManager("Combine");
roiManager("Add");

//Save only the manually selected cells and the large single ROI
roiManager("Select", newArray(158,676,704,1541));
roiManager("Save", " filepath ");

//Delete all the ROIs and open the saved ones
run("Select All");
roiManager("Select", );
roiManager("Delete");
roiManager("Open", " filepath ");

//Count mitochondria
selectImage("C1-K7A-22 astro_A1.tif");
run("Z Project...", "start=6 stop=10 projection=[Average Intensity]");
runMacro("C: filepath)
saveAs("Results", "C filepath ");
run("Clear Results");
```

```
//Measure fluorescence intensity of mitochondria

selectImage("AVG_C1-K7A-22 astro_A1.tif");

runMacro("C: filepath /Measure fluorescence intensity.ijm");

saveAs("Results", "C:/ filepath /K7A-22 astro_A1 MFI.csv");

saveAs("Results", "C:/ filepath /K7A-22 astro_A1 summary.csv");
```

mitochondria threshold and count.ijm

```
idOrig = getImageID();

run("Duplicate...", "title=[My duplicated image]");

idDuplicate = getImageID();

run("Median...", "radius=4");

imageCalculator("Subtract create", idOrig, idDuplicate);

setAutoThreshold("Otsu dark");

//run("Threshold...");

setThreshold(50, 65535, "raw");

run("Convert to Mask");

run("Watershed");


roiManager("Select", 0);

run("Analyze Particles...", "size=0.40-Infinity show=Nothing display include
summarize");

roiManager("Select", 1);

run("Analyze Particles...", "size=0.40-Infinity display include summarize");

roiManager("Select", 2);

run("Analyze Particles...", "size=0.40-Infinity display include summarize");

roiManager("Select", 3);

run("Analyze Particles...", "size=0.40-Infinity display include summarize");
```

Measure fluorescence intensity.ijm

```
roiManager("Select", 0);
roiManager("Measure");
roiManager("Select", 1);
roiManager("Measure");
roiManager("Select", 2);
roiManager("Measure");
roiManager("Select", 3);
roiManager("Measure");
```